NTNU
Norwegian University of Science and Technology
Department of Marine Technology

M.Sc.THESIS

Title:	**Delivered:**
Analysis and Design of Columns in Offshore Structures subjected to Supply Vessel Collisions	June 20, 2011
	Availability: Open
Student: Reny Watan	**Number of pages:** 98

Abstract:

The assessment had been conducted for shipside collision against unstiffened, inclined jacket leg segment (column). The inclined column has been modelled with horizontal-to-vertical ratio of 1/7. Two types of boundary conditions of the column has been modelled; perfectly clamped boundary conditions (clamped or fixed) and boundary conditions with axial flexibility (axial spring)

For clamped column, two different impact locations have been simulated, namely middle span impact and quarter span impact. For each impact location, three (3) design categories have been analysed; ductile design (Rigid Ship versus deformable column), integrated design (deformable ship versus deformable column), and strength design (Rigid column versus deformable ship). For rigid ship and integrated cases, three (3) column wall thicknesses had been simulated to present the transition from ductile to integrated and strength categories.

From the force-displacement relationships, the force demanded to generate the same displacement both on the column and shipside is slightly higher for middle span impact than for quarter span impact, for all column wall thickness assessed herein. However, the resistance to indentation appeared to be significantly higher for middle span impact after the contact area had developed until over the height of the shipside.

Considering the analysis results from fixed columns, the column with the wall thickness of 40 mm under middle span impact had been chosen as main representative model to reveal the influence of the axial flexibility to the capacity of the column. Two (2) types of the spring arrangement on each column-end have been modelled, namely the multiple springs and the single springs. For multiple springs type, two different spring coefficients have been evaluated, namely the equivalent and the unequal (nodal) spring stiffness. The spring coefficients are calculated according the analysis results generated on USFOS, taking only the linear elastic spring stiffness.

The 'real' axial flexibility proved no major contribution to the overall resistance and deformation of the column. Therefore, assuming a fixed column is prudent for practical design.

Keyword:

Shipside-column impact
Inclined or tilted column
Axial springs
Resistance-indentation

Advisor:

Professor Jørgen Amdahl

Address:
NTNU
Department of Marine Technology
N-7491 Trondheim

Location
Marinteknisk Senter
O. Nielsens vei 10

Tel. +47 73 595501
Fax +47 73 595697

MASTER THESIS 2011

for

Stud. Techn. Reny Watan

Analysis and Design of Columns in Offshore Structures subjected to Supply Vessel Collisions

Analyse og dimensjonering av offshore søyler/tårn utsatt for støt fra forsyningsskip

Supply vessels, passing merchant vessels and shuttle tankers are regarded a major threat for offshore structures and platforms are often designed intentionally to resist collisions. In Norwegian sector of the North Sea the standard design event is a supply vessel of 5000 tons displacement sailing into a platform with a speed of 2m/s. For design purposes standard force-deformation curves for bow, side and stern impacts have been defined in NORSOK N-004 Appendix A for bow, sideways and stern impact.

With respect to the distribution of strain energy dissipation there may be distinguished between three design principles, namely *strength design, ductility design* and *shared-energy design* depending upon the relative strength the ship and the platform:

Strength design implies that the platform is strong enough to resist the collision force with minor deformation, so that the striking ship is forced to deform and dissipate the major part of the collision energy. *Ductility design* implies that the platform undergoes large, plastic deformations and dissipates the major part of the collision energy.

Shared energy design implies that both the platform and the striking ship contribute significantly to the energy dissipation.

From a calculation point of view, strength design or ductility design is favourable. In strength design, it is only necessary to verify that the struck ship is capable of resisting the total collision force and the local high pressure intensities during the deformation process. In ductility design, the shape of the deformation is highly dominated by the geometry of the striking ship structure and the energy dissipation can be analysed by means of plastic methods. In shared energy design, both the magnitude and the distribution of the collision force depend upon the deformation of both ships. This interaction makes the analysis more complex and calls for nonlinear finite element analysis. In most cases ductility or shared energy design is used or assumed. However, strength design may in some cases be achieved with small changes in structural configuration or material improvement.

Force intensities to apply for strength design are only given for stern collisions in Norsok-N004. Recently, considerable work has been on supply vessel, but no recommendations exist for strength design against supply vessel beam impacts.

The purpose of this work is to investigate the integrated response of unstiffened and stiffened columns/towers of offshore structures subjected to side from supply vessels and to establish guidelines for analysis and design.

The following topics should be addressed:

Brief review simplified design procedures for calculating the force and energy dissipation of unstiffened columns accounting for local denting.

Perform modelling of different stiffened and unstiffened columns/towers. Appropriate modelling of boundary conditions shall be performed. The scantlings, e.g. the diameter, thickness and degree of internal stiffening shall be varied. Emphasis should be made on parameterizing the models so as to allow easy change of scantlings.

Perform analysis of stiffened and unstiffened columns subjected to sideway impact by a supply vessel suing LS_DYNA. An existing finite element model of the ship side may be utilized. Develop force-intensity curves for various contact areas. To the extent possible, the limit point where the response changes from strength to shared energy and ductile behaviour shall be identified. Perform sensitivity analysis where important design parameters are varied. For unstiffened columns the effect of collision point location shall be investigated.

Compare the results of numerical analysis with simplified analysis procedures, notably those for unstiffened columns. If needed suggest improved design procedures.

Conclusions and recommendation for further work

Literature studies of specific topics relevant to the thesis work may be included.

The work scope may prove to be larger than initially anticipated. Subject to approval from the supervisor, topics may be deleted from the list above or reduced in extent.

In the thesis the candidate shall present his personal contribution to the resolution of problems within the scope of the thesis work.

Theories and conclusions should be based on mathematical derivations and/or logic reasoning identifying the various steps in the deduction.

The candidate should utilise the existing possibilities for obtaining relevant literature.

The thesis should be organised in a rational manner to give a clear exposition of results, assessments, and conclusions. The text should be brief and to the point, with a clear language. Telegraphic language should be avoided.

The thesis shall contain the following elements: A text defining the scope, preface, list of contents, summary, main body of thesis, conclusions with recommendations for further work, list of symbols and acronyms, references and (optional) appendices. All figures, tables and equations shall be numerated.

The supervisor may require that the candidate, in an early stage of the work, presents a written plan for the completion of the work. The plan should include a budget for the use of computer and laboratory resources which will be charged to the department. Overruns shall be reported to the supervisor.

The original contribution of the candidate and material taken from other sources shall be clearly defined. Work from other sources shall be properly referenced using an acknowledged referencing system.

The report shall be submitted in two copies:

Signed by the candidate

The text defining the scope included

In bound volume(s)

Drawings and/or computer prints which cannot be bound should be organised in a separate folder.

The report shall also be submitted in pdf format along with essential input files for computer analysis, spreadsheets, Matlab files etc in digital format.

Deadline: June 14, 2011

Trondheim, January 17, 2011

Jørgen Amdahl

Summary

The summary of this report can be compacted into a diagram, as showed in Figure 1. A short description is outlined herein.

The assessment had been conducted for shipside collision against unstiffened, inclined jacket leg segment (column). The inclined column has been modelled with horizontal-to-vertical ratio of 1/7. Two types of boundary conditions of the column has been modelled

- Perfectly clamped boundary conditions (clamped or fixed)
- Boundary conditions with axial flexibility (axial spring)

For clamped column, two different impact locations have been simulated, namely middle span impact and quarter span impact. For each impact location, three (3) design categories have been analysed; ductile design (**Rigid Ship** versus deformable column), **integrated** design (deformable ship versus deformable column), and strength design (**Rigid column** versus deformable ship). For rigid ship and integrated cases, three (3) column wall thicknesses had been simulated to present the transition from ductile to integrated and strength categories.

From the force-displacement relationships, the force demanded to generate the same displacement both on the column and shipside is slightly higher for middle span impact than for quarter span impact, for all column wall thickness assessed herein. However, the resistance to indentation appeared to be significantly higher for middle span impact after the contact area had developed until over the height of the shipside.

Considering the analysis results from fixed columns, the column with the wall thickness of 40 mm under middle span impact had been chosen as main representative model to reveal the influence of the axial flexibility to the capacity of the column. Two (2) types of the spring arrangement on each column-end have been modelled, namely the multiple springs and the single springs. For multiple springs type, two different spring coefficients have been evaluated, namely the equivalent and the unequal (nodal) spring stiffness. The spring coefficients are calculated according the analysis results generated on USFOS, taking only the linear elastic spring stiffness.

The 'real' axial flexibility proved no major contribution to the overall resistance and deformation of the column. Therefore, assuming a fixed column is prudent for practical design.

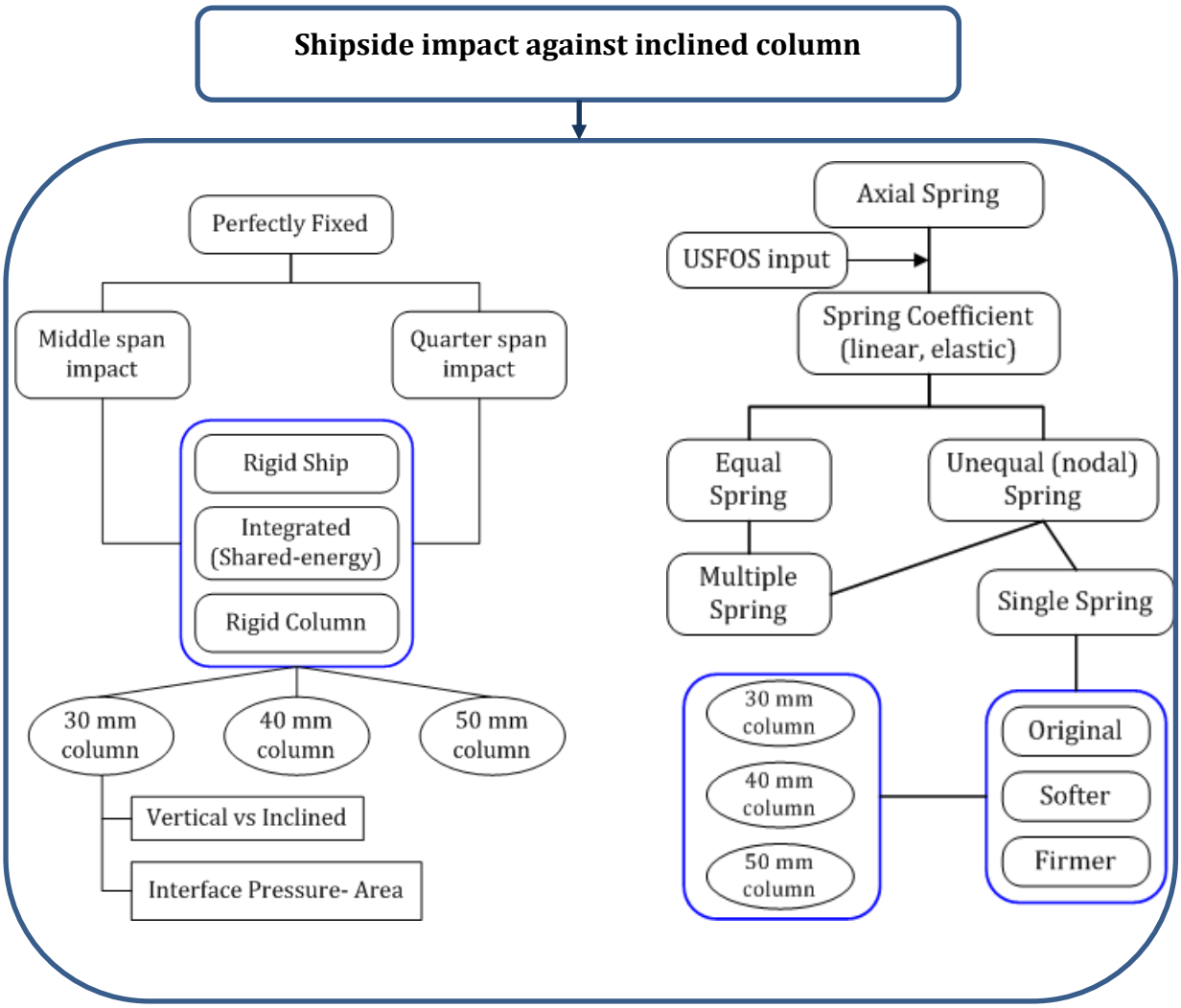

Figure 1 Summary

Preface

This document reports the thesis work results of Marine Technology master student Reny Watan during spring semester 2011 at Norwegian University of Science and Technology (*Norges Teknisk-Naturvitenskapelige Universitet*, NTNU).

This thesis work has been a broadened from the project work carried out during autumn semester 2010. Some essential background theories and features of the software which have been part of the project work are included here to emphasize.

Assessment on the force-deformation, energy-deformation and resistance-indentation relationships due to impact of shipside against the inclined column is the main feature in this report. The shipside model came from the existing model developed by previous master student, Henrik Raaholt. Three (3) thicknesses of the column wall have been investigated and compared with regard to three categories in design principle; ductile design, integrated design, and strength design. The influence of the impact location have been observed under two types of arrangement, namely middle span impact and quarter span impact for all three thicknesses concerned. The influence of the axial flexibility to the load-carrying capacity of the column had been investigated for middle span impact.

This thesis work had been a good combination of interesting, challenging, tedious yet fully learnable process. There were times when a mistake on the detail leads to the analysis results far from anticipated.

Problems and questions during the thesis work are discussed with various persons timely. Therefore, I would like to express my gratitude to:

- Professor Jørgen Amdahl for his role as my master thesis supervisor, for his guidance and motivation
- Zhenhui Liu (PhD candidate) for the time he spared to discuss my questions and for the motivational lines he shared.
- Sabril Haris for his assistance in dealing with the software at times
- Mohammad Taghi Tavakoli for his help in the material model
- Enni Lisda Lubis for discussion on USFOS results
- All the PhD candidates and master students for their help, influence and motivation in doing my thesis work, either intentionally or not.

Trondheim, June 20, 2011

Reny Watan

Table of Contents

List of Figures

List of Figures in Appendix

List of Tables

Nomenclature

Notation	Unit	Description
A	m^2	Cross sectional area
a	kg	Added mass
a_i	kg	Added mass for installation
a_s	kg	Added mass for ship
b	m	Width of identation (in longitudinal direction)
c	m/s	speed of sound in material
c	-	non-dimensional spring stiffness
D	m	Diameter of tubular section
E	Pa	Modulus of elasticity (Young's modulus)
E_a	J	Absorbed energy
E_E	J	External energy
E_I	J	Internal energy
E_s	J	Strain energy
f_y	Pa	Yield stress
I	m^4	Geometrical moment of inertia
i	m^2	Radius of gyration
k	N/m	Stiffness, spring stiffness
K_{node}	N/m	Axial Stiffness of the node with the considered member removed
L	m	Length of member
M_e	N.m	External moment
M_i	N.m	Internal moment
m_i	kg	Mass of struck object
M_p	N.m	Plastic moment
M_{red}	N.m	Reduced moment capacity
m_s	kg	Mass of striking object
N	N	Axial Force
N_p	N	Plastic Axial Force
N_{Rd}	N	Design axial compressive resistance
N_{Sd}	N	Design axial compressive force
p	Pa	Pressure
$P_{plastic}$	N	Concentrated, plastic load
q_p	N/m	Distributed, plastic load
R	N	Resistance to local denting
R_c	N	Characteristic strength factor (characteristic strength)
R_o	N	Plastic collapse load in bending
R_u	N	Increased load carrying capacity
t	s	time

Notation	Unit	Description
t	m	Wall thickness of tubular section
t_d	s	Duration of impact
v	m/s	velocity of the ship
W	m^3	Elastic section modulus
w_d	m	Depth of local denting (maximum identation)
W_P	m^3	Plastic section modulus
Δt	s	Time step
Δt_e	s	Critical time step
ν	-	Poisson's ratio of material
ρ	kg/m^3	Density

1 Introduction

Ship accidents have become public interest after several catastrophic accidents that left severe and prolonged consequences to the local communities and to overall environment.

Considering vulnerability of offshore installations to collision, supply vessels are among the potential ones to give a serious threat for offshore platforms. Therefore, offshore platforms are generally designed to resist the impact load of ship impact.

So far, the preferably design methods are either strength or ductile design. The example of strength design is shown in Figure 1-1. One of the main reasons the shared-energy design method is not widely applied is due to the computational time. Here the author had summarized the computational time required for several analyses in present work using LS-DYNA solver, as shown in Table 1-1. The computational time is indeed relatively longer for shared-energy analyses.

Table 1-1 Summary of Computational Time

	Rigid Ship		Rigid Column		Shared-Energy	
wall thickness	Quarter span	Middle span	Quarter span	Middle span	Quarter span	Middle span
30 mm	14 m 1 s	14 m 23 s	11 h 21 m 38 s	11 h 17 m 38s	11 h 52 m 47 s	11 h 53 m 53 s
40 mm	14 m 35 s	14 m 36 s			11 h 54 m 29 s	11 h 59 m 53 s
50 mm	14 m 42 s	14 m 40 s			12 h 0 m 34 s	18 h 15 m 16 s

note: h = hours; m = minutes; s = seconds

Recommendation from NORSOK applies only for vertical tubular member. In present work, the case is for column member with certain degree of inclination w.r.t. vertical axis. The column has the horizontal-to-vertical ratio of 1/7.

Under the previous work done in laboratory, a tubular member was struck by a rigid object. Effect of the impact location over the length of the tubular member was observed. The results visualized as if the tubular member is subjected to a concentrated load. The assessment to cover the integrated (shared-energy) analysis with a more realistic ship model was conducted in present work.

Agreed Scope of Work

After a discussion with Professor Jørgen Amdahl as the main supervisor, the thesis work would have more focus on the unstiffened column. Therefore, the work for the stiffened column has not been performed in this work.

(Source: http://www.2coolfishing.com/ttmbforum/showthread.php?t=146065)

Figure 1-1 Ship Collision against a Fixed Offshore Platform

2 Basic Principles

2.1 Collision Design Principles

2.1.1 Collision mechanics

The analysis procedures to solve the ship collision problems are commonly decoupled into two parts, the *external dynamics* and the *internal mechanics*. The external dynamics deal with the global inertia forces and hydrodynamic effects, while the internal mechanics deal with the energy dissipation and distribution of damage in the two structures involved in collision. There are several methods to analyze the internal mechanics problems, namely

- Statistical (empirical) methods;
- Experimental methods;
- Nonlinear finite element methods (NFEM);
- Simplified analytical methods

In this thesis work, the focus is on the internal mechanics by nonlinear finite element method and the simplified analytical method.

2.1.2 Strain energy dissipation

Collision between objects is governed by laws of momentum and energy. As for ship collision, the loads are characterised by a kinetic energy, described by the mass of the ship, including hydrodynamic added mass and the speed of the ship at the instant of impact.

NORSOK (N-004, 2004) gives the guidance to assess the strain energy dissipation based on the type of installation (compliant, fixed, or articulated installation) and the initial velocity of the installation. Since the present work deals with the typical jacket leg (fixed offshore structures), only the criteria for fixed installation will be presented.

The collision energy to be dissipated as strain energy maybe taken as

Fixed installations

$$E_s = \frac{1}{2}(m_s + a_s) \times v_s^2 \qquad \text{(2-1)}$$

Where

m_s = ship displacement [kg];

a_s = ship added mass (a_s = 0.2 for bow or stern impact; a_s = 0.4 for broadside impact)

v_s = ship (impact) velocity (should not be assumed less than 2 m/s for North Sea condition)

The installation can be assumed compliant if the duration of impact is small compared to the fundamental period of vibration of the installation. If the duration of impact is comparatively long, the installation can be assumed fixed.

Jacket structures can normally be considered as fixed. Floating platforms (semi-submersibles, TLPs, production vessels) can normally be considered as compliant. Jack-ups may be classified as fixed or compliant.

NORSOK standard (N-004, 2004) has defined three design principles based on the distribution of strain energy dissipation, namely *strength design*, *ductility design*, and *shared-energy design*.

Strength design implies that the struck structure has an adequate strength to resist the collision force and contact pressure without large (plastic) deformation. In this way, the ship is forced to deform and absorb most of collision energy.

Ductile design implies that the struck structure absorbs the most of collision energy as it undergoes large, plastic deformation, while the striking body experience minor deformation.

Shared-energy design implies that both colliding bodies will deform and contribute significantly to the energy dissipation.

A graphical representation of the categories is shown in Figure 2-1. In the design process, either strength or ductile design is favourable as the computational time is relatively shorter because one of the colliding bodies has been regarded as rigid, such that the calculation is necessary only for the deformable body.

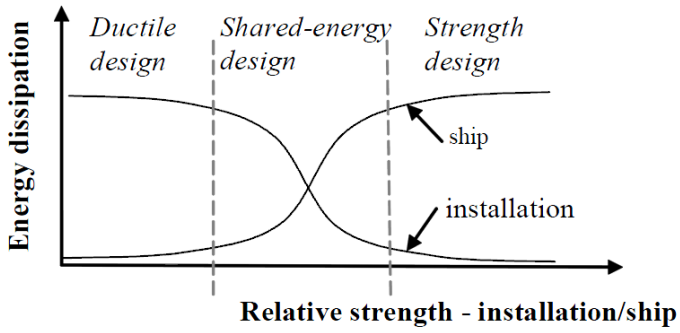

Figure 2-1 Energy Dissipation for Strength, Ductile, and Shared-energy design

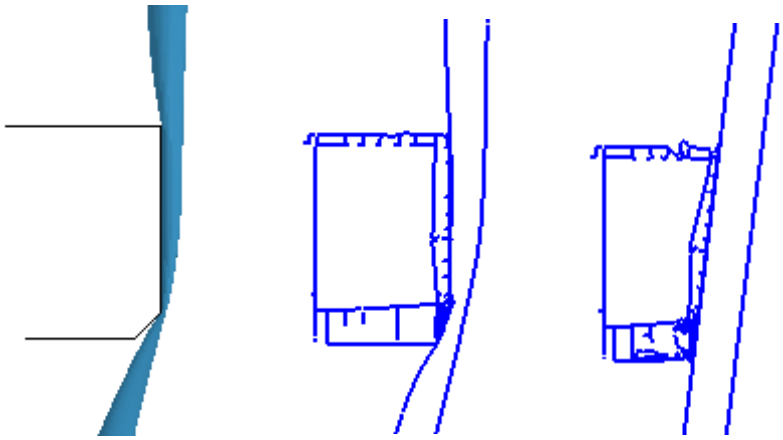

(a) Ductile (b) Shared-Energy (c) Strength

Figure 2-2 Deformed Colliding Bodies for three design principles

The load-deformation relationships for the ship and the installation are often established independently of each other assuming the other object infinitely rigid. This method may have, however, severe limitations: both structures will dissipate some energy regardless of the relative strength.

A representative of the load-deformation relationship is shown in Figure 2-3. In Figure 2-3 the force-deformation relationship from the integrated (shared-energy) analysis has been included.

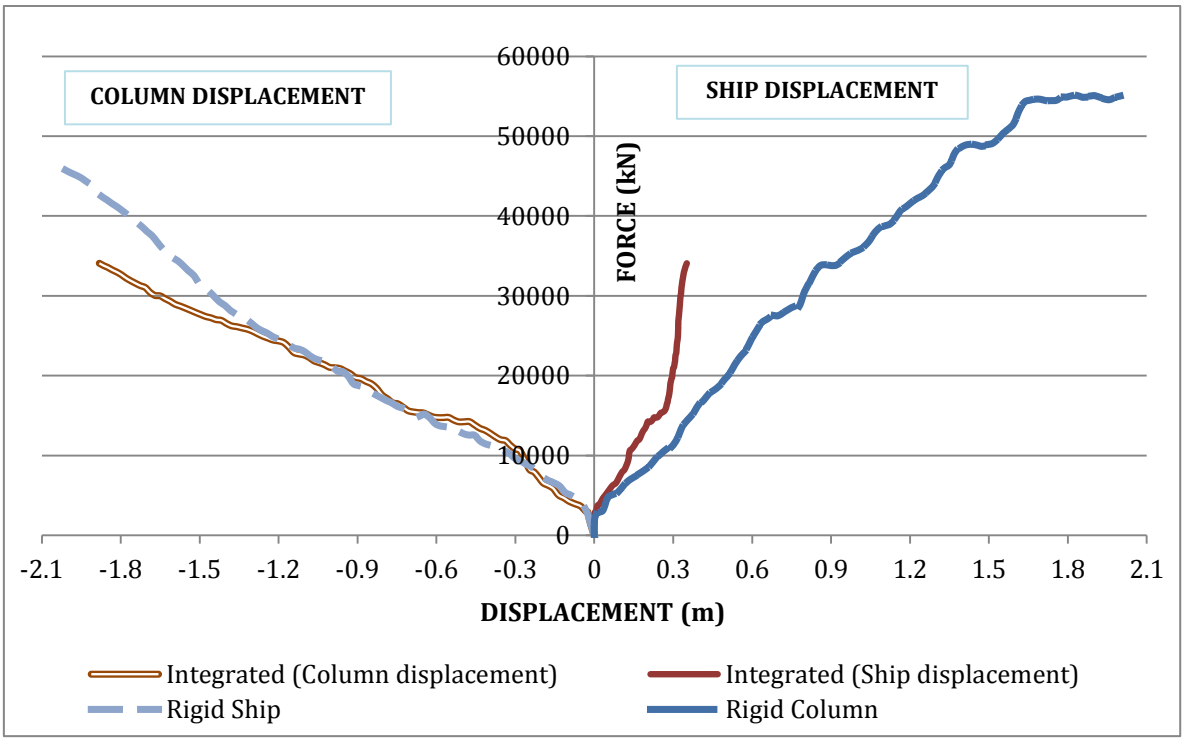

Figure 2-3 Force-Deformation Relationship for Ship and Column

The strain energy dissipated by the ship and the installation equals to the total area under the load-deformation curves and could be expressed as

$$E_{strain} = E_{strain,ship} + E_{strain,installation}$$

$$\boldsymbol{E_{strain}} = \int_0^{w_{s,max}} \boldsymbol{R_s}\, \boldsymbol{dw_s} + \int_0^{w_{i,max}} \boldsymbol{R_i}\, \boldsymbol{dw_i} \qquad \textbf{(2-2)}$$

where:

R_s = resistance of the ship;
R_i = resistance of the platform (installation);
dw_s = the deformation of the ship;
dw_i = the deformation of the platform (installation);

2.2 Simple Plastic Theory

Most structural materials undergo an elastic state before a plastic state is reached. This applies to both material behaviour of a cross section and the structure as a whole. The plastification process is important for steel in plastic design as it ensures that the material has adequate ductility for the cross section to sustain loading beyond its elastic limit (f_y).

For design purposes, it is prudent to ignore the extra strength provided by strain hardening, which becomes smaller in magnitude as the grade strength of steel becomes greater. Hence, for simplicity, steel is always idealized as an elastic-perfectly plastic material with a stress–strain relationship shown in Figure 2-4 (b).

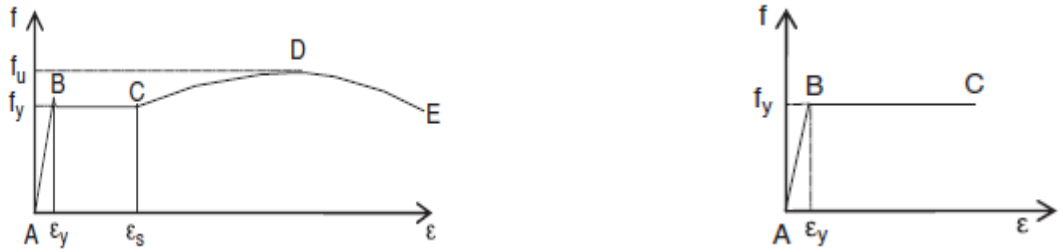

(a) General stress-strain diagram (b) idealized stress-strain diagram

Figure 2-4 Stress-strain diagram

An example to review the plastification is a simple beam subjected to increasing loading. At a relatively small displacement, before reaching the yielding strain-stress point (point B in Figure 2-4), the cross-section will undergo an elastic deformation, meaning that if the member is unloaded the strain of the cross-section will reverse back to its initial condition. The bending moment under this term is then an elastic moment. When the extreme fibers of the cross section reach the yield strain, ε_y, with a yield stress, f_y, a yield

moment M_y exists in the section. A further increase in loading causes partial plastification in the cross section, which signals the start of its elastic–plastic state. This elastic–plastic state corresponds to an increase in bending moment from B to D shown in Figure 2-5. When the cross section becomes fully plastic at point D, the maximum moment capacity, called plastic moment Mp, is reached. A further increase in loading increases the strains and hence the curvature in the cross section, but the plastic moment remains unchanged.

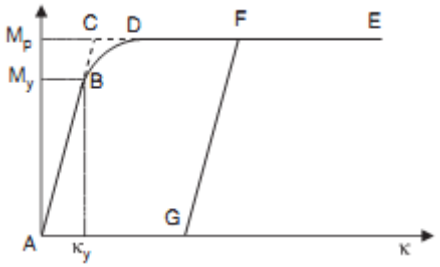

Figure 2-5 Moment–curvature relationship of a cross section

In reality, the exact value of Mp is difficult to obtain and its calculation is only approximate. There are several methods to analyse the plastic moment Mp of a structure such as incremental elasto-plastic analysis and classical rigid plastic analysis. The rigid plastic analysis has been used for plastic design over past decades because of its simplicity, especially for the plastic design of beams and frames. Its use is applicable mainly for manual calculation.

Rigid plastic analysis uses the assumption that the elastic deformation is negligibly small. Therefore in using this analysis method, the material behaves as if the structures does not deform until it collapse plastically.

Theorems of Plasticity

There are three basic theorems of plasticity from which manual methods for collapse load calculations can be developed. The basic theorems of plasticity are kinematic, static, and uniqueness. The kinematic theorem will be outlined hereafter.

Kinematic Theorem (Upper Bound Theorem)

This theorem states that the collapse load or load factor obtained for a structure that satisfies all the conditions of yield and collapse mechanism is either greater than or equal to the true collapse load. The true collapse load can be found by choosing the smallest value of collapse loads obtained from all possible cases of collapse mechanisms for the structure. The method derived from this theorem is based on the balance of external work and internal work for a particular collapse mechanism. It is usually referred to as the *mechanism method*.

Mechanism Method

This method requires that all possible collapse mechanisms are identified and that the virtual work equation for each mechanism is established. The collapse load Pw (or collapse load factor α_c if a set of loads are applied) is the minimum of the solutions of all possible collapse mechanisms for the structure. In establishing the virtual work equation, the total internal work as sum of the products of the plastic moment, M_p, and the corresponding plastic rotation, θ, at all plastic hinge locations j must be equal to the total external work. The total external work is expressed as the sum of the products of the externally applied load, α_c P, and the corresponding distance, δ, it displaces for all loads i . Mathematically,

$$E_{internal} = E_{external}$$
$$\sum_j \left(\boldsymbol{M_p} \cdot \boldsymbol{\theta}\right)_j = \boldsymbol{\alpha_c} \sum_i (\boldsymbol{P} \cdot \boldsymbol{\delta})_i \quad \textbf{(2-3)}$$

For Equation $\sum_j \left(\boldsymbol{M_p} \cdot \boldsymbol{\theta}\right)_j = \boldsymbol{\alpha_c} \sum_i (\boldsymbol{P} \cdot \boldsymbol{\delta})_i$ (2-3), a relationship between θ and δ can be established so that α_c is evaluated independently of these two terms.

2.3 Resistance-Indentation (Local Deformation)

The descriptions outlined herein have been excerpted from Chapter 7 of Skallerud & Amdahl's book (Skallerud & Amdahl, 2002).

The presence of local deformation due to ship collision on a tubular section depends on the slenderness of the cross section and the area of contact. Local deformation may form as a dent. The effect of the dent is two-fold:

(1) The impact energy is dissipated in the denting process.
The contribution of local denting to energy dissipation is significant for jacket legs, but relatively small for braces in typical jacket structure.
The dented cross section had been assumed consisting of a flattened part and the virtually undamaged part (Figure 2-6). The dented region is modelled by idealized yield-line model mechanism. It is assumed the tubular flattened at the contact area direct to the ship, and then the flattening gradually decreases in the adjacent, triangular regions towards the fixity points.

The resistance-deformation relationship is assessed by applying the principle of virtual work and conceding the contribution from plastic rotation along the yield lines, the change of curvature in circumferential direction and elongation of the tube generators.

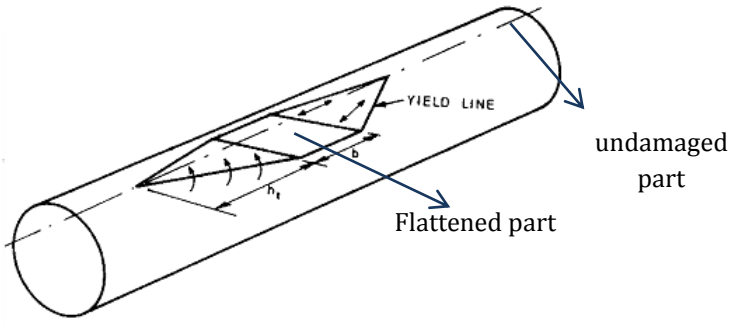

Figure 2-6 Yield-line model of dented tubular

NORSOK standard N-004 (N-004, 2004) recommends the resistance-to-indentation of unstiffened tubes to be taken from the curves as given in Figure 2-7. Alternatively, the non-dimensional resistance $\left(\frac{R}{R_c}\right)$ may be calculated from Equation (2-4). This equation has considered the effect of axial force on denting resistance.

$$\frac{R}{R_c} = k \times c_1 \times \left(\frac{w_d}{D}\right)^{c_2} \tag{2-4}$$

Where

Rc = characteristic resistance = $R_c = f_y \times \frac{t^2}{4} \times \sqrt{\frac{D}{t}}$

$$k = \begin{cases} 1.0 & ; \frac{N_{Sd}}{N_{Rd}} \leq 0.2 \\ 1.0 - 2\left(\frac{N_{Sd}}{N_{Rd}} - 0.2\right) & ; 0.2 < \frac{N_{Sd}}{N_{Rd}} < 0.6 \\ 0 & ; \frac{N_{Sd}}{N_{Rd}} \geq 0.6 \end{cases}$$

$$c_1 = 22 + \left(1.2 \times \frac{b}{D}\right)$$

$$c_2 = \frac{1.925}{3.5 + \frac{b}{D}}$$

N_{Sd} = design axial compressive force

N_{Rd} = design axial compressive resistance

NORSOK (N-004, 2004) noted that the curves should not be used to verify a design where the dent damage is required to be less than $0.05\left(\frac{w_d}{D} < 0.05\right)$.

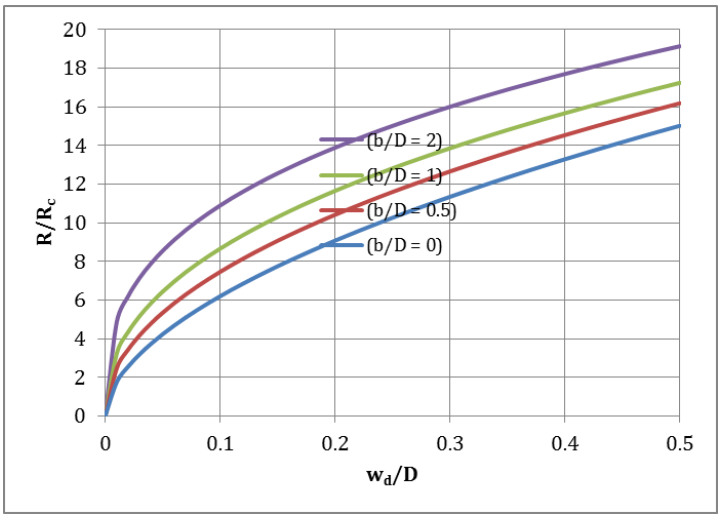

Figure 2-7 Resistance curve for local denting

(2) The dent may trigger ovalisation which reduces the effective bending capacity of the section and causes secondary bending moment from the axial force through the eccentricity created in damaged section. For conservative reason, it may be assumed that only the damaged part of the dented section contributes to the bending moment. This yields:

$$\frac{M_{red}}{M_p} = \cos\frac{\theta}{2} - \frac{1}{2}\sin\theta \qquad (2\text{-}5)$$

Where

$\theta = \arccos\left(1 - \frac{2w_d}{D}\right)$

$M_p = f_y \times D^2 \times t$

2.4 LS-DYNA Keywords

LS-DYNA keyword file is built up by command lines (keywords) which are customizable to comply with the type of analysis being concerned. The background theories of several important keywords described herein are excerpted from the theory manual (LS-DYNA Theory Manual, 2006).

2.4.1 Material Model

Rigid Material (*MAT_RIGID)

Assigning rigid material on parts comprised of elements will turn the parts into a rigid body. This is a preferable practice in many applications because the rigid elements are bypassed in the element processing and no storage is allocated for storing history variables; consequently cut down the computational time.

Inertial properties for rigid materials may be defined in either of two ways; from the geometry of the constituent elements of the rigid material and the density specified for the part ID; or by defining directly the inertial properties and initial velocities for a rigid body.

Realistic values of Young's modulus, E, and Poisson's ratio, ν, and density, ρ, should be defined to avoid the numerical problem in contact when determining sliding interface parameters if the rigid body interacts in a contact definition.

Power Law Isotropic Plasticity (*MAT_POWER_LAW_PLASTICITY)

This material model used to define material with elastoplastic behavior with isotropic hardening. The parameters below are used for the material. The material was recommended by Alsos (Alsos, 2008) as a good approximation of ship steel. The yield stress and the elastic strain are given by:

$$\boldsymbol{\sigma_y = k\,\varepsilon^n = k\left(\varepsilon_{yp} + \bar{\varepsilon}^p\right)^n} \qquad \textbf{(2-6)}$$

Where

ε_{yp}= elastic strain to yield, given by: $\varepsilon_{yp} = \left(\frac{\sigma_y}{k}\right)^{\left[\frac{1}{n}\right]}$

$\bar{\varepsilon}^p$= effective plastic strain (logarithmic)

σ_y = yield stress

k = strength coefficient

n = hardening parameter

This material also includes a stress strain effect, but is not including in this thesis work.

Elastic Spring (*MAT_SPRING_ELASTIC)

This is an isotropic elastic material for discrete springs and damper, which provides either translational or rotational elastic spring located between two nodes. Only one degree-of-freedom is connected.

This material has been assigned in present work for the elastic linear springs modelled to define the axial flexibility of the column.

2.4.2 Element Model

Belytschko-Lin-Tsay Shell Elements

While the Hughes-Liu shell element formulation had been used for years as the default shell element in the older version of LS-DYNA, the Belytschko-Lin-Tsay shell element had been implemented in recent LS-DYNA as the default shell element formulation for

explicit calculations, because it is computationally efficient compared to the Hughes-Liu shell element.

The Belytschko-Lin-Tsay shell element is based on a combined co-rotational and velocity-strain formulation. The efficiency of the element is obtained from the mathematical simplifications that result from these two kinematical assumptions. The co-rotational portion of the formulation avoids the complexities of nonlinear mechanics by embedding a coordinate system in the element. The choice of velocity-strain or rate-of-deformation in the formulation facilitates the constitutive evaluation, since the conjugate stress is the physical Cauchy stress.

2.4.3 Time Step

The dynamic FE analysis can be solved by either implicit or explicit method. The implicit method is unconditionally stable, but demands significantly long computational time, thus is costly and generally not preferred to be applied. In contrast, the explicit method is preferred since the computational time is relatively shorter. However, the explicit method is conditionally stable. The stability of this method can be assured by setting its time step size to be lower than the critical time step for the model.

The critical time step is governed by several parameters. To fulfil the conditions for stability the time step needs to be smaller than the time a pressure wave uses to pass through the element. If this was not the case, uncontrolled pressure waves could pass through the model and the results would at best be inaccurate. Another important factor regarding time step size is contact between bodies, as this requires a low time step to be stable.

In LS DYNA the next time step ensuring a stable solution is found by cycling through all the elements and checking their minimum time step size from the respective equations. A safety factor of 0.9 is then applied to the smallest step size found to ensure that the critical time step size is not violated.

For shell elements the critical time step is given by:

$$\Delta t_e = \frac{L_s}{c} \tag{2-7}$$

where

Ls = characteristic element length

c = sound speed in the material, given by: $c = \sqrt{\frac{E}{\rho(1-\nu^2)}}$

The characteristic element length can be defined in three different ways:

- The default option; based on the length of the element sides.
- A conservative option; based on the diagonals of the element, which gives a larger characteristic length, thus smaller time steps.

In this thesis work, the default alternative is used. The time step is then given by

$$L_S = \frac{(1-\beta)A_S}{\max(L_1, L_2, L_3, (1-\beta)L_4)} \qquad (2\text{-}8)$$

where β = 0 for quadrilateral and 1 for triangular shell elements,

A_s is the area, and

L_i (i = 1...4) is the length of the sides defining the shell elements

2.5 NORSOK (N-004, 2004)Recommendations

To determine the impact force for broad side and stern end impacts, NORSOK Standard N-004 recommended the force-deformation relationships for a supply vessels with a displacement of 5 000 tons for broad side, bow, stern end and stern corner impact for a vessel with stern roller, as given in Figure 2-8.

The basis for the curves in Figure 2-8 is strength design, i.e. limited local deformations of the installation at the point of contact. In addition to resisting the total collision force, large diameter columns have to resist local concentrations (subsets) of the collision force, as given in Table A.3-1 and Table A.3-2 of NORSOK (N-004, 2004).

NORSOK recommends a ductile design to be applied instead of the strength design, if the installation is not purposed for to be ductile.

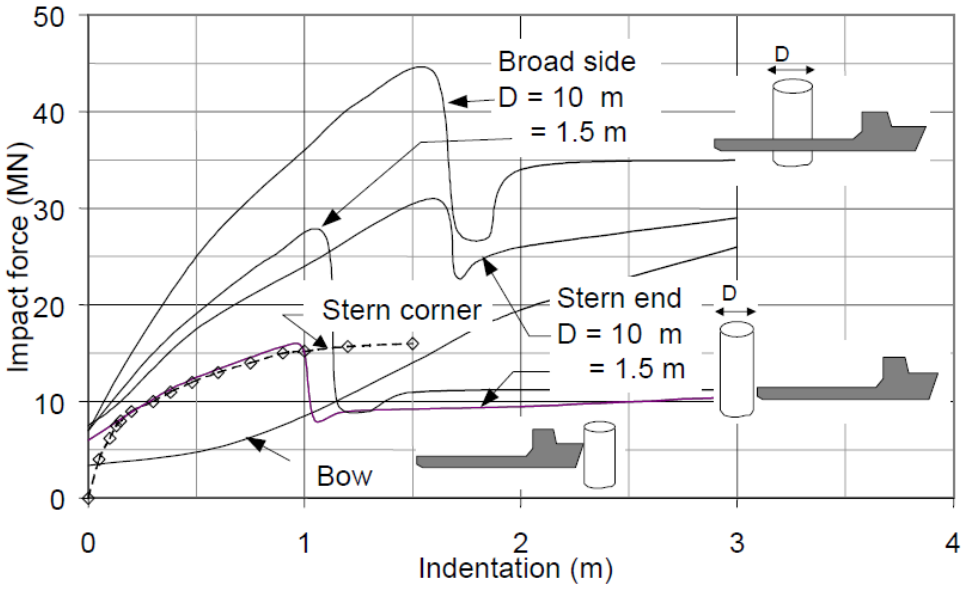

Figure 2-8 Recommended-deformation curves for beam, bow and stern impact

3 Finite Element Modelling

3.1 Modelling Aid Software

There are several softwares which have been utilized to build the model, MSC Patran 2008r1, MSC Patran 2010 1.2. x64 and LS-PrePost version 3.1. These are some of powerful software available for both pre-processing and post-processing. The MSC Patran, shortened as Patran, has been for years widely used for developing the finite element model. While LS-PrePost is initially used most for post-processing, for modifying the model and for building a relatively simple model it can replace Patran's role for pre-processing tasks.

The ship model had been built using Patran 2008r1 and later verified in Patran 2010 1.2. x64 and LS-PrePost for the quality of the elements. For the column model, since it is a simple model, LS-PrePost is preferred for modelling.

3.2 Ship Model

The ship model is adopted from the existing model built by Henrik Raaholt (Raaholt, 2009). The descriptions hereafter are mostly excerpted from his thesis report.

3.2.1 Reference Ship

The reference vessel is an Ulstein design with 4600 dwt. This supply vessel was chosen by considering that it is designed to operate in areas around platforms and wind turbines. Moreover, the total structural drawing available was also an important factor. The main dimension of the vessel is presented in Table.

Table 3-1 Principle Dimensions of Reference Ship

Length O.A.	90.90 m
Length P.P.	78.80 m
Breadth Moulded	18.80 m
Depth Moulded	7.60 m
Draught Scantling	6.20 m
Docking load app.	4600 tons

Figure 3-1 Reference Ship

3.2.2 Geometry Model

The mid shipside model consisting of 24 frames in the middle of the cargo deck had been selected. This was considered sufficient to obtain good results for collision with a relatively small diameter column. Due to the complexity of the mid ship section most of the details in this section had been left out or simplified in the modelling process. Simplifications reduced the modelling and meshing time and also the calculation time. The following figure (Figure 3-2) indicates where the mid ship section is situated in the reference ship.

Table 3-2 Principle dimensions for mid shipside model

Length	15.60 m
Width (Breadth)	4.20 m
Height	7.60 m
Frame spacing	0.65 m
Double bottom height	1.2 – 1.45 m
Thickness of outer plating	9 / 10.5 / 25 mm
Thickness of bottom plate	13.00 mm
Cross section of side stiffeners	HP180x8 / HP200x9

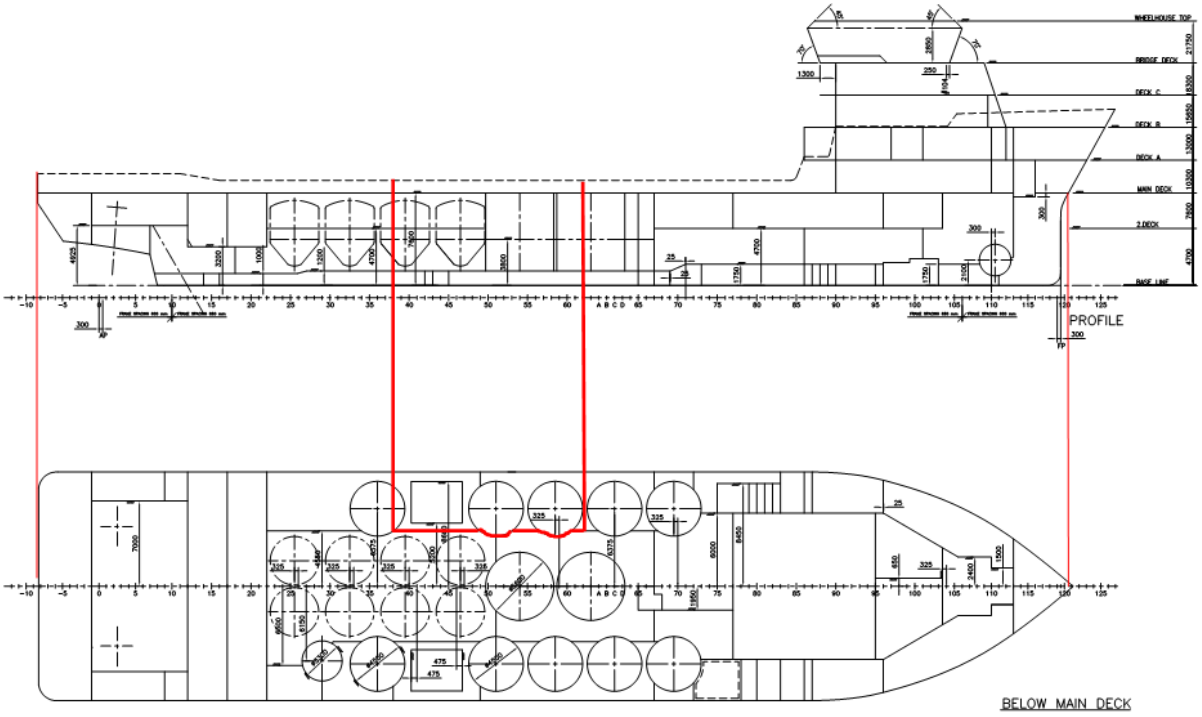

Figure 3-2 Mid-shipside model shown in reference ship

The mid ship side model is shown in the Figure 3-3. The simplifications made are:

- The circular cut-outs are modelled squared with approximately the same area;
- Small brackets and other small detailed geometry are neglected; and
- Bulbous stiffeners are modelled with L-profile with the same height, thickness and area as the original profiles.

These simplifications do not influence the results significantly, but it is beneficial for both modelling and computation time of the analyses.

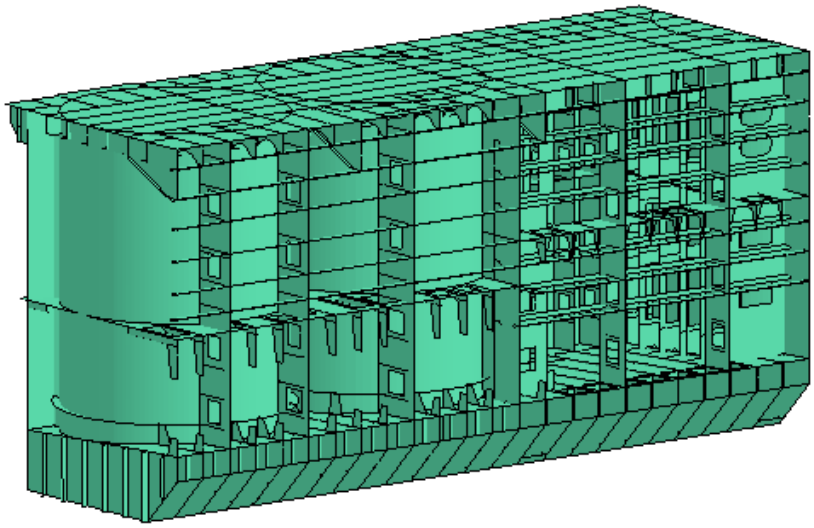

Figure 3-3 Mid-shipside model showed without the front side plate

3.2.3 Meshing

The four-node quadratic shell elements have been preferred to be applied for the entire model. Compared to three-node triangular elements, for structures subjected to bending, the four-node quadratic elements will give more accurate results. For areas with sophisticated geometry, simplifications had been made to allow use of four-node elements.

The size and shape of the elements will strongly affect the results and computation time. Alsos (Alsos, 2008) presented a convergence study on the mesh size when performing a grounding analysis, which is in many ways similar to a collision analysis, and it was found that with an element length between 5 and 10 times the plate thickness yielded good representation of the shell folding and a good physical model. In the mid ship section the plate thickness varies between 8 to 25 mm and the element length is therefore varied between 80 and 150 mm and between 6 and 10 times the plate thickness. This mesh gave a total of 100 000 elements.

3.2.4 Boundary Conditions

The nodes on the transversal edges of the mid shipside model, which parallel to the impact direction, have been restrained in all degrees-of-freedom except in the translational degree-of-freedom parallel to the direction of motion.

There is no boundary limitation assigned to the nodes on the longitudinal edge, as the velocity of the ship motion will be generated from this edge. This implies that the forces in the transverse direction must be transferred as shear forces in the plates. The boundary conditions on the mid shipside model are depicted in the following figure.

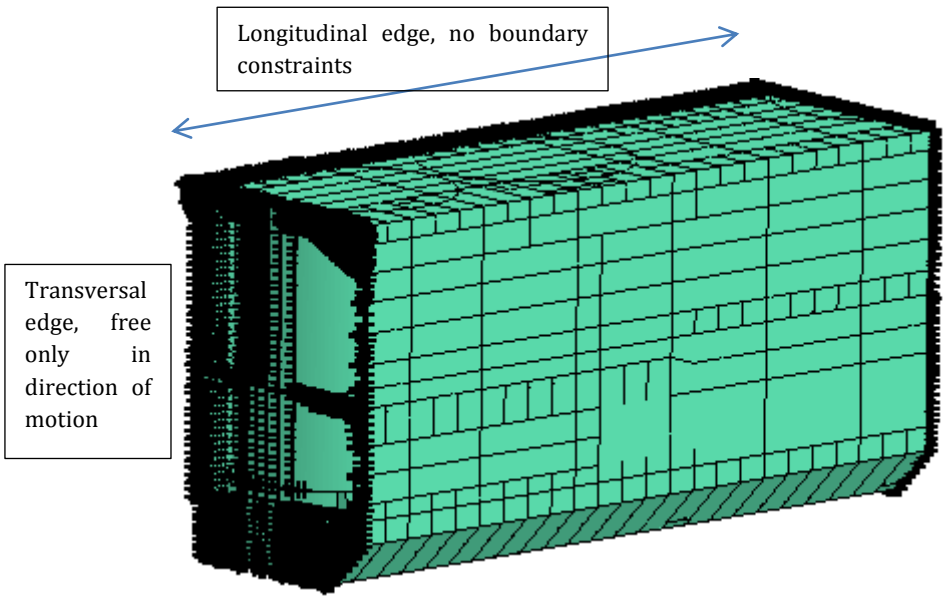

Figure 3-4 Boundary conditions on mid-shipside model

3.2.5 Material Model

There are mainly types of material used for the mid ship section. The material is assigned to the model to comply with the type of analysis being concerned (*rigid ship*, *rigid column*, or *shared-energy (integrated)* analysis).

(a) Rigid material is used in *rigid ship* analyses, where the impact energy is absorbed only by the column.
(b) Elasto-Plastic Power-Law material is used in both *Rigid Column* and *Shared-Energy* analyses, where the shipside is deformable. The following material parameters are used.

Table 3-3 Power Law material parameters for ship steel

Yield stress, σ_y	260 MPa
Young's modulus, E	210 GPa
Density, ρ	7850 kg/m3
Poisson's ratio, ν	0.3
Strength coefficient, k	740 MPa
Hardening exponent, n	0.24

3.3 Jacket Leg Segment Model

3.3.1 Geometric

The jacket leg segment is a typical inclined tubular section with batter ratio of $^1/_7$ (see Figure 3-5). The diameter and length of the segment is 1.50 m and 17.0 m, respectively. The simulations are then varies in the thickness of the tubular section. The dimensions and geometrical properties of the jacket leg with several thicknesses used in this thesis work are tabulated below. For short, the jacket leg segment will further be named as ***column***.

Table 3-4 Jacket Leg Geometric Properties

Outside Diameter =			1.5 m		
Total length =			17 m		
No	thickness (m)	D/t	Area (m^2)	I (m^4)	$i = \sqrt{\frac{I}{A}}$
1	0.030	50	0.139	0.037	0.520
2	0.040	37.5	0.183	0.049	0.516
4	0.050	30	0.228	0.060	0.513

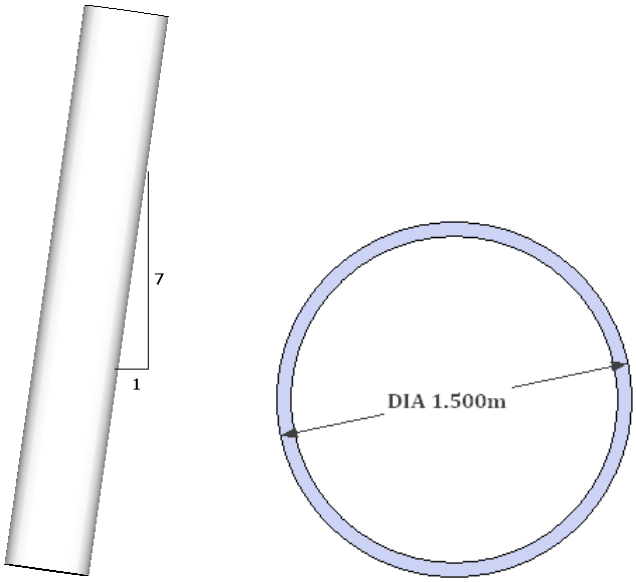

Figure 3-5 Sketch of Jacket Leg

3.3.2 Boundary Conditions

The model of leg segment is 17.0 m long, while the total jacket leg which may exceed 100 m long. The length of the leg segment is determined based on the braced length of the jacket leg of which potentially subjected to ship impact. Since the leg segment is supported by the braces and the jacket is piled, it is acceptable to assume the leg segment ends are clamped in all translational and rotational degrees-of-freedom, provided that the load transfer from the leg segment to other members and braces is carried out ideally. Thus, in this chapter all the analyses have been simulated under the assumption that the jacket leg (column) is clamped at it ends.

However, one should be aware that the fixed-ends assumption does not represent the real boundary conditions as the jacket structure also subjected to other loads (environmental, gravitational, etc.). These loads contribute to the global deformation of the jacket structure and interact with the local deformation of the leg segment. Thus, the ideal boundary conditions should have the flexibility range in between the clamped and the pinned supported.

In Chapter 5, a review on the modified boundary conditions will be presented.

3.3.3 Meshing

The column is built up with four-node quadrilateral elements. The wall thicknesses of the column chosen in present work are 30 mm, 40 mm, and 50 mm. The element length is set 100 mm, which is between 2 and 3.3 times the wall thickness. The element size of 100 mm is applied for column model to avoid the element intrusion at the contact interface during the impact.

3.3.4 Material

Similar to the material model for shipside model, the following two materials have been assigned for the jacket leg model.

(a) Rigid material is used in *rigid column* analyses, where the impact energy is absorbed only by the ship.
(b) Elasto-Plastic Power-Law material is used in both *Rigid Ship* and *Shared-Energy* analyses, where the column (jacket leg) is deformable. The following material parameters are used. The

Table 3-5 Power Law material parameters for jacket leg model

Yield stress, σ_y	355 MPa
Young's modulus, E	210 GPa
Density, ρ	7850 kg/m3
Poisson's ratio, ν	0.3
Strength coefficient, k	790 MPa
Hardening exponent, n	0.19

3.4 Collision Preparation

3.4.1 Velocity

The velocity of the colliding bodies will determine the total energy released during the collision, which will then influence the energy absorbed by the strain energy dissipation. Figure 3-6 shows the influence of the velocity to the impact force and energy. The analysis arrangement used for the comparison is based on the shipside impact on the middle span of the jacket leg with 30 mm wall thickness.

The figure shows that within the same displacement range, the force-deformation and energy-displacement relationship for the velocity of 5 m/s will be relatively higher than the other two velocities.

Nevertheless, the constant velocity of 2 m/s will be used further in this thesis work for all impact scenarios and cases.

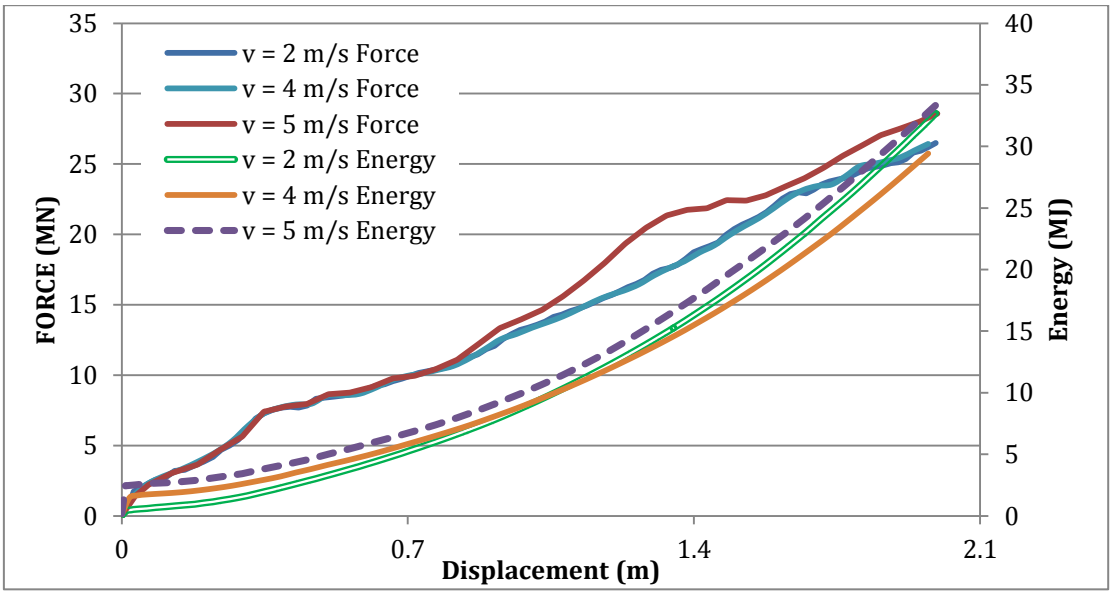

Figure 3-6 Force-Energy-Displacement comparison (various constant ship speeds)

3.4.2 Impact location on the jacket leg

The collision location is determined from the very first point where the ship touches or interacts with the struck object (column). From this point of view, in order to observe the effect of the collision point location, two scenarios have been set with regard to the length (span) of the column.

a. Scenario 1 (Quarter Span)
   By this scenario, the shipside model is located such that the half-height of its flat front interface is at the same level with the half-length of the column. The first strike shipside will then strike the column at about 5 m up from the bottom-end of the column. For the 17 m of the column, this arrangement does not represent strike at its exact quarter span. This arrangement has been set initiatively by the author, considering that at the final state of the impact the contact area will be covering the middle zone of the column, which is presumed to be the weakest part along the column span. This arrangement has been used in present work to represent the effect of impact at the quarter span of the column, thus will be further regarded as "***quarter span*** impact". This scenario is illustrated in Figure 3-7(a).

b. Scenario 2 (Middle Span)
   The shipside will first hit the column by its bottom hull, as indicated in Figure 3-7(b). This point will be regarded as the reference impact-point. In this scenario, the shipside is arranged such that level of reference impact-point has the same level with the middle span of the column. Consequently, at the first contact, the shipside will hit the column at around its middle span (half-length).
   In present work, this scenario will be regarded as "***middle span*** impact".

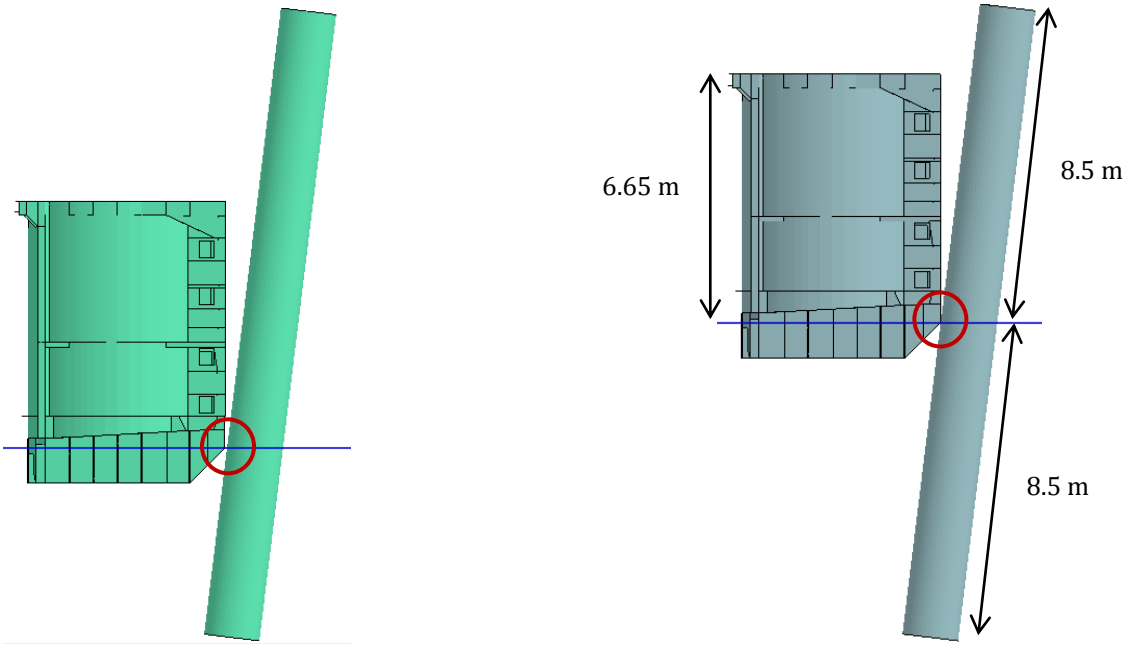

(a) Scenario-1 (Quarter Span) (b) Scenario-2 (Middle Span)

Figure 3-7 Impact location scenarios

The colliding objects are arranged as close as possible to each other, but still detached before the execution of the simulation, to dismiss the unnecessary computational effort to move the striking body until the first contact takes place.

3.4.3 Inclined Column Compared to Vertical Column

The leg of a jacket typically has certain degrees of inclination with respect to the vertical axis. In this thesis work, the column observed is the inclined one. However, to observe the difference between the inclined and the vertical column, a brief review is presented herein. The analyses had been conducted for the column with the wall thickness of 30 mm. The shipside is located such that the half-height of its flat interface is at the same level as the half-length of the column. In this way, the shipside will hit the column at its middle span area. Sketch of the model arrangement for this case is presented in Figure 3-8.

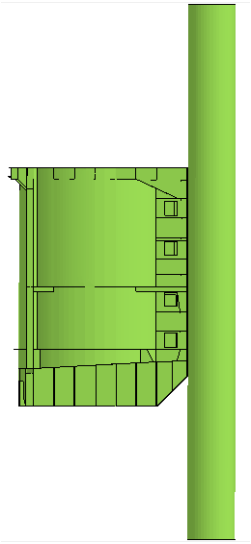

Figure 3-8 Collision arrangement for Vertical (straight) Column

The analyses conducted cover the assumption of rigid column, rigid ship, and integrated (shared-energy). The force-displacement relationships for these three categories are presented in Figure 3-9.

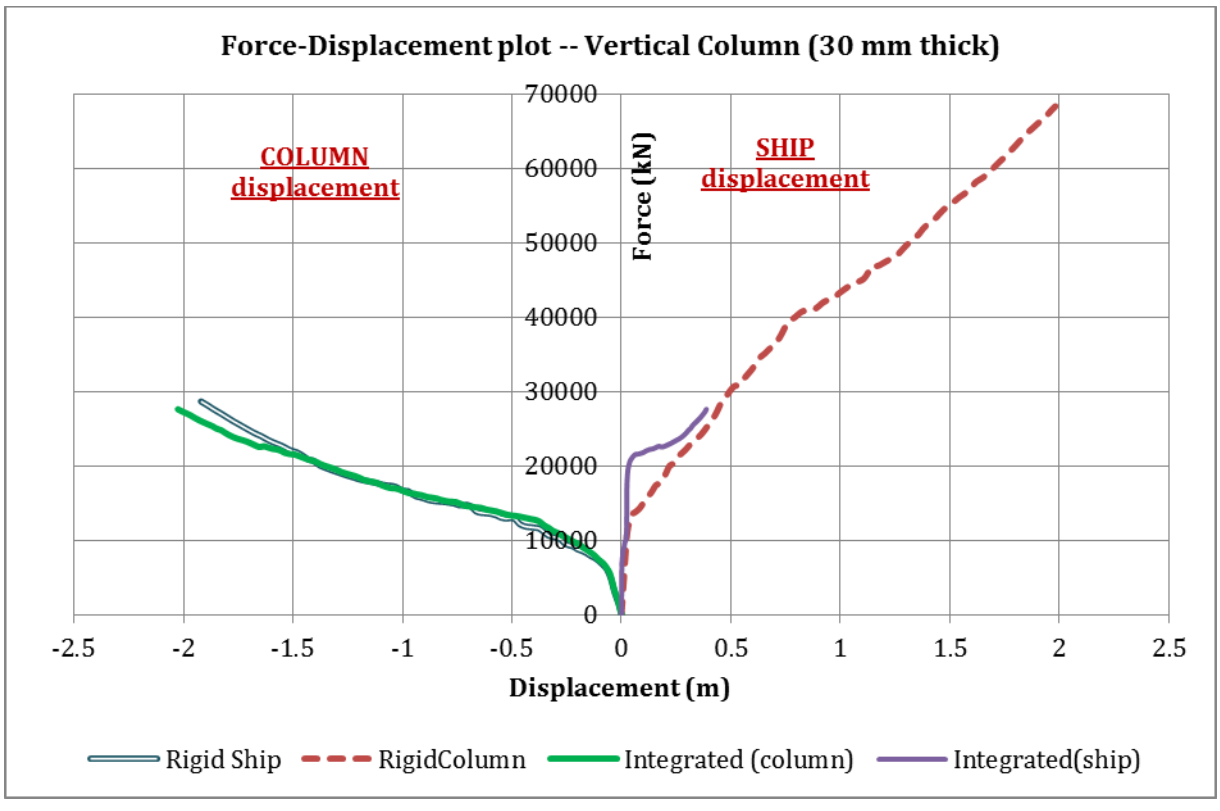

Figure 3-9 Force-Deformation – Vertical Column

Figure 3-9 shows that under the integrated (shared-energy) analysis, the column force-deformation relationship agrees well with the rigid-ship assumption. At the early stages

of the impact, the shipside behaves as a rigid body penetrating the column. At the end of the impact, as the column develops additional resistance due to its fixed-ends boundary conditions during the impact, there occurs a slight deformation on the ship. The deformation contour of both shipside and column are presented in Figure 3-10.

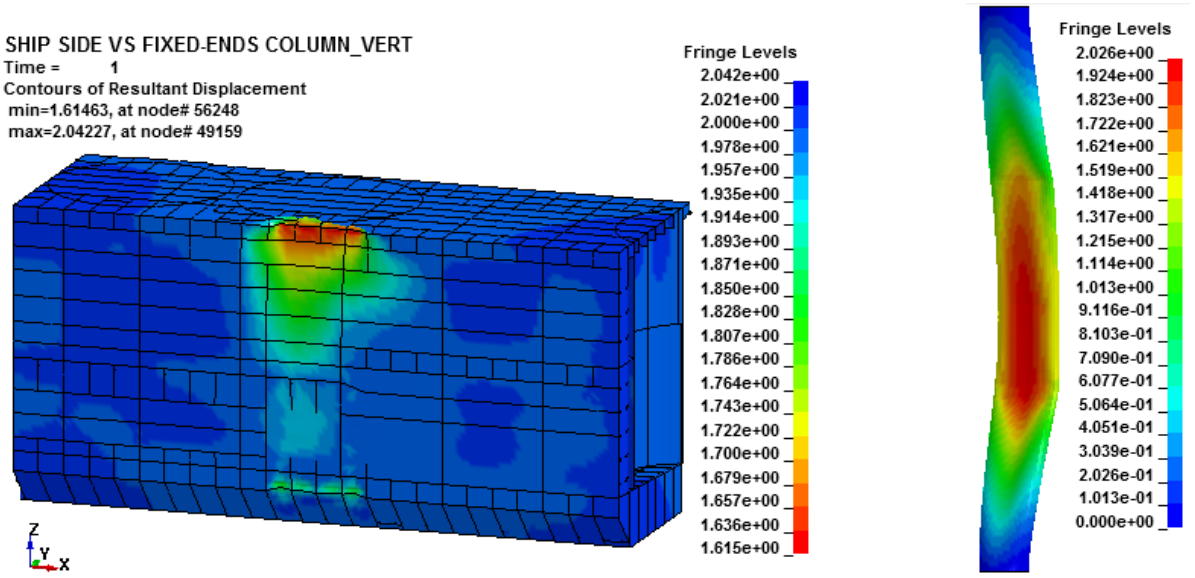

Figure 3-10 Shipside and Column Deformation at Final State—Vertical Column

The comparison of the force-deformation relationship between two columns is presented in Figure 3-11. Only the shared-energy category has been plot for this comparison purpose.

Figure 3-11 shows that there is a significant change of the force-deformation relationship. Under the same boundary conditions (fixed-ends) and the same wall thickness of the jacket leg (column), this can be understood as

(a) On the impact of shipside to vertical column, the total contact area from the first time state until the final state is slightly changed. While as on the inclined column, the contact area of the impact changed gradually for every time state.
(b) For vertical column, the contact area is relatively large and constant such that the impact load can be viewed as a distributed load on the impact interface. While as on the inclined column, since the contact area changes gradually, so does the impact load. The impact load can be assumed as a concentrated load at the early state of the impact, and then gradually changes to distributed load with the time state.

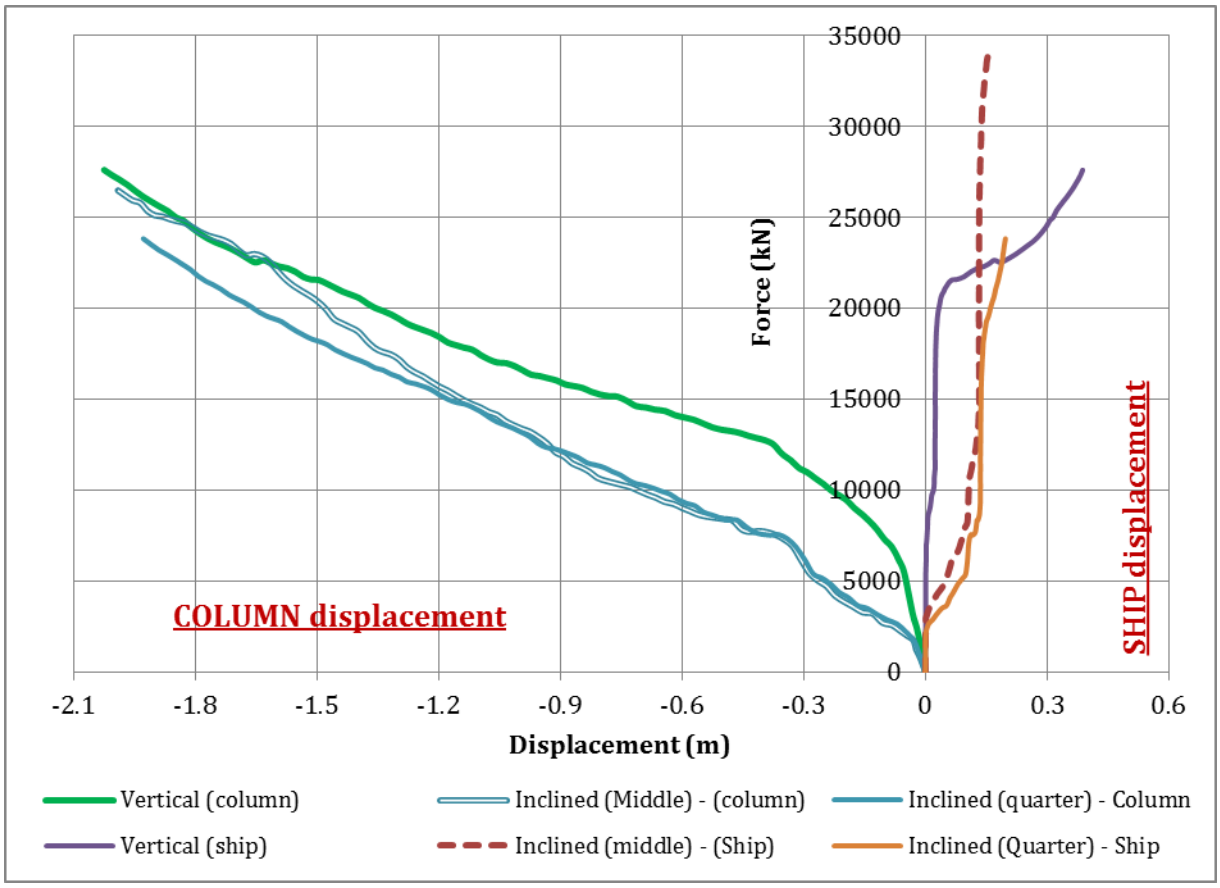

Figure 3-11 Force-Deformation (Integrated case) —Vertical vs. Inclined Column

3.4.4 Contact interactions

When the collision occurs, there are two (2) potential contact interactions, as described herein.

(1) Contact interaction between two colliding bodies (master-and-slave contact). This type of contact interface will further be noted as "external contact" in this report. The LS-DYNA keyword used to define the external contact is *CONTACT_AUTOMATIC_SURFACE_TO_SURFACE. The jacket leg (struck body) has been assigned as the master-contact and the ship (striking body) as the slave-contact. This keyword enables an automatically updating surface-to-surface penalty algorithm.

(2) Contact interaction between the structural components and elements inside each colliding body itself (self-contact). This contact interface will be noted as "internal contact". If both colliding bodies are deformable structures, there are two separated internal contacts will be defined. In other hand, if one of the colliding bodies is assumed as rigid, only the deformable body should have the internal contact defined. The keyword used to define the internal contact is *CONTACT_AUTOMATIC_SINGLE_SURFACE. This keyword enables the single-surface penalty algorithm to be automatically updated.

For both contact interactions described above, the static and dynamic friction coefficients of 0.3 has been used, similar to (Storheim, 2008), (Tavakoli, Amdahl, Alsos, & Klæbo, 2007), and (Raaholt, 2009).

3.4.5 The Execution Syntax

The syntax applied to instruct LS-DYNA to start processing the keyword file of all simulations in this thesis work is as follows:

LS-DYNA I = **inf** S = **iff** NCPU = **ncpu**

Where:

LS-DYNA = version of ls-dyna execution file used to perform the analysis. (in this thesis work the execution file is ***ls971_d_R5_0_intel64_redhat54***

inf = user specified input file (the name of the keyword file)

iff = interface force file (user defined). This option will be defined whenever it is required to keep the output files consisting interface pressures of the colliding bodies.

ncpu = number of cpu (defining the number of processors for shared memory computers to control parallel processing usage). This number determines the computational time required for a simulation to complete.

4 Results for Clamped Ends Column

The default output by LS-DYNA is controlled by keyword *CONTROL_OUTPUT. The output of ASCII databases and binary files output by LS_DYNA is controlled by the keyword *DATABASE (with a combination of options), while the default output is controlled by *CONTROL_OUTPUT. By *DATABASE, the frequency of writing various databases can be defined.

In this present work, several ASCII databases have been defined to be written out by LS-DYNA, such as GLSTAT (global data), RCFORC (resultant interface forces), MATSUM (material energies), NODOUT (nodal point data), NCFORC (nodal interface force) and SPCFORC (SPC reaction forces). Refer to (LS-DYNA Keyword User's Manual Volume 1: Version 971/Rev. 5, 2010).

In present work, the impact duration (terminating time of impact) is 1.0 s., whereas for the time interval between outputs of the ASCII databases is 0.01 s. This setting will give more than 100 points of data output for each node and element over the impact duration.

The most important analysis results to be reviewed hereafter are the displacements, the interface (contact) forces between two colliding structures and the corresponding interface pressures, and the dissipated energy.

For the reference ship with ship displacement of 4600 tons, the impact energy for shipside (broad side) collision towards fixed installation (jacket structure) can be calculated by equation ($\boldsymbol{E_s = \frac{1}{2}(m_s + a_s) \times v_s^2}$ (2-1):

$$E_s = \frac{1}{2}(m_s + a_s) \times {v_s}^2$$

$$E_s = \frac{1}{2}\left((1 + 0.4) \times 4.6 \cdot 10^6\right) \times 2.0^2 = 12.88\ MJ$$

The force-deformation with the corresponding energy-displacement relationships will be outlined and observed next. Following these curves are the non-dimensional resistance-indentation relationships and the corresponding resistance-bending plots to observe the effect of the local indentation to the global bending of the leg segment (column). The interface pressure-contact area plots will be observed next in the sequence by comparing to the formulas developed by Lin Hong (Hong & Amdahl, 2007) and Tavakoli (Tavakoli, Amdahl, Alsos, & Klæbo, 2007).

The NLFEA demands a lengthy time to compute and write out the output results because of the iteration process. For each analysis in present work, eight (8) CPUs had been occupied on the server system consists of shared-memory computers to complete the computation. The output files are equally demanding to store. Depending on the complexity of the FE model and also the number of output databases demanded by the user, disk memory required to store a complete analysis output ranges from 1 GB (Gigabyte) up to 15 GB.

4.1 Force-Deformation

The ductile (rigid ship), strength (rigid column) and integrated (shared-energy) analyses had been conducted. The interface forces are reported in ASCII database (RCFORC) and equal for both colliding bodies (in equilibrium, action force = reaction force). The deformation is determined by the deepest penetration a body experienced due to the collision. The column deformation is relatively easy to determine since the column is fixed. Therefore the deformation is plot merely based on the maximum nodal displacement.

The shipside deformation is determined based on some considerations:

a. The shipside is the moving body, while the displacement output by LS-DYNA is including the displacement due to the motion. Thus the deformation is calculated based on the relative displacement, by subtracting the deepest nodal displacement with the displacement due to motion.
b. The bottom part of the shipside appears to be stronger than the upper part because of the stiffeners structure at the bottom hull. Even though the bottom part will be in contact with the column most of the impact duration, the displacement at the upper part could relatively be larger at the final state. This is also influenced by the resistance of the column, which will be discussed further sequentially.

4.1.1 Force-Deformation - Scenario 1 (Quarter Span)

The following figures show the deformed contour of the shipside and the column (Figure 4-1 up to Figure 4-3) at final state due to quarter span impact with various column thicknesses under the integrated (shared-energy) analyses.

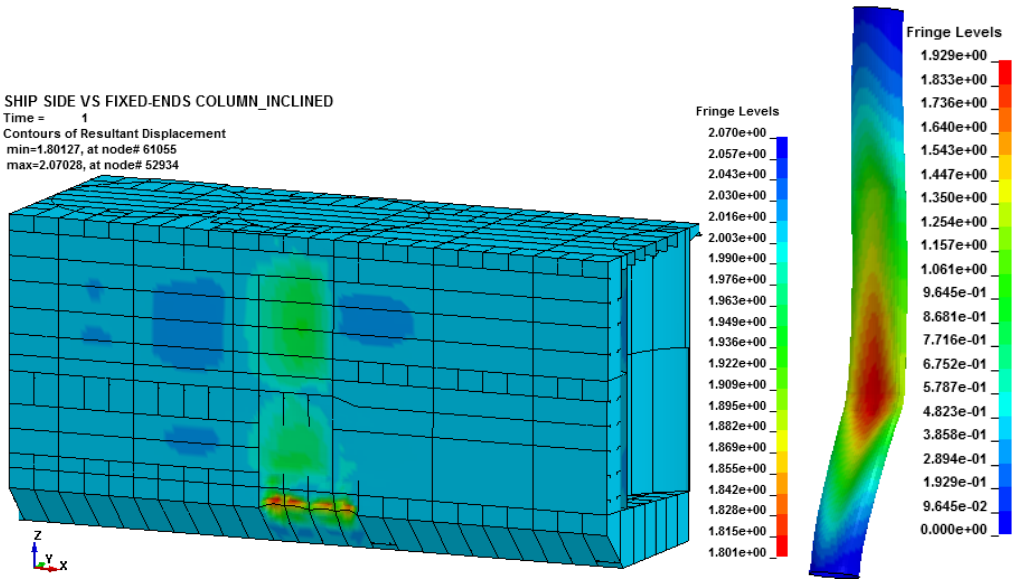

Figure 4-1 Displacement fringe (Integrated) – Quarter Span (30 mm thk. Column)

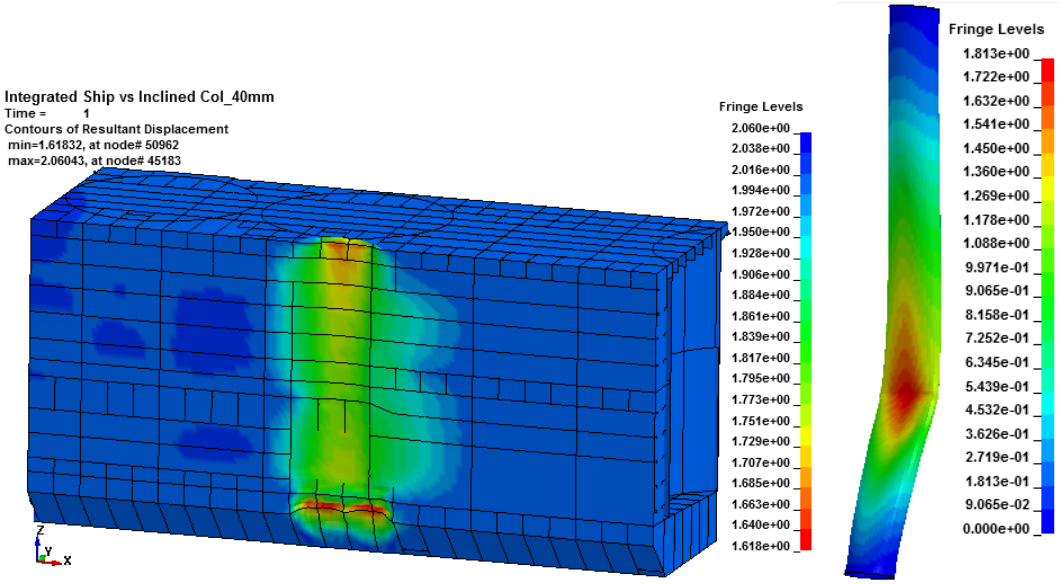

Figure 4-2 Displacement fringe (Integrated) – Quarter Span (40 mm thk. Column)

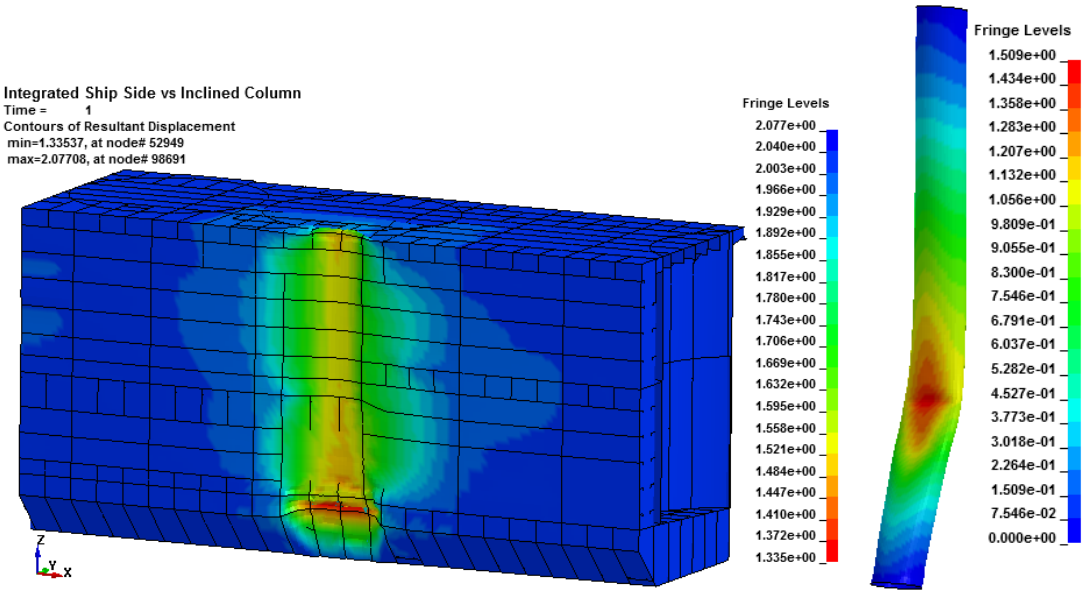

Figure 4-3 Displacement fringe (Integrated) – Quarter Span (50 mm thk. Column)

The figures show an obvious transformation from relatively ductile column (30 mm thick column) to integrated (40 mm thick column), and to a more rigid column (50 mm thick column). A sensitivity analysis had also been conducted for column with wall thickness of 45 mm and 60 mm under the shared-energy (integrated) simulation. The force-deformation plot that includes these two thicknesses is presented in Fig. A-9.

The force-deformation relationships for three main column thicknesses (30 mm, 40 mm, and 50 mm) are presented in Figure 4-4.

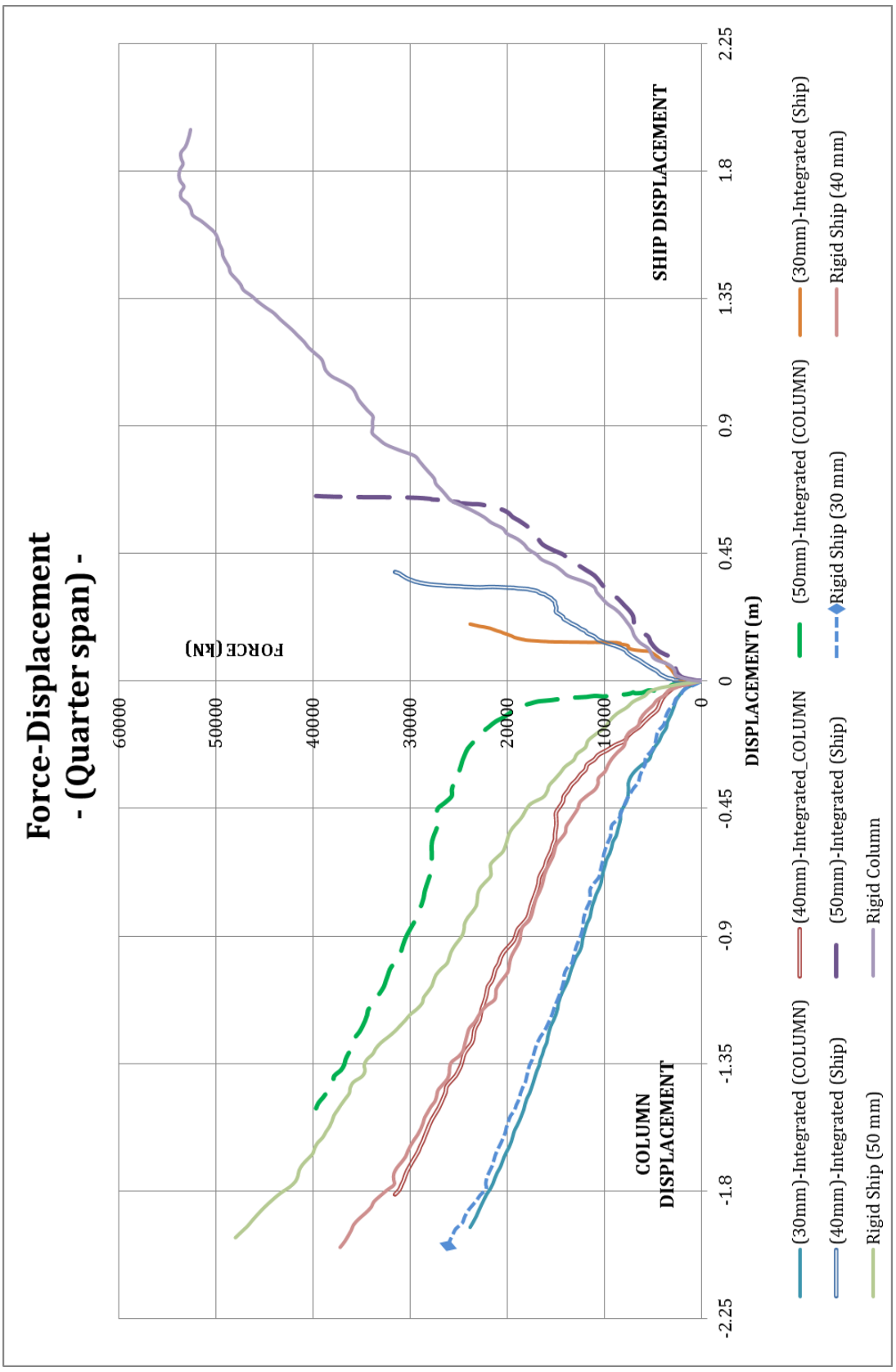

Figure 4-4 Force-Deformation – Quarter Span

From Figure 4-4, some observations can be pointed out:

(1) Impact on 30 mm thick column

Under the shared-energy analysis, the force-deformation of the column ("*(30mm)-Integrated (COLUMN)*") follow closely to the rigid ship analysis ("*Rigid Ship (30mm)*"). The shipside, in contrast to the column, suffered only minor deformation, as can be seen from the fringe contour on Figure 4-1. Several top-cut sections of the deformation on both bodies are provided in Figure 4-14.

The column appears to be ductile. The column then can be carried out under ductile category. For clearer detail on the force-deformation relationship for the shipside impact against 30 mm thick column, see Fig. A-5.

(2) Impact on 40 mm thick column

The column developed resistance higher than the 30 mm thick column. At the early stage of impact (smaller displacement) the shipside impact tried to penetrate the column. Thus, a local displacement is generated on the column. The column resistance was then causing local deformation on the shipside. Simultaneously, the contact area extended further up giving more resistance to the column. On the other side, the extending contact area was directed to the middle part of the shipside, which is weaker than its bottom part. As the results, the force demand becomes higher.

The energy is dissipated by both colliding body, resulting damages on both bodies. The independent plot of force-deformation relationship for this case is provided in appendix A (Fig. A-6). Some details on the deformed colliding structures are provided by Figure 4-16.

(3) Impact on 50 mm thick column

The force-deformation of this collision scenario is significantly higher than the previous two. Comparing between the integrated curve and the rigid-ship curve shows that the early stage of impact the shipside is still sufficiently rigid to create a local deformation on the column. Therefore the integrated curve agrees well with the rigid-ship curve at this stage. Leaving this zone, the column works in reverse; the column behaves sufficiently rigid to generate damages on the ship. This is indicated by the (integrated) force-displacement curve of the shipside follows the rigid-column curve. Nevertheless, at the ending stage the impact force is distributed over larger contact area, the impact energy is then dissipated on both structures. Cut section details for certain column indentation are provided by Figure 4-18. The independent force-displacement curve for this case is shown in Fig. A-7.

The local deformation of the column has a significant influence to the resistance of the column. The resistance-indentation relationship for this case will be discussed further in section 4.2.

4.1.2 Force-Deformation - Scenario 2 (Middle Span)

Figure 4-5 up to Figure 4-7 present the resultant displacement fringe of the shipside and the column at final state due to middle span impact with various column thicknesses under the integrated (shared-energy) analyses.

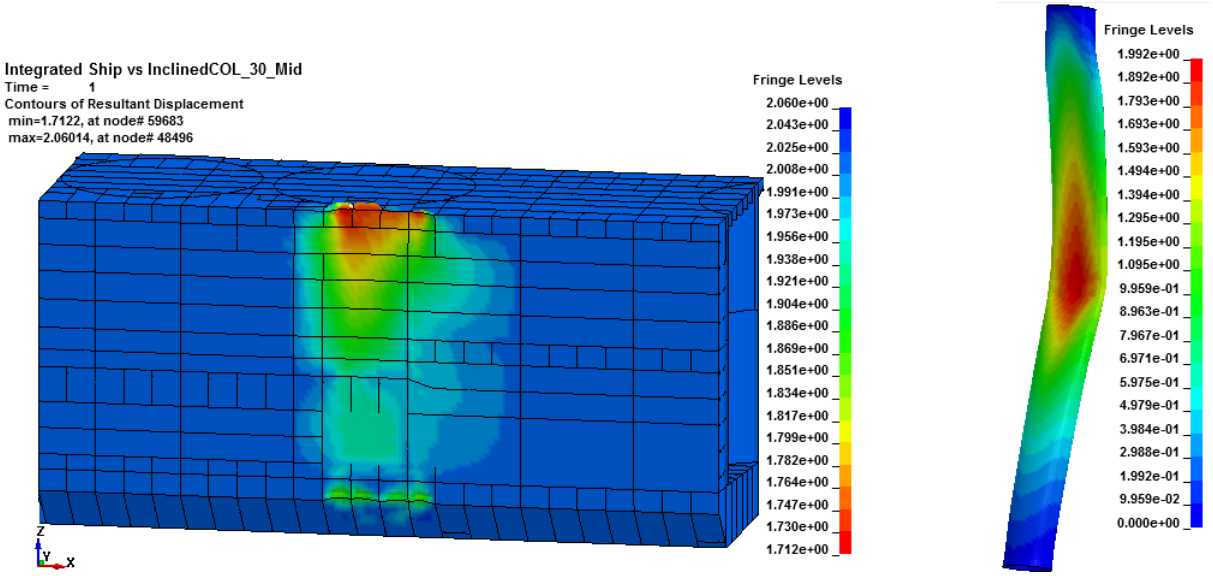

Figure 4-5 Displacement fringe (Integrated) – Middle Span (30 mm thick Column)

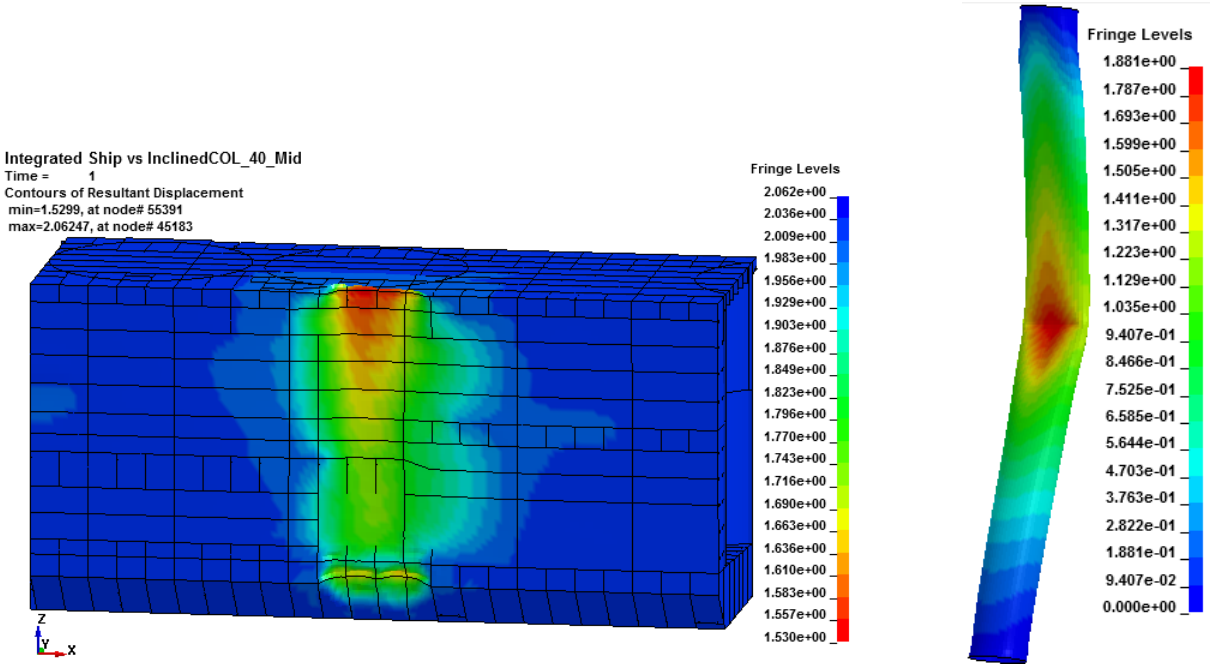

Figure 4-6 Displacement fringe (Integrated) – Middle Span (40 mm thick Column)

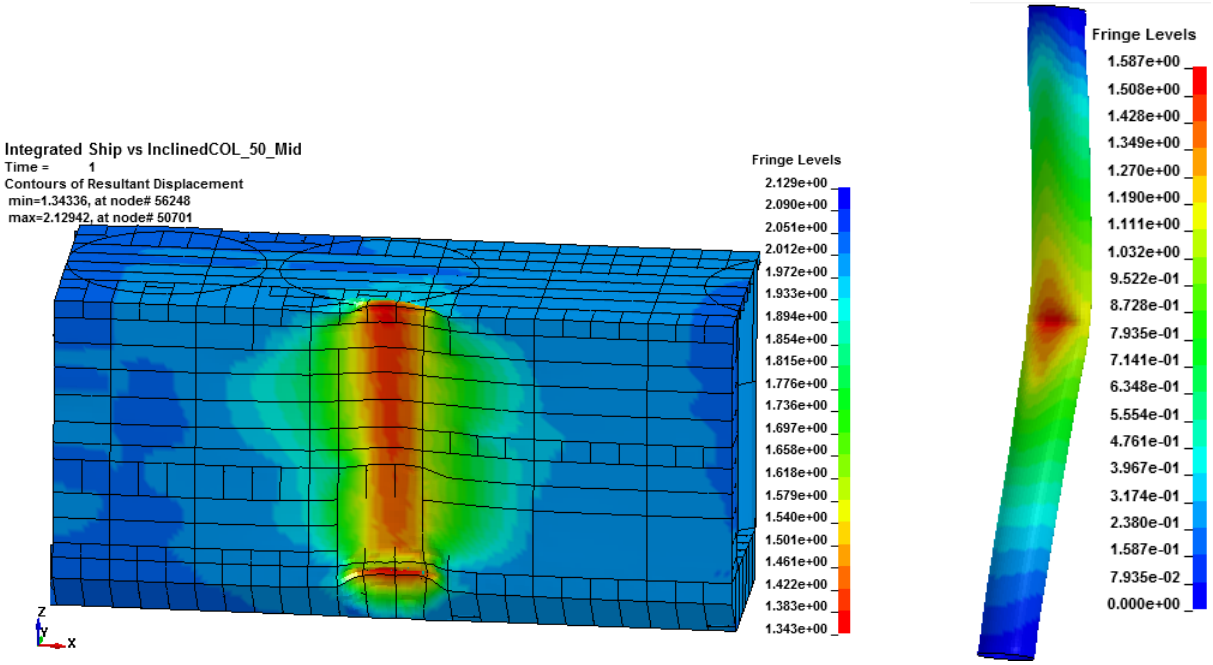

Figure 4-7 Displacement fringe (Integrated) – Middle Span (50 mm thick Column)

In term of the three design categories, the middle span impact scenarios prove the similar behaviour of the column with the quarter span impact. However, for the shipside, some distinctions are spotted.

Compared to the quarter span impact, the shipside had more visible damage under this impact scenario, particularly on the upper deck of the shipside. Under this scenario, the shipside was arranged such that the shipside will have the first strike point at the centre of the column span. Figure 3-7(b) shows that the upper deck of the ship is closer to the clamped-end of the column compared to the arrangement of quarter span impact. The restraints give a certain level of additional resistance to the column-end zone. The column-ends are not free to displace in all degrees-of-freedom, thus the shipside will take the major rule to dissipate the energy when the upper deck finally touches the column, near to the column end. Moreover, the upper part of the shipside is relatively weaker than its bottom part and the influence of the restraints is a distance away from the bottom part. Simultaneously, the impact force is also distributed over a larger contact area. Therefore, the displacement of the ship side at the first-impact zone (bottom part) is relatively constant after a certain deformation on the ship.

While in quarter span impact the energy sharing is easier to be categorized into the three design categories, under the middle span impact scenarios both structures suffer visible damages.

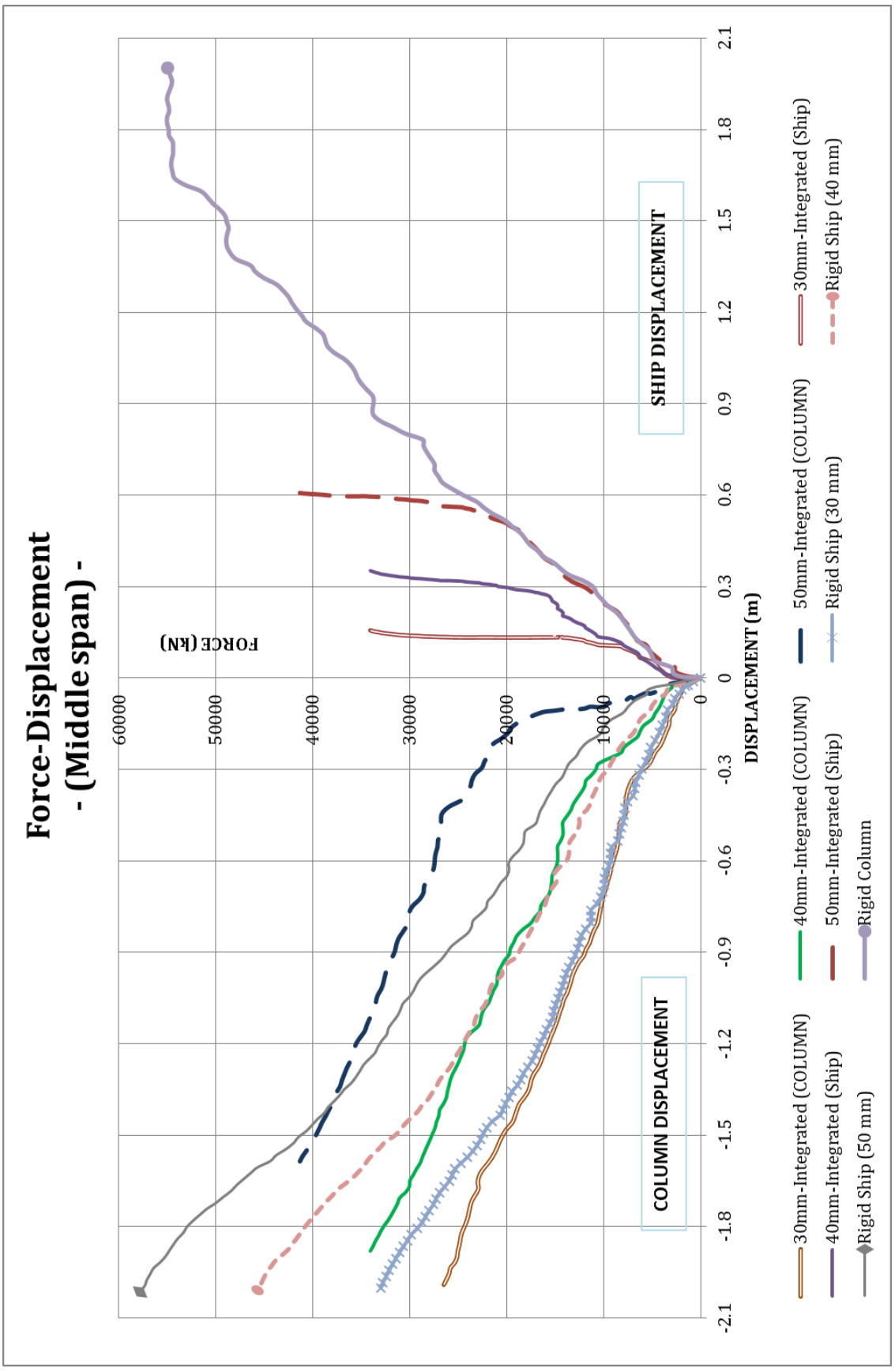

Figure 4-8 Force-Deformation –Middle Span - Inclined Column

4.1.3 Comparison between Scenario-1 and Scenario-2

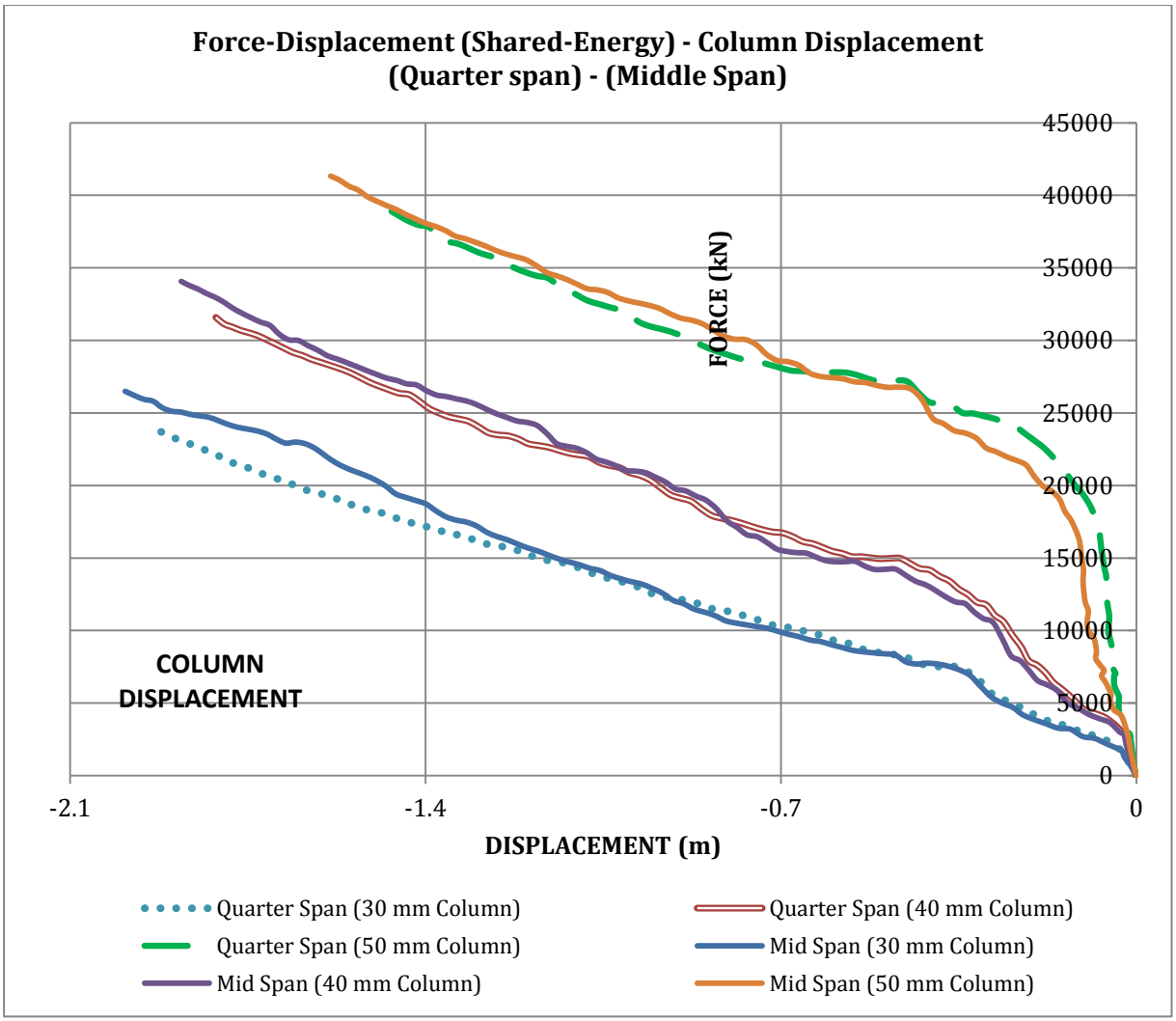

Figure 4-9 Force-Deformation – Quarter vs. Middle Span (Column Displacement)

Figure 4-9 indicates that the first-point-of-impact location have a slender influence on the column force-deformation relationship for all column thicknesses observed. The interface forces of impact on middle span cases are slightly higher, particularly on the larger displacement.

The force-deformation relationship for the shipside shown on Figure 4-10 indicates the similar tendency on the influence of the impact location.

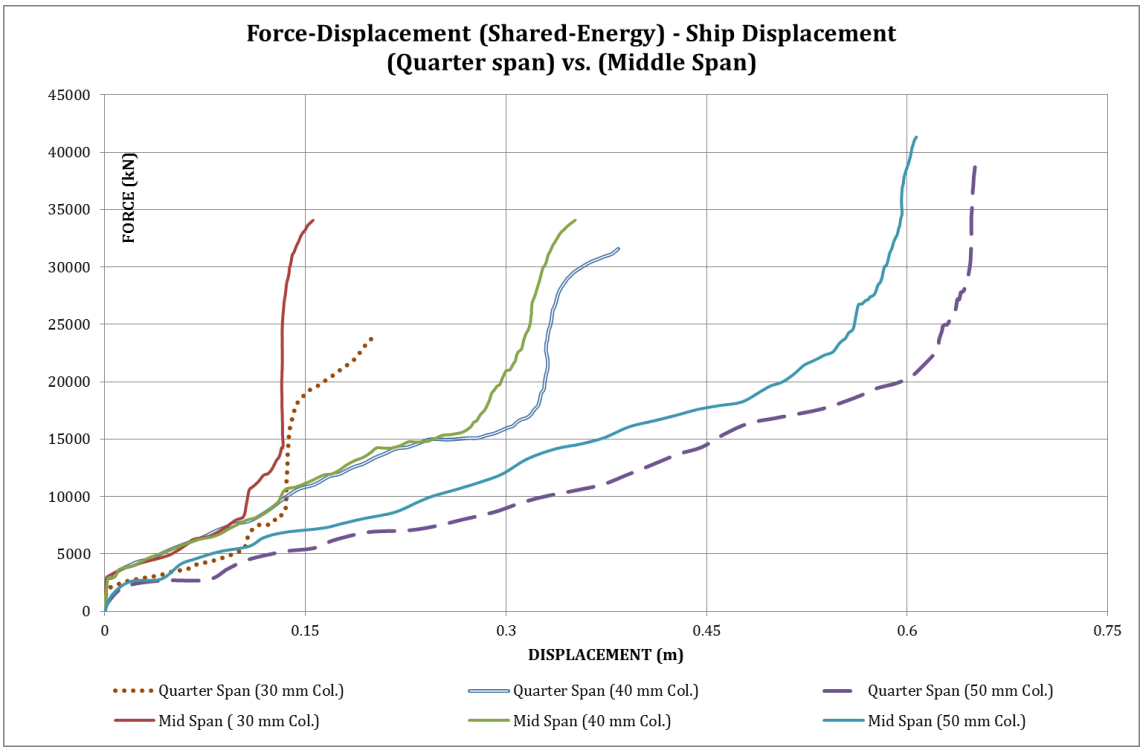

Figure 4-10 Force-Deformation – Quarter vs. Middle Span (Ship Displacement)

The following figures (Figure 4-11 and Figure 4-12) compare the Energy-displacement relationships for both impact locations (middle span versus quarter span). For the displacement on the column, the energy-displacement relationships appear to be relatively similar between the middle span impact and the quarter span impact.

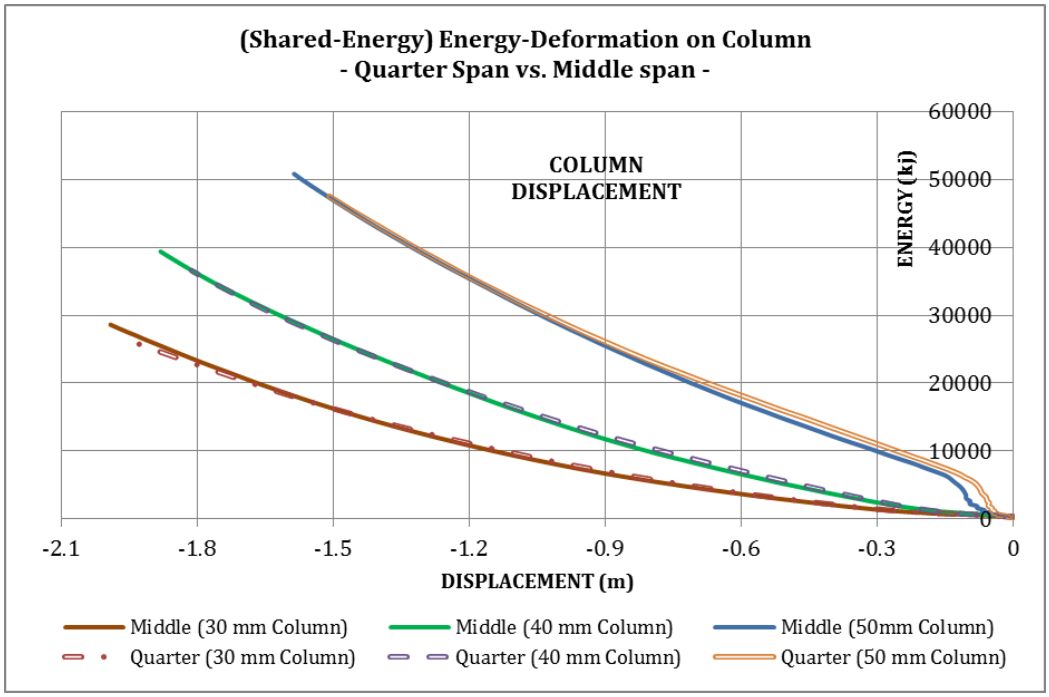

Figure 4-11 Energy-Deformation - Quarter vs. Middle Span (Column Displacement)

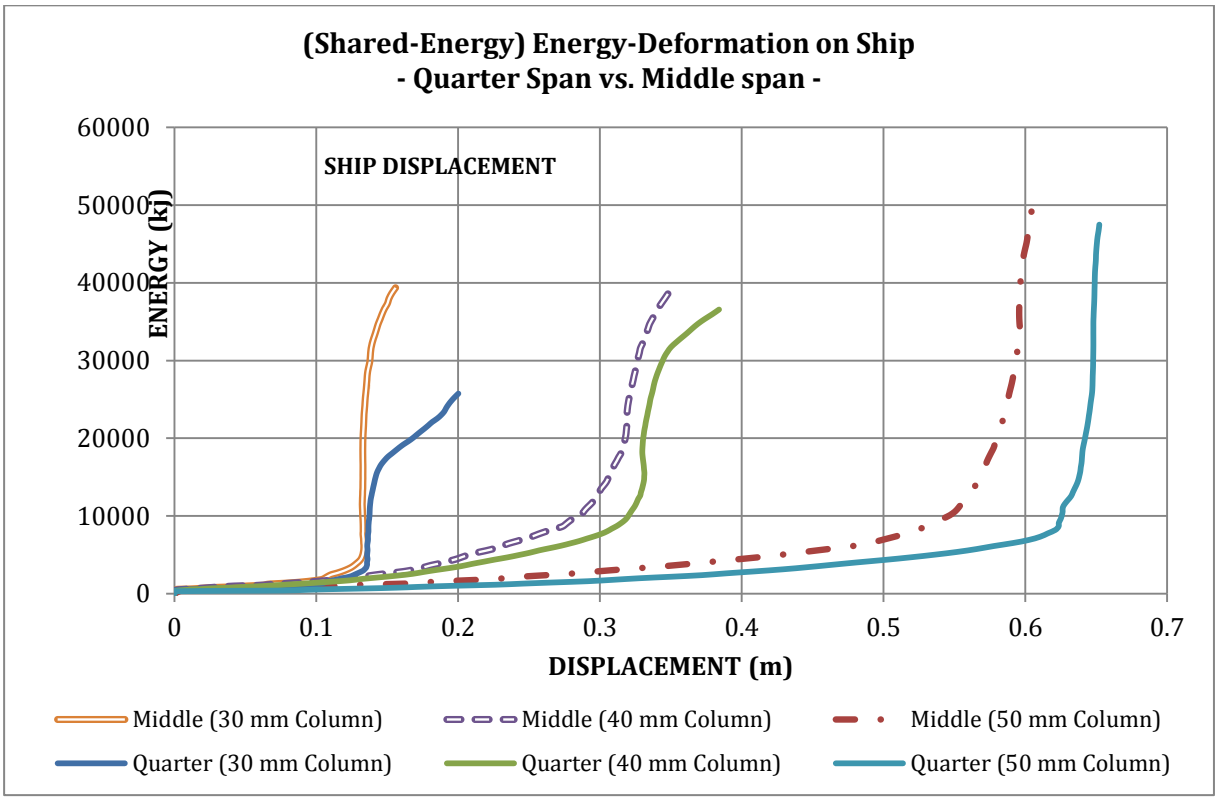

Figure 4-12 Energy-Deformation - Quarter vs. Middle Span (Ship Displacement)

4.2 Resistance-Indentation

The local deformation has a significant contribution to the overall resistance of the column. After reviewing the force-deformation of all the terms in previous section, one might agree that the *shared-energy* assumption is more ideal to represent the real occurrence of the collision, regardless the computational time. Therefore, it will be outlined next the resistance-indentation relationship of the column for various wall thickness based on the *shared-energy* assumption, both for quarter-span impact and middle-span impact.

The simulation results will be compared to the theory to see how the simulation results agree with the current theory, see Section 2.3.

4.2.1 Resistance-Indentation under Scenario 1 (Quarter Span)

Column with wall thickness of 30 mm

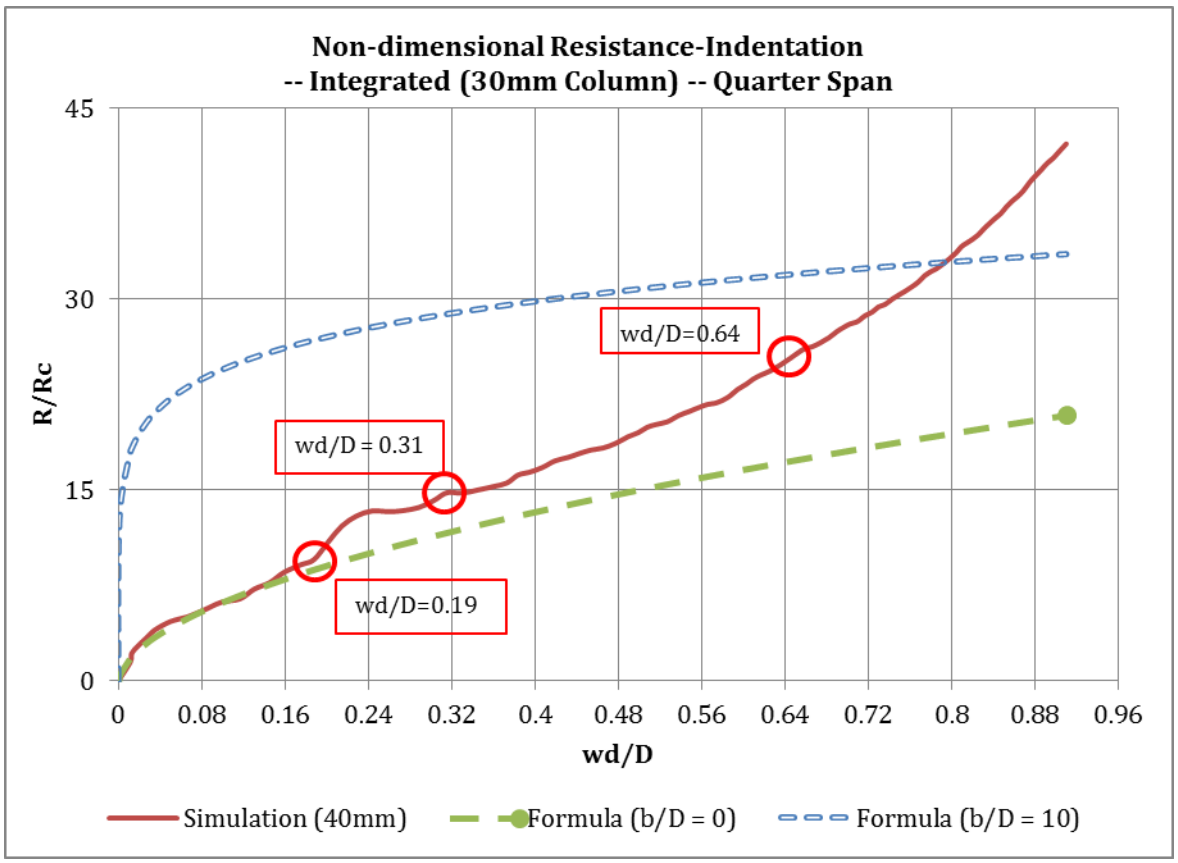

Figure 4-13 Resistance-Indentation – Quarter Span (30 mm thick Column)

At the early states, the shipside strikes the column by its bottom part which appears to be stronger than its upper part. The shipside was then penetrating the column, giving a local deformation on the column. This explains how the curve from simulation results agrees well with the theory curve for (b/D =0) (see Figure 4-13). The strength capacity of column itself gives only a minor local deformation on the shipside, as shown in Figure 4-14 (a).

As the contact area extends larger, the resistance also gets higher. The curve then starts to deviate away from the theory curve. However, the curve appears to have a relatively constant deviation until the indentation becomes deeper. At this state, the deformation on the ship remains virtually unchanged, while the column takes more deformation; see Figure 4-14 (b).

At the larger displacement (Figure 4-14 (c)), the simulation results deviate further up. As the shipside continues to push the column, the contact area develops further, raising more resistance to the column. At this state the column will also bend, utilize its bending capacity. The boundary conditions have been thought to have a contribution to the increase of the column resistance.

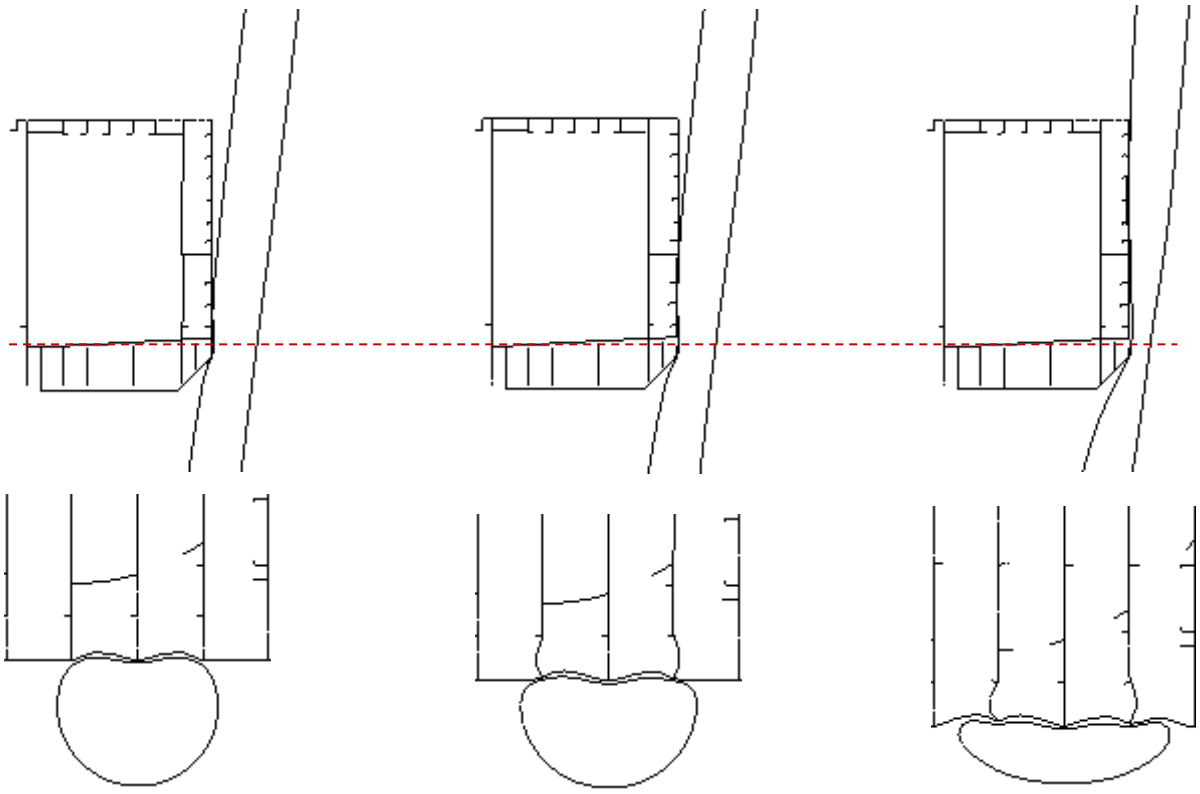

(a) $w_d/D = 0.19$ (b) $w_d/D = 0.31$ (c) $w_d/D = 0.64$

Figure 4-14 Detail of Resistance-Indentation (Quarter Span; 30 mm Column)

Figure 4-14 indicates there is only a small local displacement on the ship throughout the impact duration, while the push of the ship generates more displacement on the column.

Column with wall thickness of 40 mm

The first strike of the ship caused a relatively small local deformation on the column. Then the resistance of the column started to balance the impact force, enforced local deformation on the shipside. The balancing continues so that both colliding structures deformed simultaneously along with the increasing of the contact area. Until the contact area covers the total height of the shipside, and then the resistance increase of the column becomes more rapid.

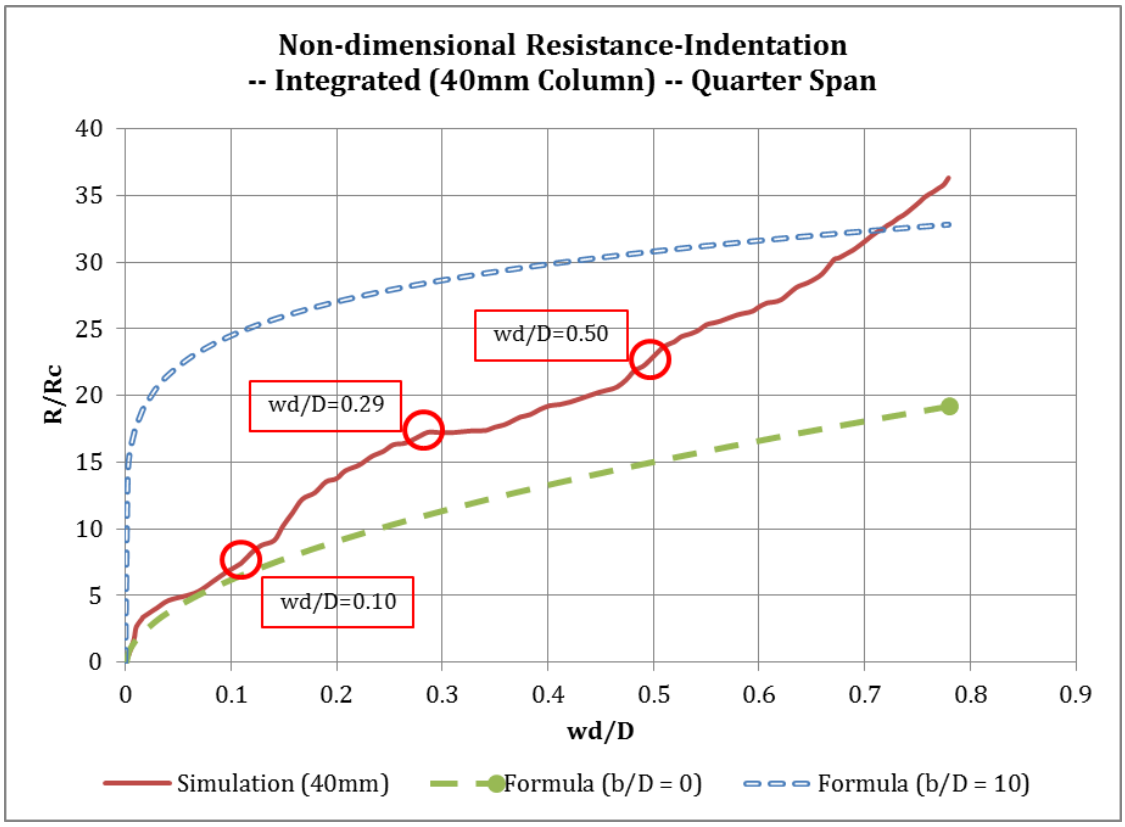

Figure 4-15 Resistance-Indentation – Quarter Span (40 mm thick Column)

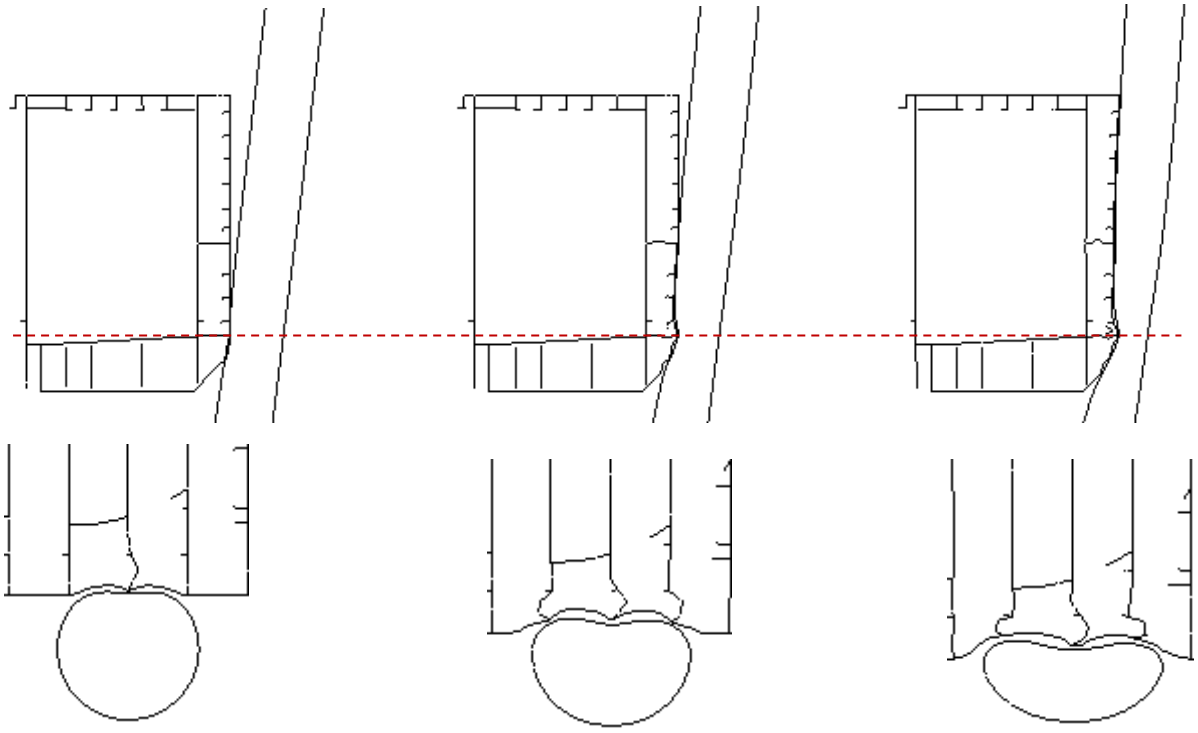

(a) $w_d/D = 0.10$ (b) $w_d/D = 0.29$ (c) $w_d/D = 0.50$

Figure 4-16 Detail of Resistance-Indentation (Quarter Span; 40 mm Column)

Column with wall thickness of 50 mm

The 50 mm thick column, as expected, has more resistance to the indentation than the columns discussed in prior sequence. The shipside caused only minor indentation when the column started developing its resistance. In reverse, the shipside generates local deformation to dissipate the impact energy. See Figure 4-18.

After the rapid deviation (compare to the theory) at small deformation, the resistance-indentation to have a relatively constant deviation until the indentation ratio reaches 0.4 (wd/D=0.4). See Figure 4-17.

The boundary conditions of the column, in addition to the increase of contact area had been thought to give a significant contribution to the increase of the resistance at the end of the impact state. The resistance increase is indicated as the deviation at the tail of the curve, see Figure 4-17.

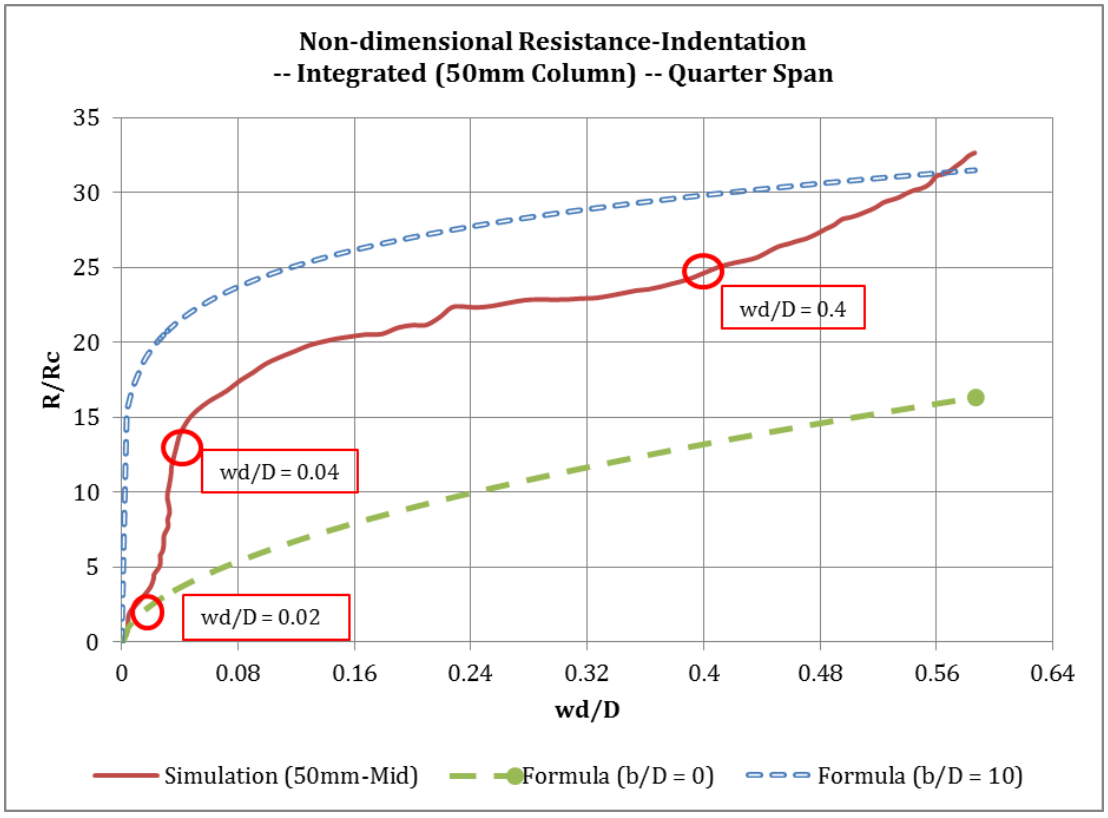

Figure 4-17 Resistance-Indentation – Quarter Span (50 mm thick Column)

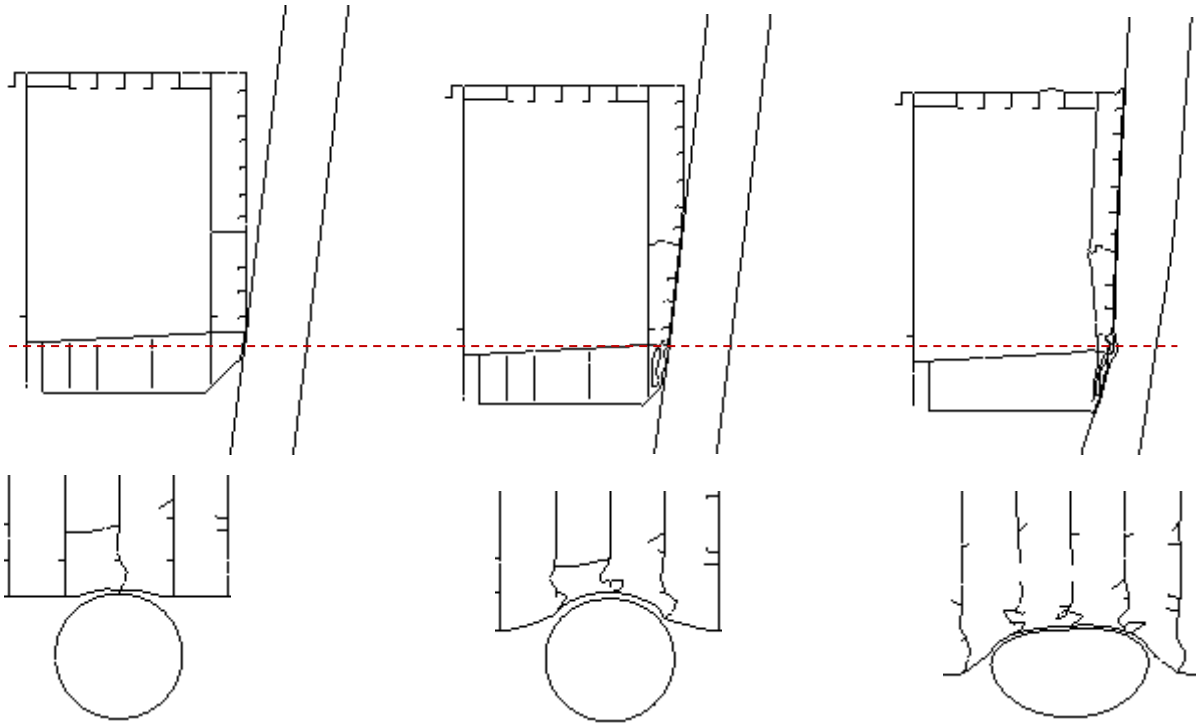

(a) $w_d/D = 0.02$ (b) $w_d/D = 0.04$ (c) $w_d/D = 0.4$

Figure 4-18 Detail of Resistance-Indentation (Quarter Span; 50 mm Column)

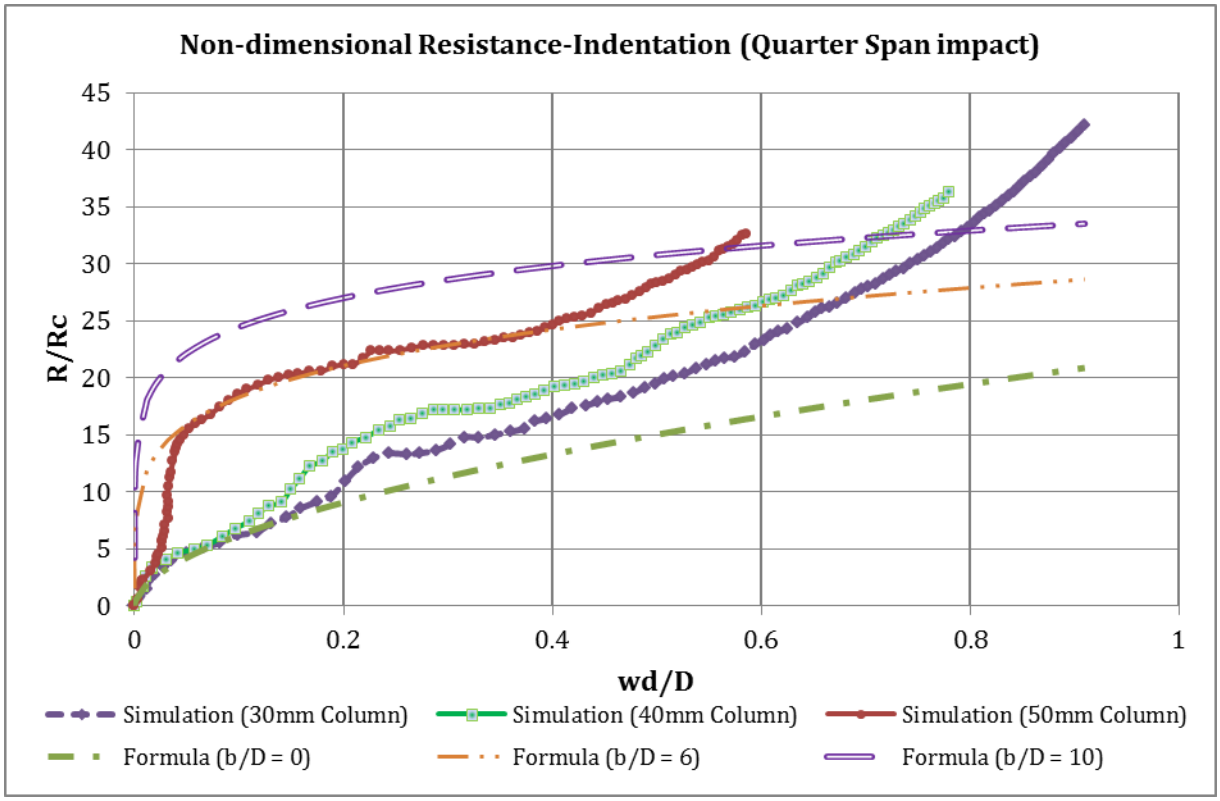

Figure 4-19 Resistance-Indentation – Quarter Span Impact

For all thicknesses analysed under quarter span impact, the resistance-indentation relationships shown in Figure 4-19, for the thicknesses concerned, appear to develop resistance as the indentation width grows from (b/D = 0) to (b/D = 10). The simulation curves are crossing diagonally between these two theory curves.

One could predict that for a thicker column, the resistance increase will be more rapid at the early stage, while the thinner column would develop its resistance slower.

It is also interesting that the resistance-indentation relationship for 50 mm column at a certain w_d/D range agrees well with the theory (b/D=6). This gives indication that the resistance of the column is comparable with the theory under the assumption of (b/D=6).

4.2.2 Scenario 2 (Middle Span)

The resistance-indentation relationships for the impact on middle span, which will be outlined hereafter, prove there is a typical behaviour and tendency compared to the quarter span impact, for the same thickness; 30 mm, 40 mm, and 50 mm. The comparison between two impact scenarios towards column of wall thickness of 30 mm, 40mm, and 50 mm respectively are provided in appendix B .

Column with wall thickness of 30 mm

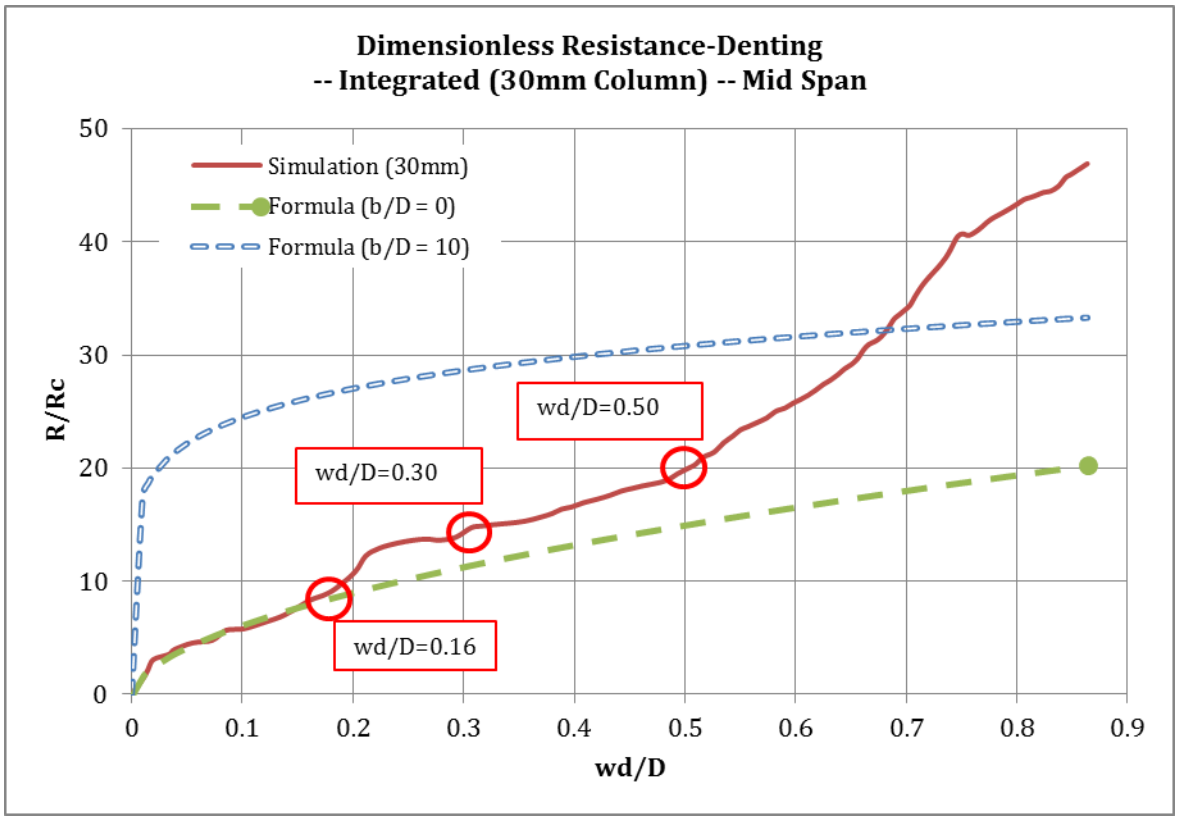

Figure 4-20 Resistance-Indentation – Middle Span (30 mm thick Column)

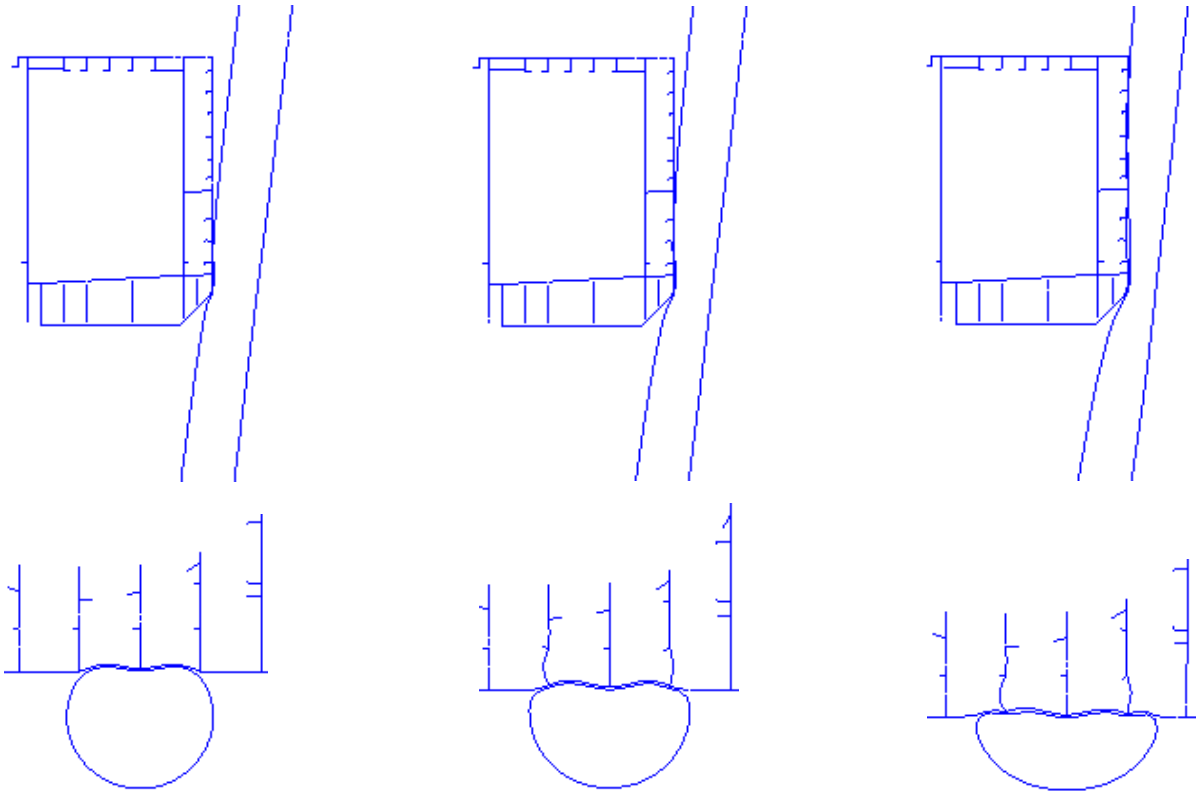

(a) $w_d/D = 0.16$ (b) $w_d/D = 0.30$ (c) $w_d/D = 0.50$

Figure 4-21 Detail of Resistance-Indentation (Middle Span; 30 mm Column)

Column with wall thickness of 40 mm

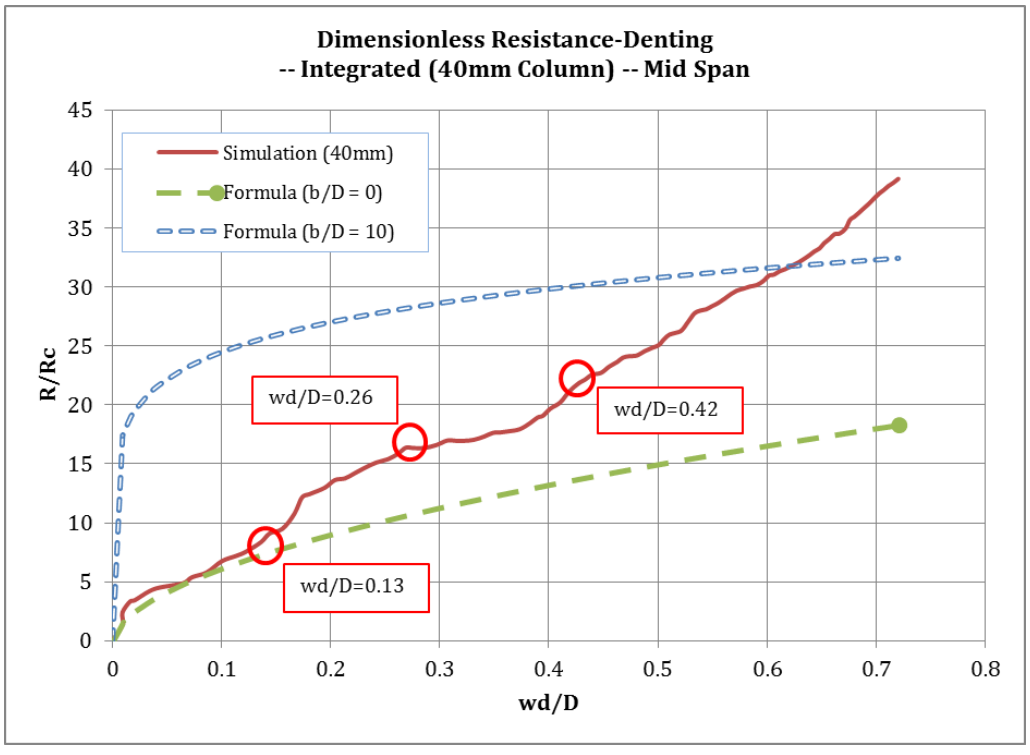

Figure 4-22 Resistance-Indentation – Middle Span (40 mm thick Column)

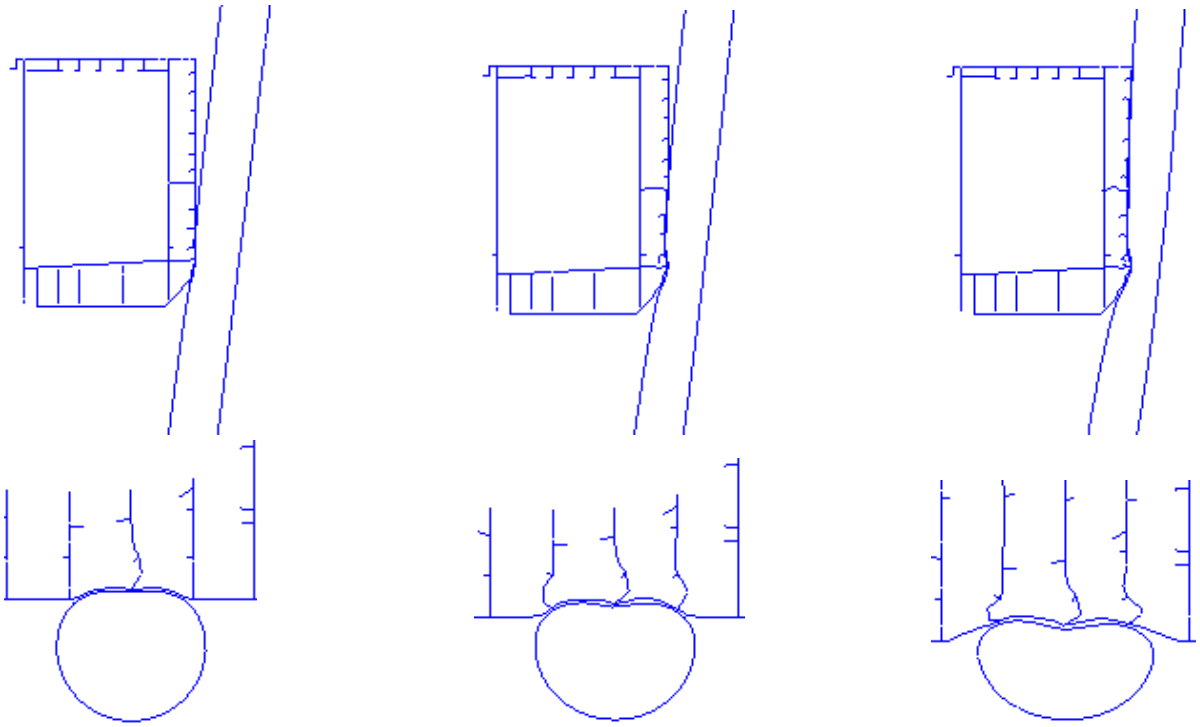

(a) $w_d/D = 0.13$ (b) $w_d/D = 0.26$ (c) $w_d/D = 0.42$

Figure 4-23 Detail of Resistance-Indentation (Middle Span; 40 mm Column)

Column with wall thickness of 50 mm

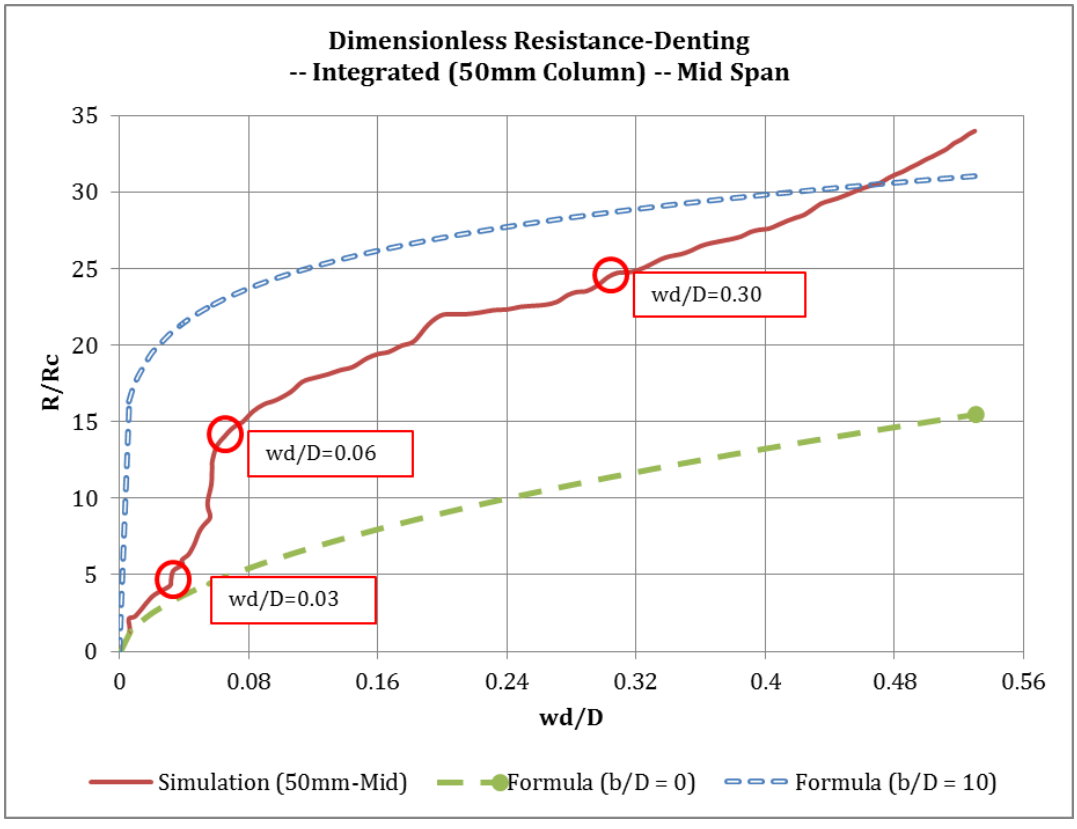

Figure 4-24 Resistance-Indentation – Middle Span (50 mm thick Column)

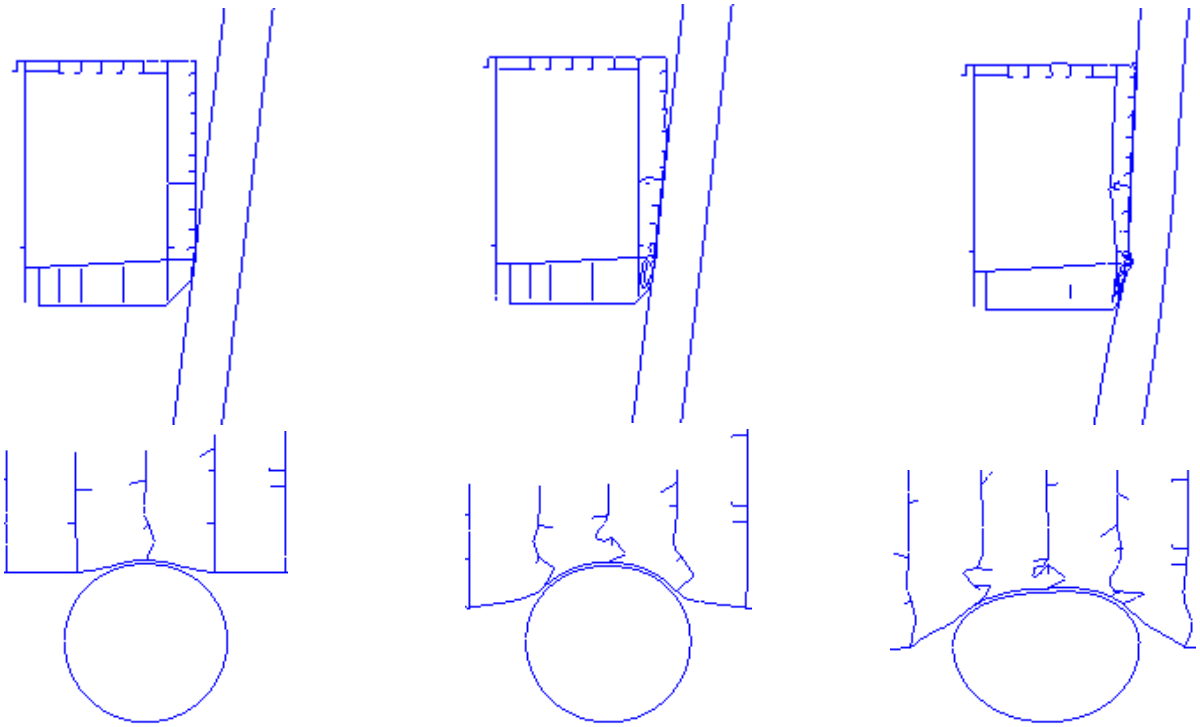

(a) $w_d/D = 0.03$ (b) $w_d/D = 0.06$ (c) $w_d/D = 0.30$

Figure 4-25 Detail of Resistance-Indentation (Middle Span; 50 mm Column)

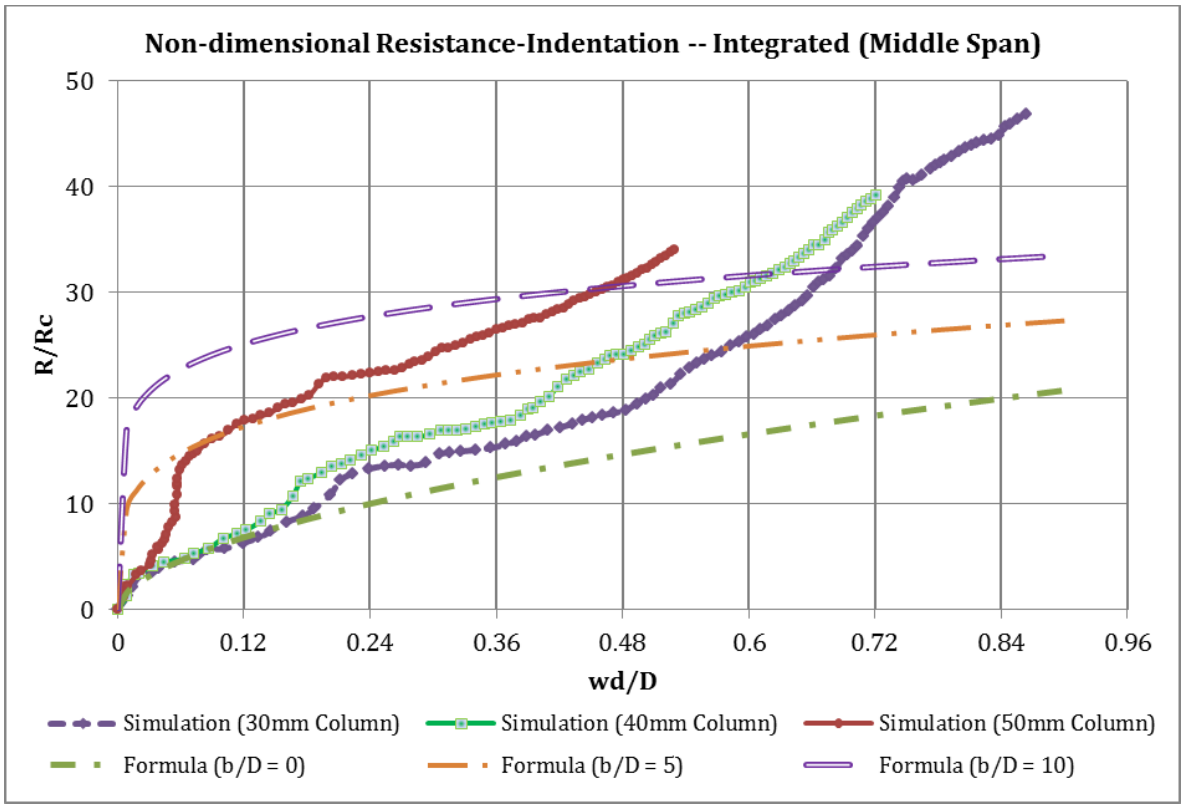

Figure 4-26 Resistance-Indentation – Middle Span Impact

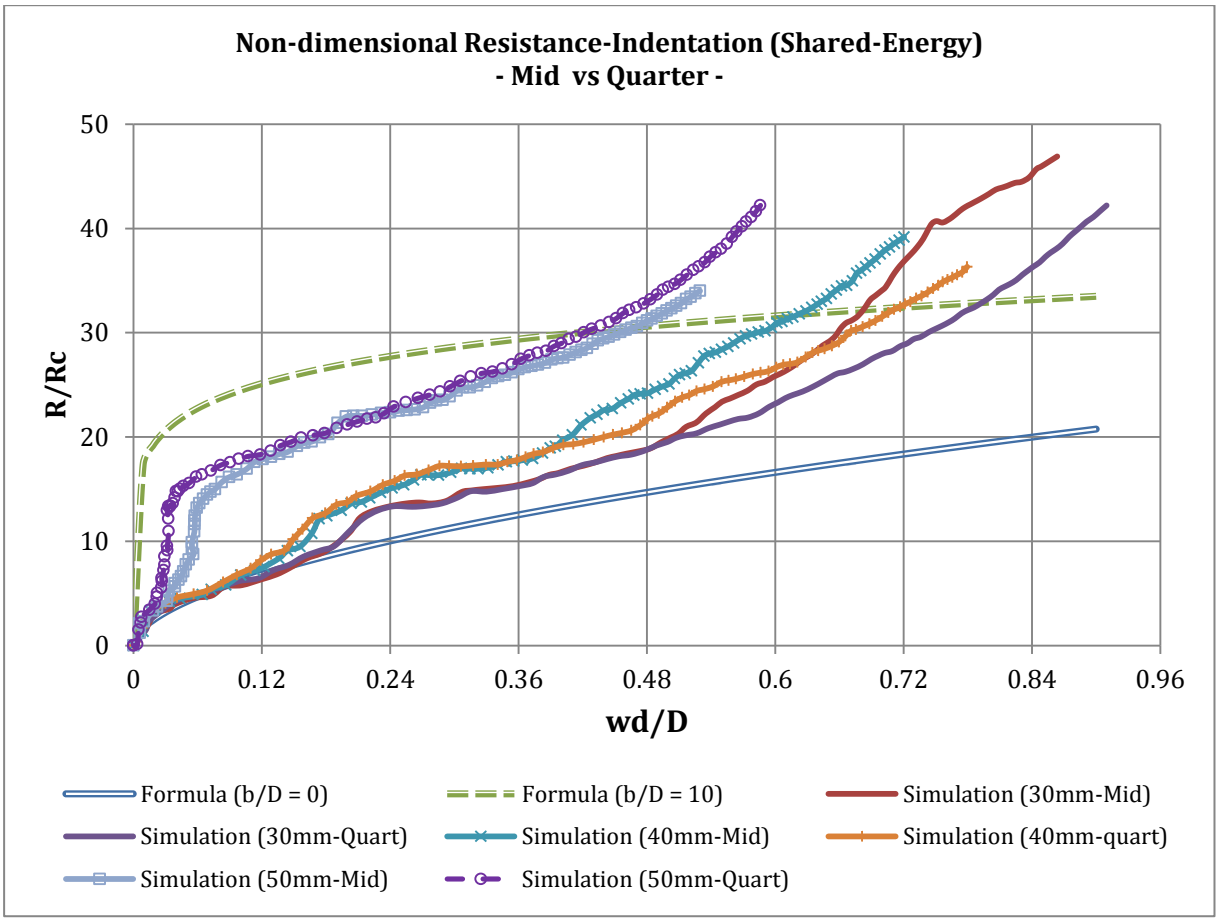

Figure 4-27 Resistance-Indentation – Middle span versus Quarter span impact

Compared to the quarter span impact scenarios, the rapid increase of resistance at the larger displacement for middle span impact occurred at a smaller w_d/D magnitude. Moreover, the increase is significantly higher at the middle span impact scenario, particularly for the 30 mm column.

From all the simulations performed, we can pull out the main conclusion that under integrated (shared-energy) simulations, the resistance-indentation relationship of various tubular leg thicknesses can be grouped into three (3) ranges of $^{w_d}/_{D}$ ratio depending on how close does the agreement of each curve to the simplified-formula curve (with various $^{b}/_{D}$ ratios).

a. Under small $^{w_d}/_{D}$ (small indentation) at the very early phase of the contact/impact), the curve will agree quite well with the simplified-formula. Figure 4-19 and Figure 4-26 show that as the leg thickness increases, the simulation results deviate away from the simplified-calculation at the smaller $^{w_d}/_{D}$ magnitude.

Under this phase, it can be concluded that the impact energy is mainly dissipated to the column causing the deformation to be occurred on the column. Here the contact area of the collision is relatively small, such that the impact force can be considered as concentrated force penetrating the column.
We will further refer this range as Phase #1.

b. The simulation results deviate further up away from the simplified-calculation results. We will further refer this term as Phase #2. Under this phase, the contact area of the collision grows larger and thus generates more resistance on the column interface. The resistance increase is due to the switch of the impact force character. The concentrated force becomes distributed or area force with the growth of the contact area.
Within this range, the ship probably will also start to deform depending on the thickness of the jacket leg. A thicker leg will cause a larger penetration/damage to the ship compared to the thinner leg. The resistance characteristic of the column determines the damage on the ship.

c. Phase #3. Within this phase, the contact area grows even larger, generating deeper indentation both on the leg and on the ship. If the ship is considerably rigid, the penetration on the leg will be deeper than on the ship. The leg will develop the membrane action as the indentation goes deeper due to the fixed (fully constrained) boundary condition assigned on the leg-ends. The membrane action and the larger contact area generate a higher resistance on the jacket leg. This condition stimulates the simulation curves deviate much further up, away from the simplified-formula curves.

The conditions that thought might drive this phenomenon are briefly explained below.

a. The boundary condition and the developed membrane actions (forces)
In the FE simulation, the column is assumed as constrained in all 6 degrees-of-freedom (3 rotational, 3 translational). Since the deformation increased by time the membrane actions (or forces) start to develop. The membrane actions generated the axial forces at the column-ends through the shear stress on the elements of the column wall.
The column is a flexural member which transfers the loads by developing moment and shear stresses under low deformations, and also by in-plane stresses under large deformations. These in-plane or membrane stresses generate compressive membrane forces at the column ends. As the result, the resistance of the column increases as the compressive axial forces cannot be released due to the restraints. The compressive forces will decease after much larger deformation occurs.

For the fully-restrained steel column subjected to large displacements, membrane force will develop utilizing its full tensile capacity. The column supports the load by tensile membrane action occurring in the area of contact and the compressive membrane action around the support (column-ends). The *tensile membrane action* which develops at large displacements is dependent on geometry with increasing vertical displacements resulting in an *increase in load-carrying capacity*.
It is logical to thick that the membrane action due to the fully-restrained condition might contribute to the increase of resistance. However, in chapter 5, the effect of the boundary conditions will be reviewed.

b. The global deformation
The column modelled here is merely a section length of the whole jacket leg. The local deformation will expectedly encourage global deformation to occur. The global deformation will influence the local deformation and vice versa. However this global deformation is not accounted in this case. This assumption can be utilized provided that the braces of the jacket support the leg section adequately such that the loads transferred to the ends of leg-section are carried by the connected braces and other members.

c. The simplified formula is based on the laboratory experiment in which the striking object is considered as a rigid body.
For the 30 mm column, referring to the force deformation curves, the column (leg-section) deformation and the ship penetration depth proved that the column is more ductile than the striking ship. Therefore the ship can be assumed as a rigid body, thus the Resistance-indentation curve resulting from the simulation agrees rather well at the small indentation. However, this does not apply for a thicker column.

4.3 Resistance-Bending

According to mechanism method, the plastic moment capacity of a beam subjected to a concentrated load at its quarter and middle span is as follows.

For impact on the quarter span of the column:

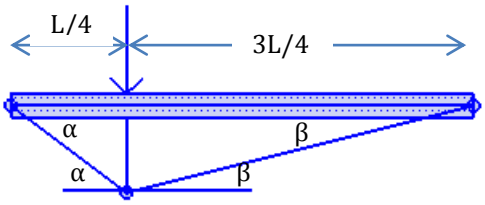

$$M_p \cdot \alpha + M_p(\alpha + \beta) + M_p \cdot \beta = P \cdot \left(\frac{L}{4} \cdot \alpha\right) = P \cdot \left(\frac{3L}{4} \cdot \beta\right) \quad (4\text{-}1)$$

Solving equation $M_p \cdot \alpha + M_p(\alpha + \beta) + M_p \cdot \beta = P \cdot \left(\frac{L}{4} \cdot \alpha\right) = P \cdot \left(\frac{3L}{4} \cdot \beta\right)$ (4-1) will give the plastic moment capacity:

$$\boldsymbol{M_{p,quart} = \frac{3PL}{32}} \quad \textbf{or} \quad \boldsymbol{P_{plastic} = \frac{32M_p}{3L}} \quad \textbf{(4-2)}$$

For impact on the middle span of the column:

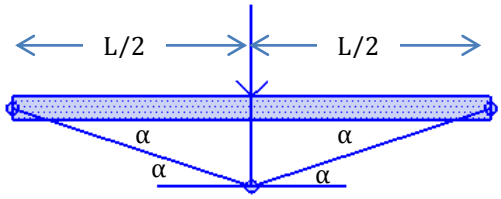

$$M_p \cdot \alpha + M_p(\alpha + \alpha) + M_p \cdot \alpha = P \cdot \left(\frac{L}{2} \cdot \alpha\right) \quad (4\text{-}3)$$

Solving equation $M_p \cdot \alpha + M_p(\alpha + \alpha) + M_p \cdot \alpha = P \cdot \left(\frac{L}{2} \cdot \alpha\right)$ (4-3) will give the plastic moment capacity:

$$M_{p,mid} = \frac{PL}{8} \quad \textbf{or} \quad P_{plastic} = \frac{8M_p}{L} \quad \textbf{(4-4)}$$

Where: $M_p = f_y \times Z_p$

For tubular members, NORSOK (N-004, 2004) recommends:

$$Z_p = \frac{1}{6} \times [D^3 - (D - 2t)^3]$$

The calculation of the plastic moment capacity is tabulated below.

Table 4-1 Plastic Moment Capacity

	fy =	355	MPa		
	D =	1.5 m	(1500 mm)		
	L =	17.0 m	(17000 mm)		
No	thickness (m)	Wp (m^3)	Mp (MN.m)	$P_{plastic}$ (MN) - mid span-	$P_{plastic}$ (MN) - quarter span-
1	0.030	0.065	23.02	10.83	14.44
2	0.040	0.085	30.28	14.25	19.00
3	0.050	0.105	37.33	17.57	23.43

The normalized of the column resistance (R) to the plastic load capacity $P_{plastic}$ is plotted with respect to the corresponding normalized lateral deformation, as provided in Figure 4-28 and Figure 4-29 for quarter span impact and the middle span impact respectively.

For the clamped-ends column subjected to central, concentrated load, the R_u/R_o ratio shown in the diagrams is given by (Skallerud & Amdahl, 2002):

$$\frac{R_u}{R_o} = \sqrt{1-\left(\frac{w}{D}\right)^2} + \frac{w}{D}\arcsin\left(\frac{w}{D}\right) \qquad \text{for} \quad \frac{w}{D} < 1 \tag{4-5}$$

$$\frac{R_u}{R_o} = \frac{\pi}{2} \times \left(\frac{w}{D}\right) \qquad \text{for} \quad \frac{w}{D} > 1 \tag{4-6}$$

Where w is the lateral deformation and D is tube diameter.

Compare to the R_u/R_o ratio (formula) given by equation (4-5) and (4-6), Figure 4-28 and Figure 4-29 show a significant increase of load carrying capacity regardless the local deformation (indentation) on the column. This differs from the load-deformation characteristic given by Amdahl (Amdahl, Consequences of Ship Collisions, 1991). In (Amdahl, Consequences of Ship Collisions, 1991), the estimate of "true" load-deformation is lower than the curve given by the above formula.

The present work deals with shipside impact against the inclined column. At the first time of contact, the assumption of concentrated impact load might be valid since the contact area is rather narrow. However, the contact area rises gradually, leaving this assumption doubtable. A closer estimate of the load carrying capacity when the contact area becomes broader will be the assumption of distributed or area load. By mechanism method, the plastic load capacity for uniformly distributed load over the full span is given by:

$$q_{p,uniform} = 16 \times \frac{M_p}{L^2} \quad \text{or} \quad P_{p,uniform} = q_{p,uniform} \times L = 16 \times \frac{M_p}{L} \tag{4-7}$$

The plots of the normalized resistance over $P_{p,uniform}$ are given in appendix D .

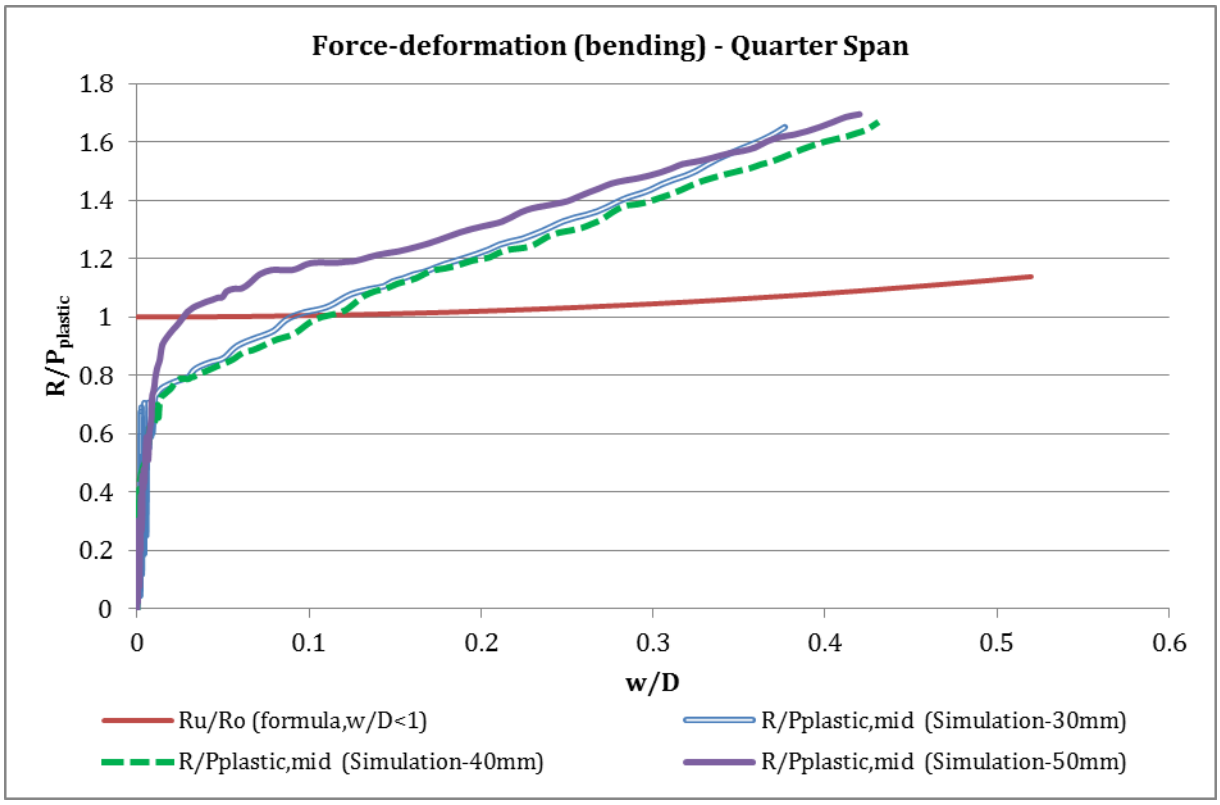

Figure 4-28 Force-deformation (bending) – Quarter span impact

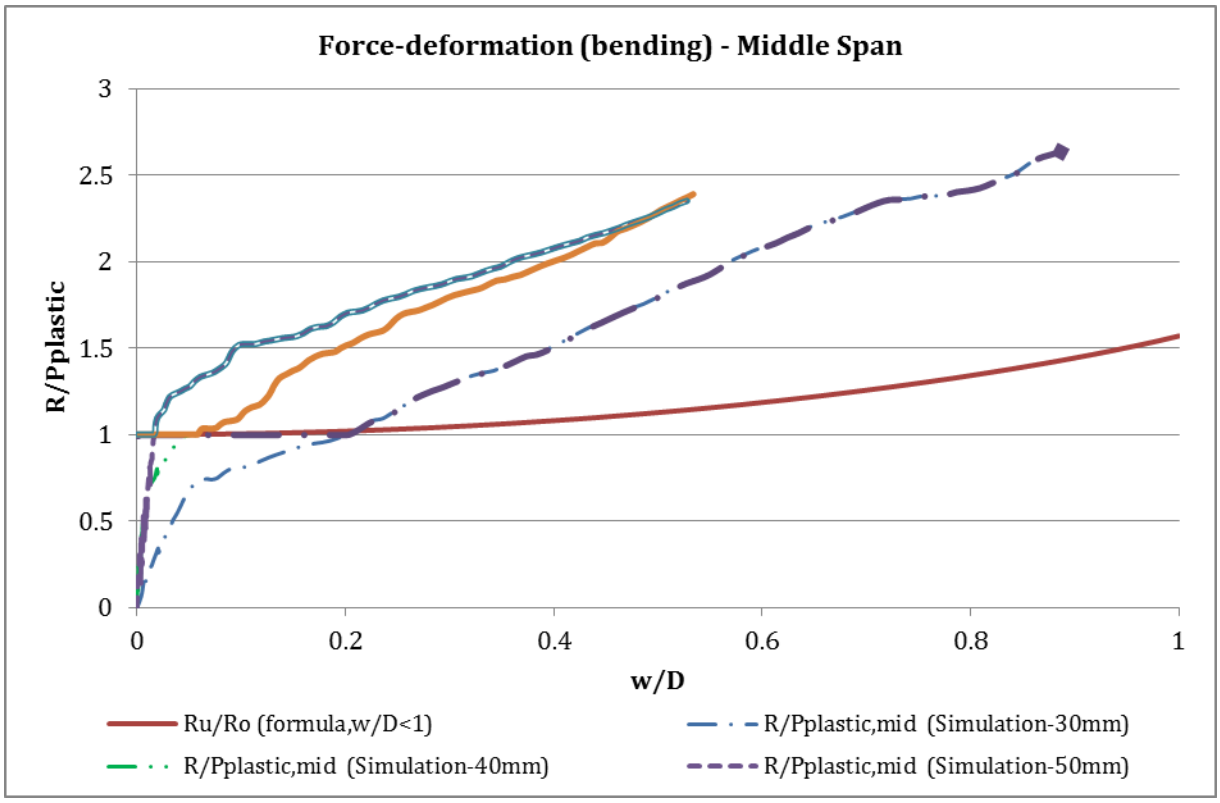

Figure 4-29 Force-deformation (bending) – Middle span impact

4.4 Interface Pressure-Area curves

The pressure-area relationship is important in the design to predict the load level the structure must resist. For instance, if the strength design is aimed for, then the interface forces must be calculated using the rigid column case.

Tavakoli (Tavakoli, Amdahl, Alsos, & Klæbo, 2007) developed pressure-area relationship for stern-corner and stern-end collisions against rigid body as:

$$P = 6.8 \times A^{-0.5} \quad (4\text{-}8)$$

Whereas Lin Hong (Hong & Amdahl, 2007) pressure-area relationship for bulb impact against rigid wall is expressed as:

$$\mathrm{P} = 7.0 \times \mathrm{A}^{-0,7} \quad \textbf{(4-9)}$$

Where A is area and [MPa] is the pressure unit

The author had been through the observation processes as described herein.

- Determining several aspect ratios of the area in which the pressure will be captured. The aspect ratio of 1-2 means that in the area matrix consisting of rows and columns, for two elements in row there will be four elements in column, and so forth. This can be visualized as if a certain area is 'framed' according to the aspect ratio.
- Capturing the pressure of the elements under the 'framed' area. The pressures of each element are evaluated one at a time. Then, calculate the average pressure for each area concerned. The maximum value of the average pressure within the timeframe (t = 0 to t = 1 s) will be plotted as the pressure of the corresponding area. To determine and locate the area with the highest possible average pressure for all time steps is a tedious process since it depends on the manual judgement and adjustment.
- The fit-to-data equation resulted from one aspect ratio will then be merged with the equation from other aspect ratio under one impact case and dissolved into one single equation for each impact case by taking the average values of the pressure calculated based on each fit-to-data equation.

The observation done here was under the assumption that the area of a single element is constant, equal to initial area before deformation. The approximate initial area is $100\ mm \times 100\ mm = 0.1\ m \times 0.1\ m = 0.01\ m^2$.

The interface pressure-area relationships shown in Figure 4-30 and Figure 4-31are developed from the impact scenarios of the shipside against 30 mm thick column, both for inclined and vertical column. For the inclined column the impact is at the quarter span of the column, whilst for the vertical is the middle span impact.

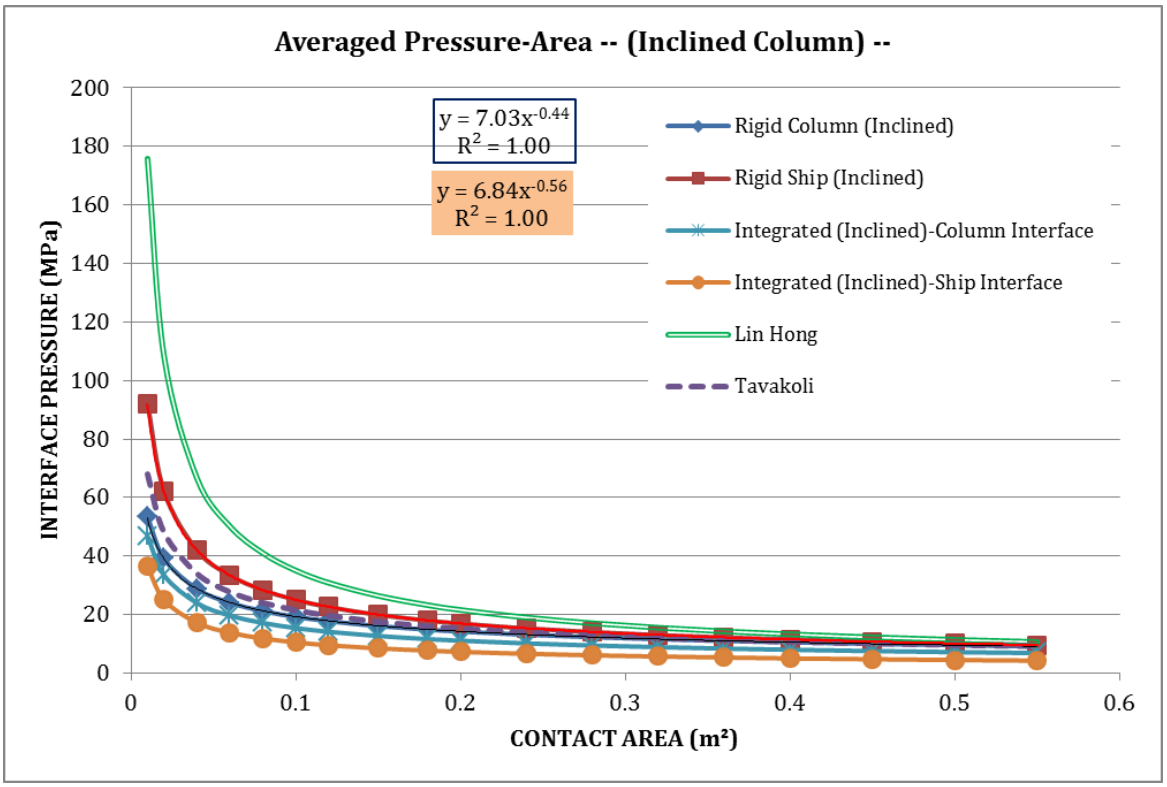

Figure 4-30 Interface Pressure-Area for Inclined Column (Quarter span impact)

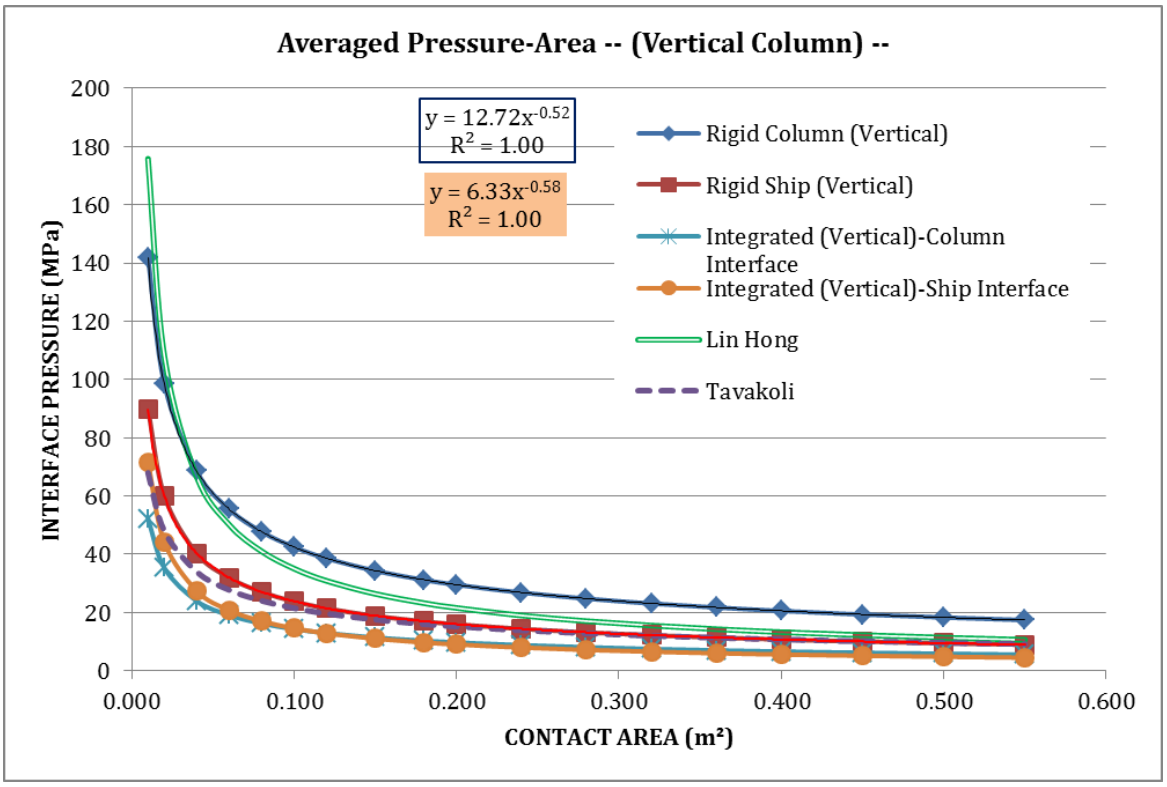

Figure 4-31 Interface Pressure-Area for Vertical Column (middle span impact)

The comparisons of the interface pressure-area relationship between inclined and vertical column for each case (rigid column; rigid ship; integrated) are presented in appendix C .

The summary of all the resulted fit-to-data equations is presented in the following table.

Table 4-2 Formula Summary of Interface Pressure-Area

Case			Inclined Column	Vertical Column
1	Rigid Column	(ship interface)	$P = 7.03\ A^{-0.44}$	$P = 12.72\ A^{-0.52}$
2	Rigid Ship	(column interface)	$P = 6.84\ A^{-0.56}$	$P = 6.33\ A^{-0.58}$
3	Integrated	(ship interface)	$P = 3.07\ A^{-0.54}$	$P = 2.98\ A^{-0.69}$
		(column interface)	$P = 5.13\ A^{-0.48}$	$P = 3.96\ A^{-0.56}$

There are several points can be observed from the results above

a. The results are subjected to the observer's judgement on how to capture the area and the related pressure. Since the column consists of many deformable elements, the area of each element alters with time. Thus, the assumption of fixed area does not represent the real condition. However, the assumption is taken to simplify the time-consuming process.

b. Since the interface shape between two colliding bodies determines the difference between the pressures captured on each body. The shipside model has a relatively flat interface while the column has a round/curved interface when the two bodies collide.

5 Effect of Boundary Conditions

For conservative reason, the leg ends will generally assumed as clamped, though this can lead to overestimating the strength of the jacket leg. In the real jacket structure, the leg is supported by the bracing system. The braces function to redistribute the loads from one to another member in the jacket structural system. The jacket leg-brace system will give a certain degree of flexibility for both leg and brace at the connection points in all degrees-of-freedom; axial, lateral, and rotational. Nevertheless, the concern is on the influence of axial flexibility, mainly because under the large deformation the response is governed by the tension (axial) forces. Even relatively small axial displacements have a significant influence on the development of tension forces under large lateral deformations (Skallerud & Amdahl, 2002).

A jacket leg typically has a certain degree of inclination or tilt and eccentricity at each segment length due to fabrication, the loading from the upper part, etc. These factors will also influence the flexibility at the adjacent points. However, as the concern is and because the degree of inclination of the jacket leg used in present work is relatively small, the influence is simply waived.

5.1 Axial Spring Stiffness

The jacket leg model is then modified by modelling the axial restraint as linear springs with stiffness k. The spring stiffness k was calculated based on the static analysis results of a jacket subjected to boat-impact load (BIMPACT) modelled in USFOS (USFOS A/S). A capture of the reference jacket is shown in Figure 5-1. By the discussion with Prof. Amdahl (Amdahl, Discussion, 2011), the spring stiffness has been calculated as outlined herein. The element force to node displacement curves for node 508 and 608 are shown in Figure 5-2 (a) and (b), respectively. These curves consist of nonlinear relationship as there occurred loading-unloading phases during the impact process. Only the linear part of the curves is used to calculate the spring stiffness for each node, as indicated in the figures. From the gradient of linear regression lines, the stiffness of nodes 508 and 608 are:

- Lower node (node 508): $k_{dn} = 1307.7\ MN/m$
- Upper node (node 608): $k_{up} = 49.5\ MN/m$

The unequal stiffness may be represented by two equal springs. The stiffness for each spring is calculated below.

$$2 \times \frac{1}{K_{equiv}} = \frac{1}{k_{dn}} + \frac{1}{k_{up}} \quad \textbf{(5-1)}$$

$$K_{equiv} = \frac{2}{\left(\frac{1}{k_{dn}} + \frac{1}{k_{up}}\right)} = 95.5\ {}^{MN}/_{m}$$

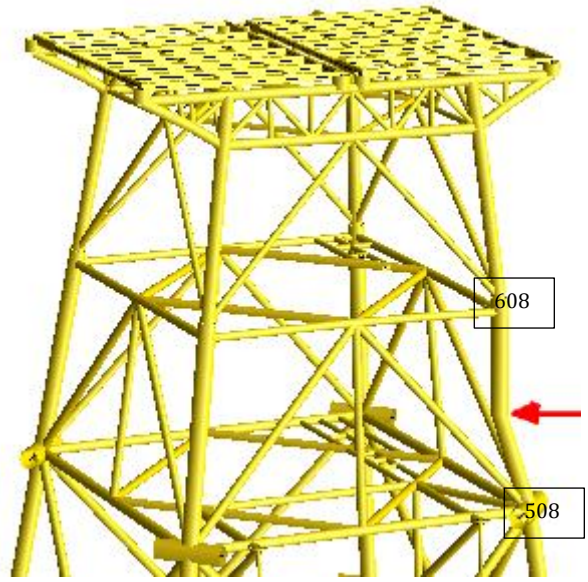

Figure 5-1 Reference Jacket subjected to ship impact

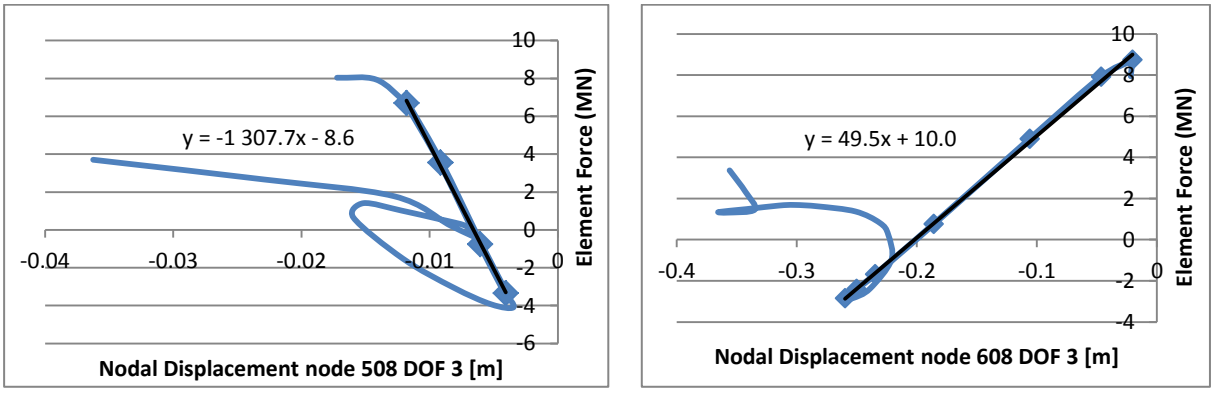

(a) Node 508 (b) Node 608

Figure 5-2 Element Force-Nodal Displacement plots from USFOS

The effect of elastic straining of the tube may be taken into account by defining an equivalent elastic, axial stiffness (Skallerud & Amdahl, 2002):

$$\frac{1}{K} = \frac{1}{K_{node}} + \frac{1}{2EA/L} \tag{5-2}$$

Where K_{node} = axial stiffness of the node with the considered member removed.

The dimensionless spring stiffness can be computed by:

$$c = \frac{2 \cdot K \cdot D}{\pi \cdot L \cdot t \cdot f_y} \tag{5-3}$$

5.2 Model for Simulation

There are 2 groups of model which have been assessed, as described hereafter.

(1) Multiple springs

This model is illustrated in Figure 5-3(a). This model consists of forty seven (47) axial springs on each end, compatible with the number of shell element in circumference. Thus, each single spring will have the stiffness of $\frac{1}{47}$ of the total spring stiffness at each node.

For this model, two simulations have been conducted, according to the spring stiffness assigned at each end:

a. Unequal spring stiffness

The spring stiffness at each node had been assigned according to the real spring stiffness calculated from the USFOS results. Therefore each single spring on lower and upper end has the spring stiffness of 27.8 MN/m and 1.05 MN/m respectively. This setting will next be regarded as ***Spring-2.***

b. Equal spring stiffness

Each single spring attached will have the same spring stiffness. The total spring stiffness will be equal to the equivalent spring calculated in prior. Therefore, each spring will have the stiffness of 2.03 MN/m.

This setting is regarded as ***Equal-Spring***.

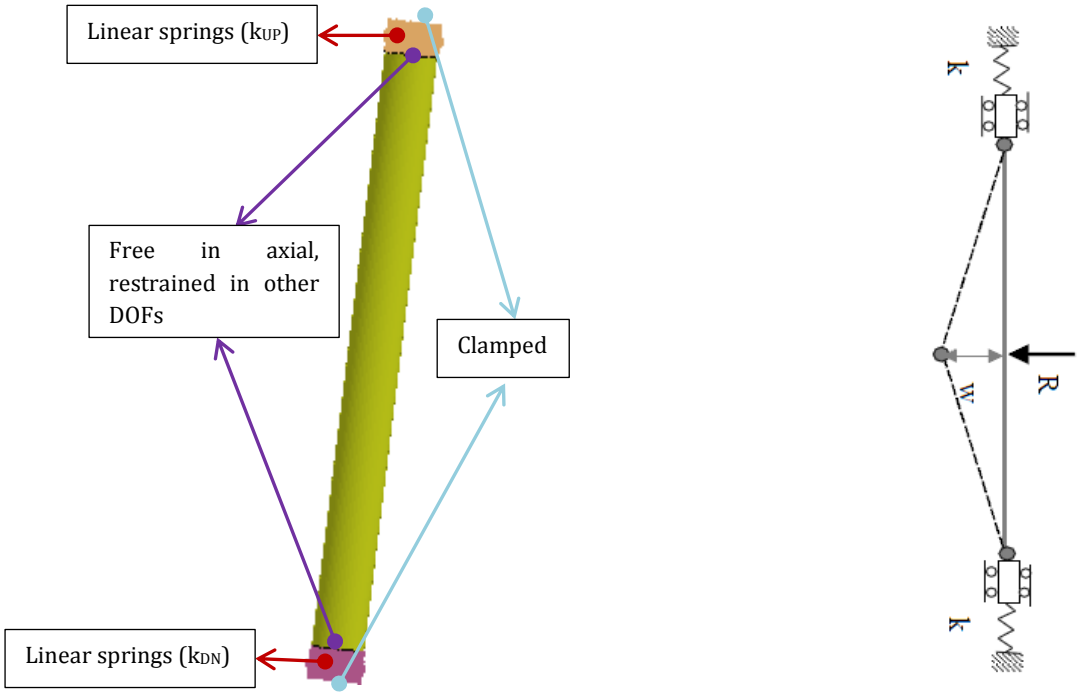

(a) Finite element model (b) Simplified model

Figure 5-3 Column Model with axial springs (Model-1)

(2) Single spring

This model consists only two single springs, one spring for each column-end. The spring is connected to the column wall by a rigid diaphragm which is allowed to have translational displacement in axial direction. A local coordinate had been generated to define the local axial coordinate of the column. The model is illustrated in Figure 5-4.

A finer mesh had been generated at the column-end zone to allow a smoother transition of section and material properties between the column wall and the rigid diaphragm.

The spring stiffness assigned for upper and lower springs are 49.5 MN/m and 1307.7 MN/m respectively.

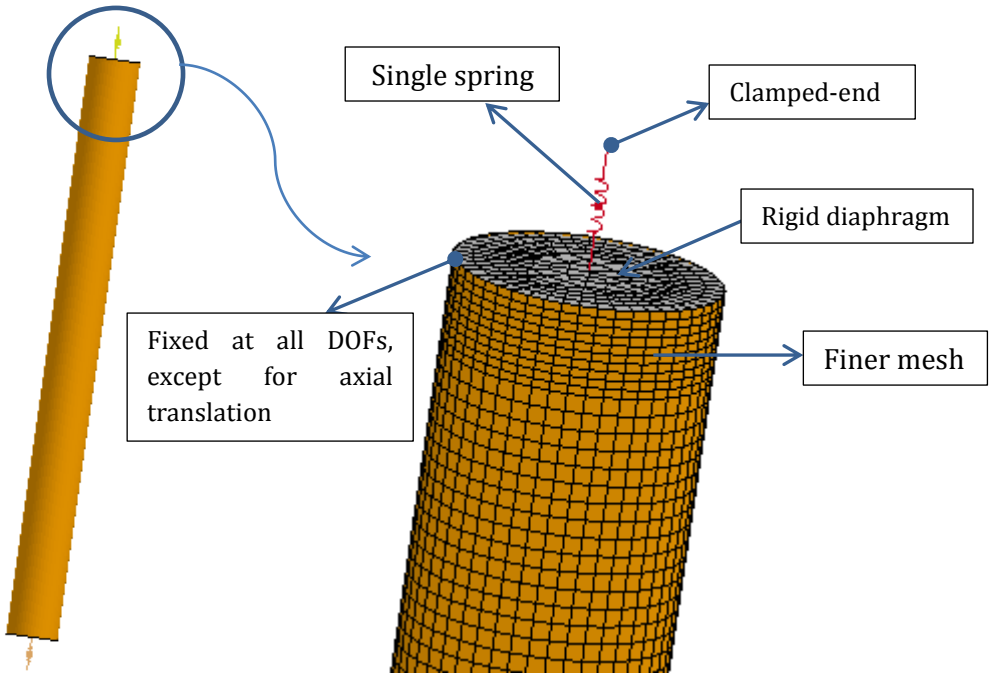

Figure 5-4 Column Model with axial springs (Model-2)

The multiple spring models are later found not the good models to represent the real boundary conditions because every single spring works independent from each other. The spring stiffness at the column end is dependent on the single spring coefficient. This could be identified by the uneven displacement at the column-ends shown in Figure 5-5 and Figure 5-6. The stiffness of each column end under the applied load is then the average spring coefficient. The uneven displacement at the column end does not represent the real behaviour since the column is attached to the other leg segment circumferentially around its wall thickness, thus the displacement at the cross section of column-end should be relatively even.

Later in present work, the focus would be on the single spring models since it is believed to be a better model to represent the real behaviour of the column-ends.

5.3 Results

The deformation fringes of three first models (multiple – equivalent spring, multiple – unequal spring and single – unequal spring) are shown below.

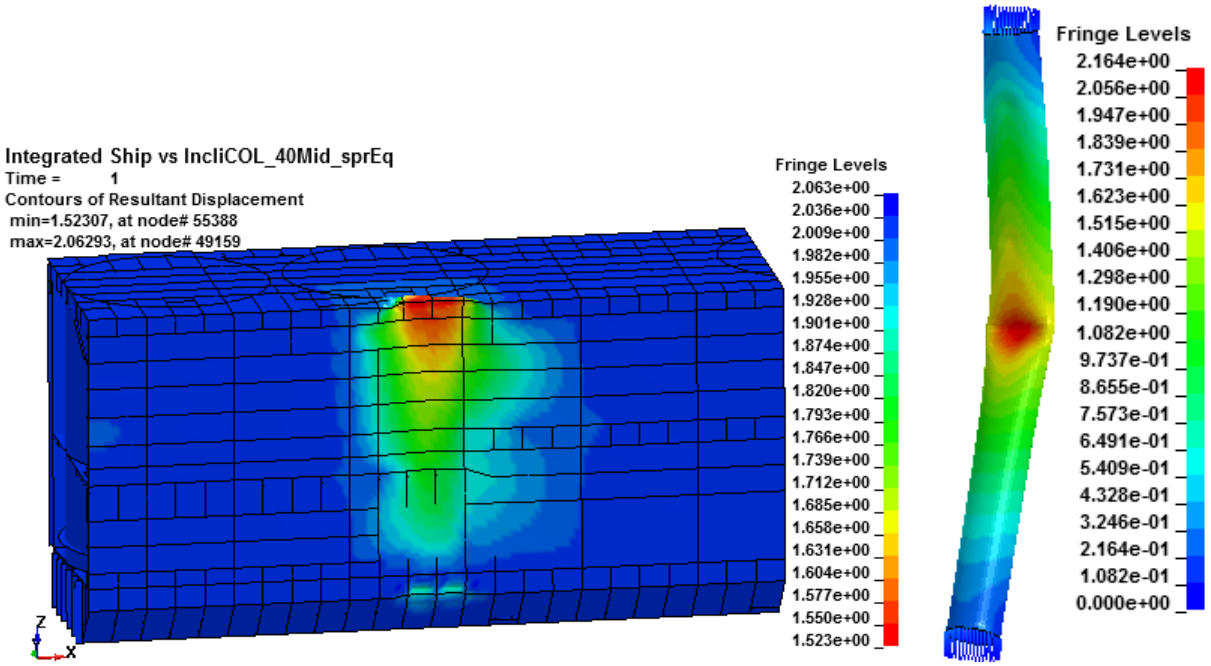

Figure 5-5 Deformation fringe – impact on column with Equal-Spring

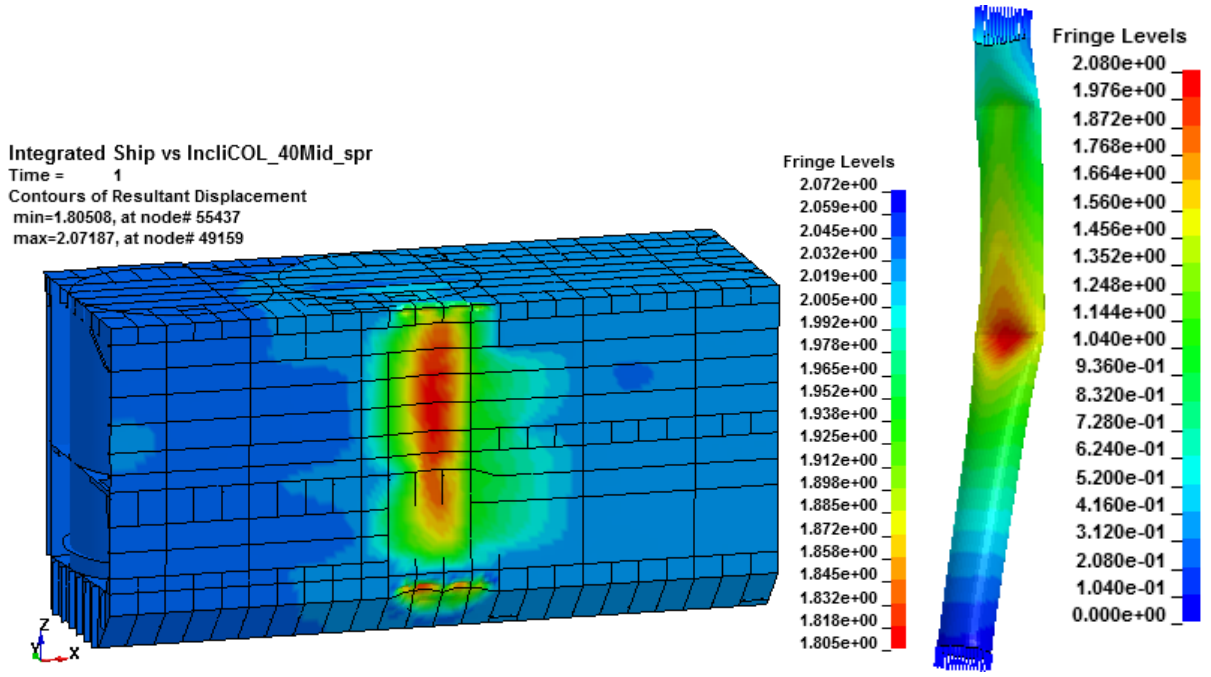

Figure 5-6 Deformation fringe – impact on column with Spring-2

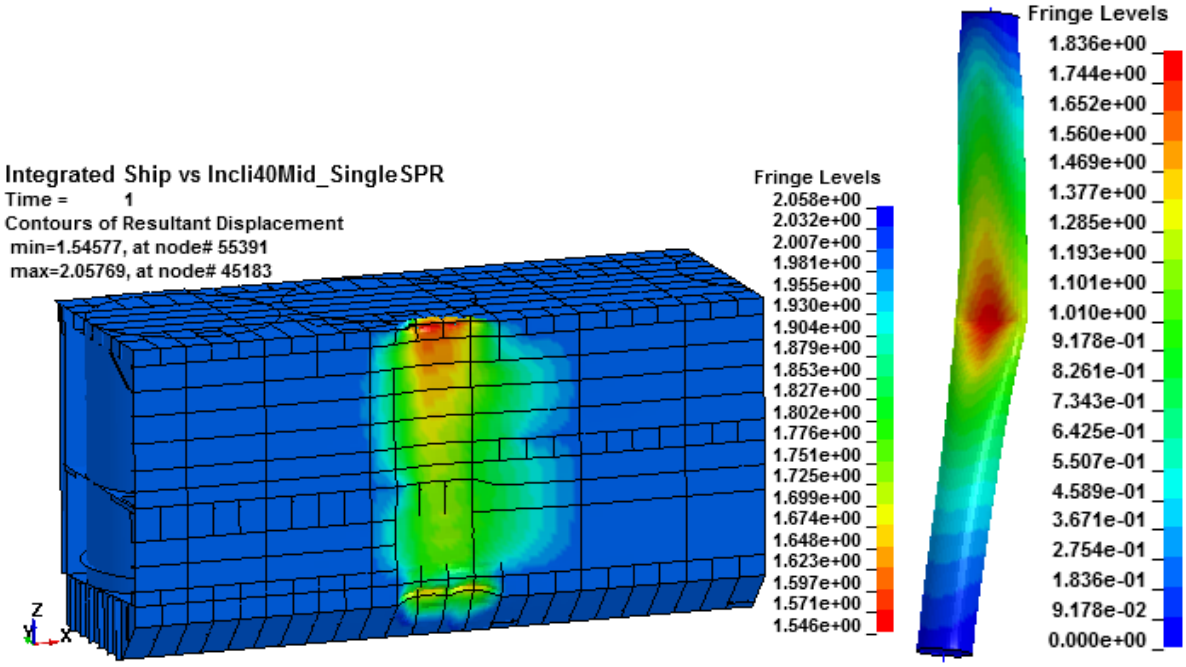

Figure 5-7 Deformation fringe –impact of column with Single Springs

The cut sections of the deformed bodies for the three models shown above are provided in the figures below to have more detail view.

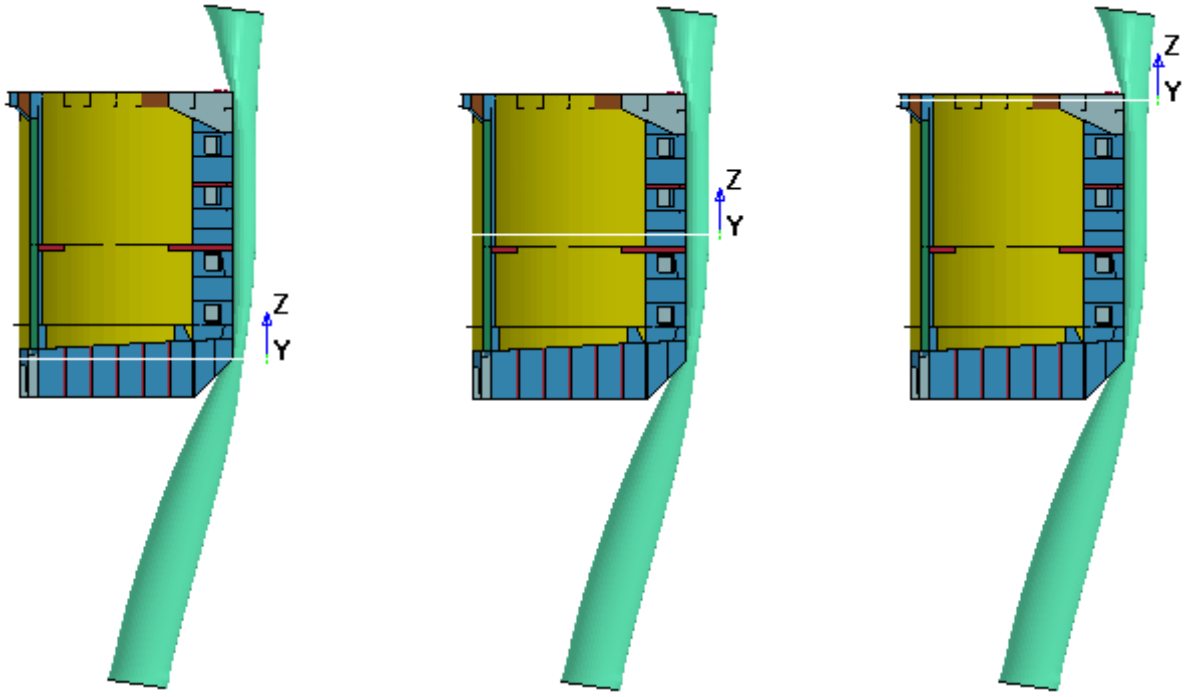

(a) Lower level (b) Middle level (c) Upper level

Figure 5-8 Elevation reference for top cut sections of deformation at final state

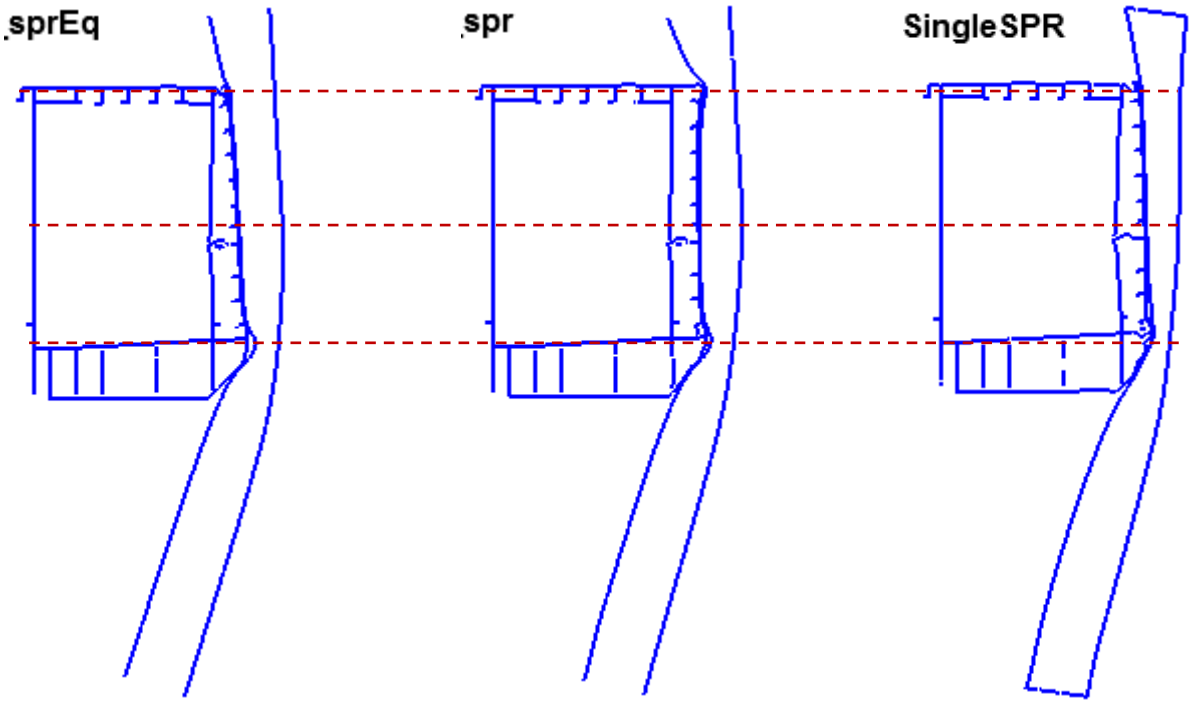

(a) Equal Spring (b) Spring-2 (nodal spring) (c) single springs

Figure 5-9 Side-cut sections of deformations at final state

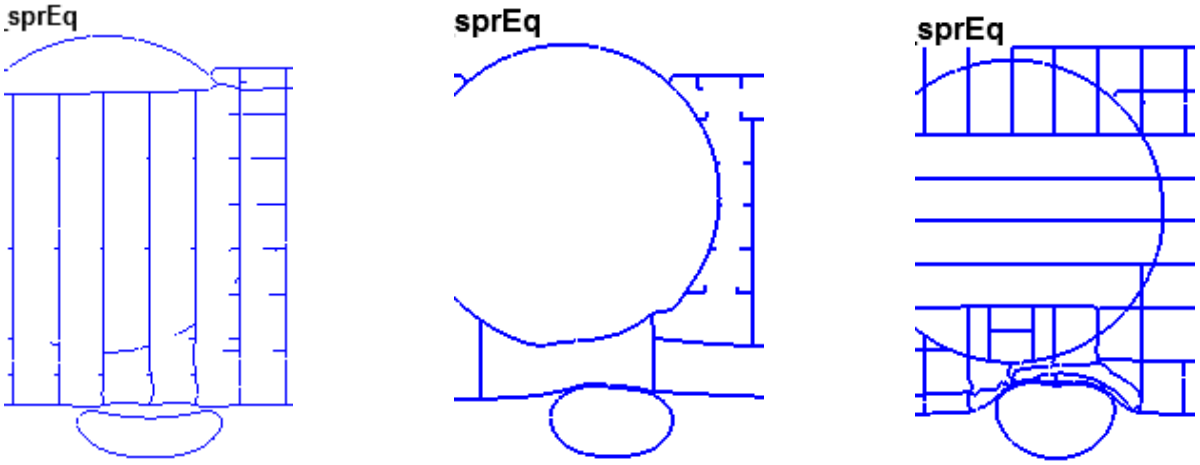

(a) Lower level (b) Middle level (c) Upper level

Figure 5-10 Top-cut sections of deformation at final state – Equal-spring

From Figure 5-5, the 'equal-spring' column model appears to behave as if the concentrated load is applied to the centre of the column. The visible deformation on the shipside is particularly due the upper deck of shipside hit the column close to its end at the final stage. The push of the shipside trigger the spring to utilize its stiffness as the column tried to pull in for getting more resistance against the impact force. This pull-in can be visualized as a rubber band tying a deformable rectangular body. The interface

pressure on the edges of the body will be higher than at its middle zone. Therefore there will be more deformation on the edges than the middle zone.

The column attempted to fail by bending moment. At the end of the impact state, as shown in Figure 5-9(a) and Figure 5-10 (a), the column is detached from the shipside.

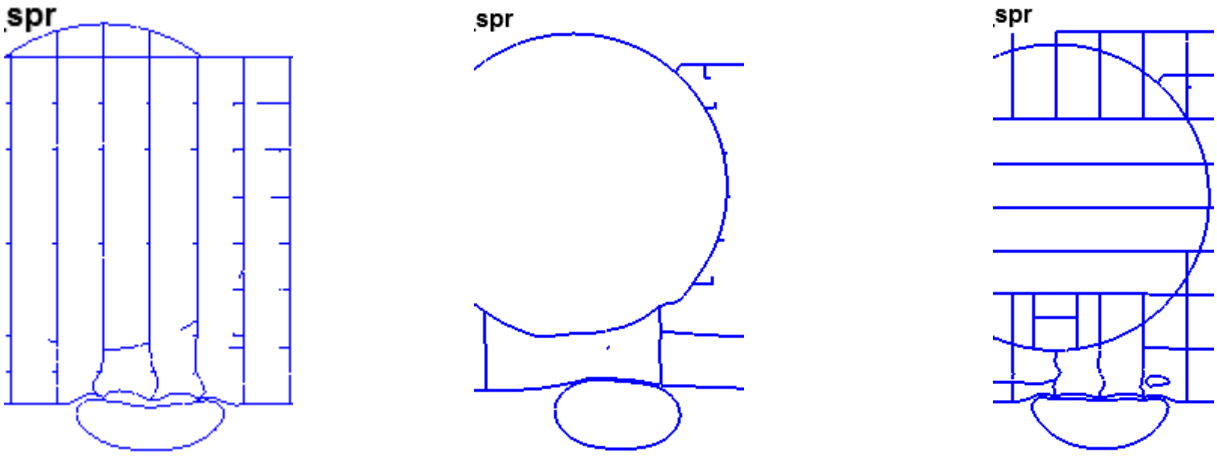

(a) Lower level (b) Middle level (c) Upper level

Figure 5-11 Top cut sections of deformation at final state – (Spring-2)

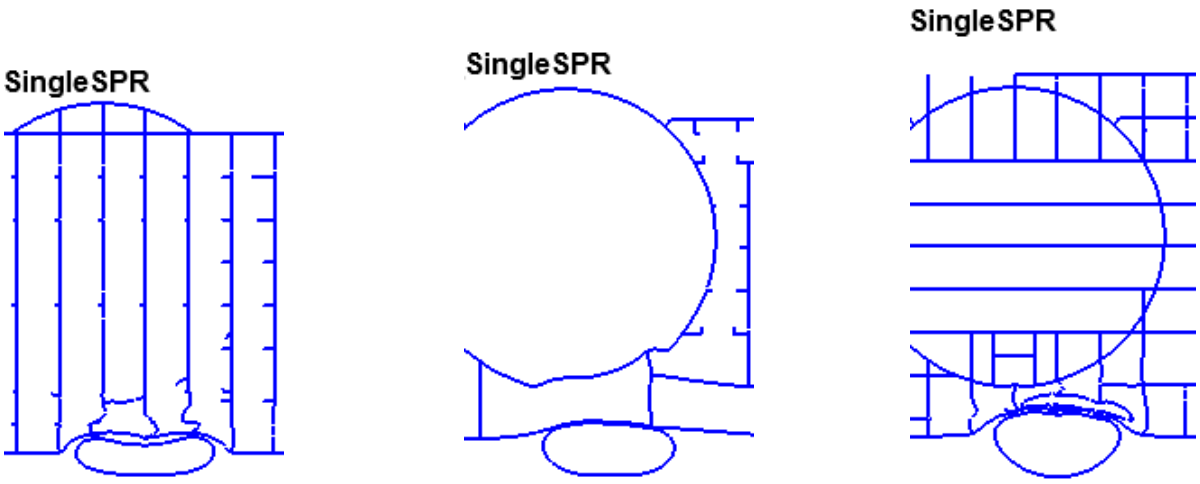

(a) Lower level (b) Middle level (c) Upper level

Figure 5-12 Top cut sections of deformation at final state – (single springs)

The deformation on the multiple-unequal spring model are shown in Figure 5-6, Figure 5-9(b), and Figure 5-11. This model generated more distributed damage over the height of the shipside. The development of the resistance over the contact area by this model occurs more significant than the previous model.

The deformation fringe of single springs model shown in Figure 5-7 is visually comparable to the deformation fringe of fixed-end model (Figure 4-6). The cut-sections shown by Figure 5-9(c) and Figure 5-12 indicated the behaviour close to the fixed-end model.

The comparison of the force-displacement relationships for the three models discussed above to the fixed-end model is shown on Figure 5-13 and Figure 5-14 for the column and the shipside displacement respectively. For the models with the springs, the displacements are the relative displacement with regard to the displacement on the springs.

As for the column displacement (Figure 5-13), under the same column displacement the force demanded for the multiple spring models appeared to be significantly lower than for the fixed one, whilst the single spring model follow closely to the fixed-ends model. The displacement on the column at the final stage in general is relatively smaller in magnitude than for the fixed-ends model. This apply also for the shipside displacement, as shown in Figure 5-14.

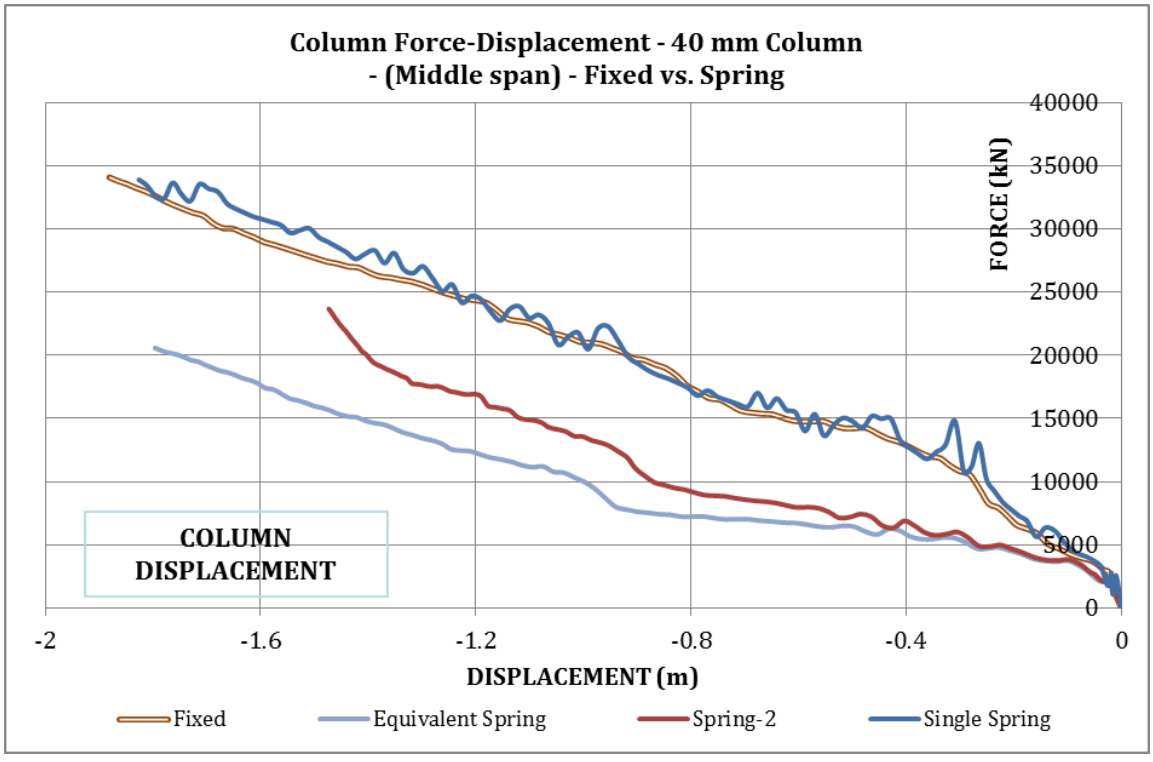

Figure 5-13 Force-deformation plots of Column (fixed vs. spring models)

The energy-displacement plots for the three models are compared with the fixed-end model in Figure 5-15 and Figure 5-16. The trends comply with the force-displacement plots on Figure 5-13 and Figure 5-14 for column and shipside displacement respectively.

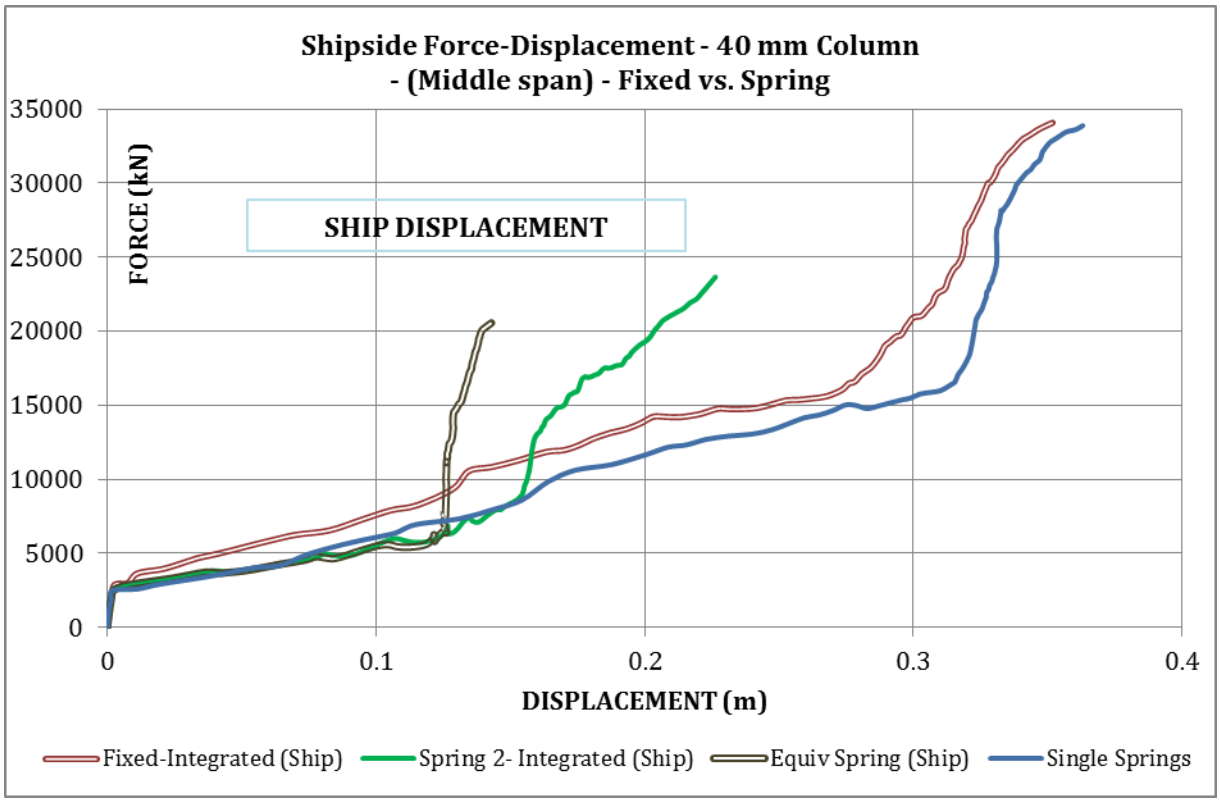

Figure 5-14 Force-deformation plots of Shipside (fixed vs. spring models)

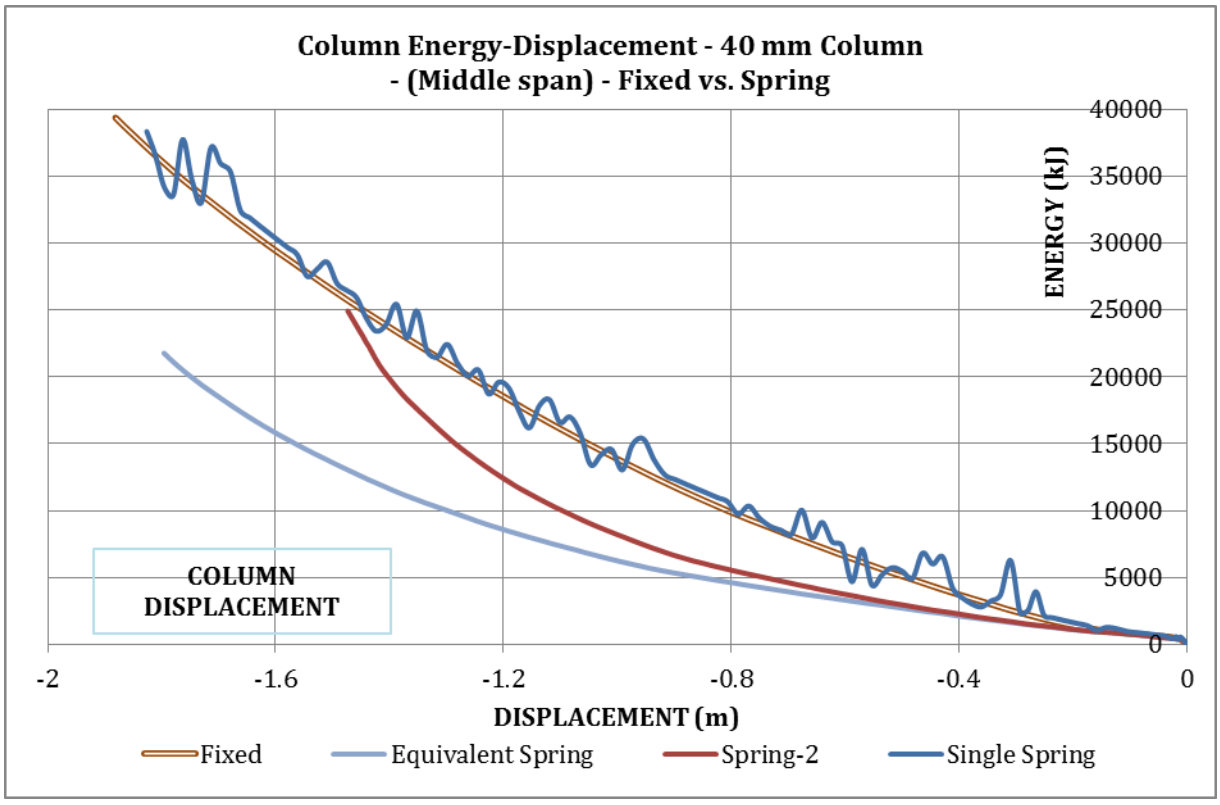

Figure 5-15 Energy-displacement plots of Column (Fixed vs. Spring Models)

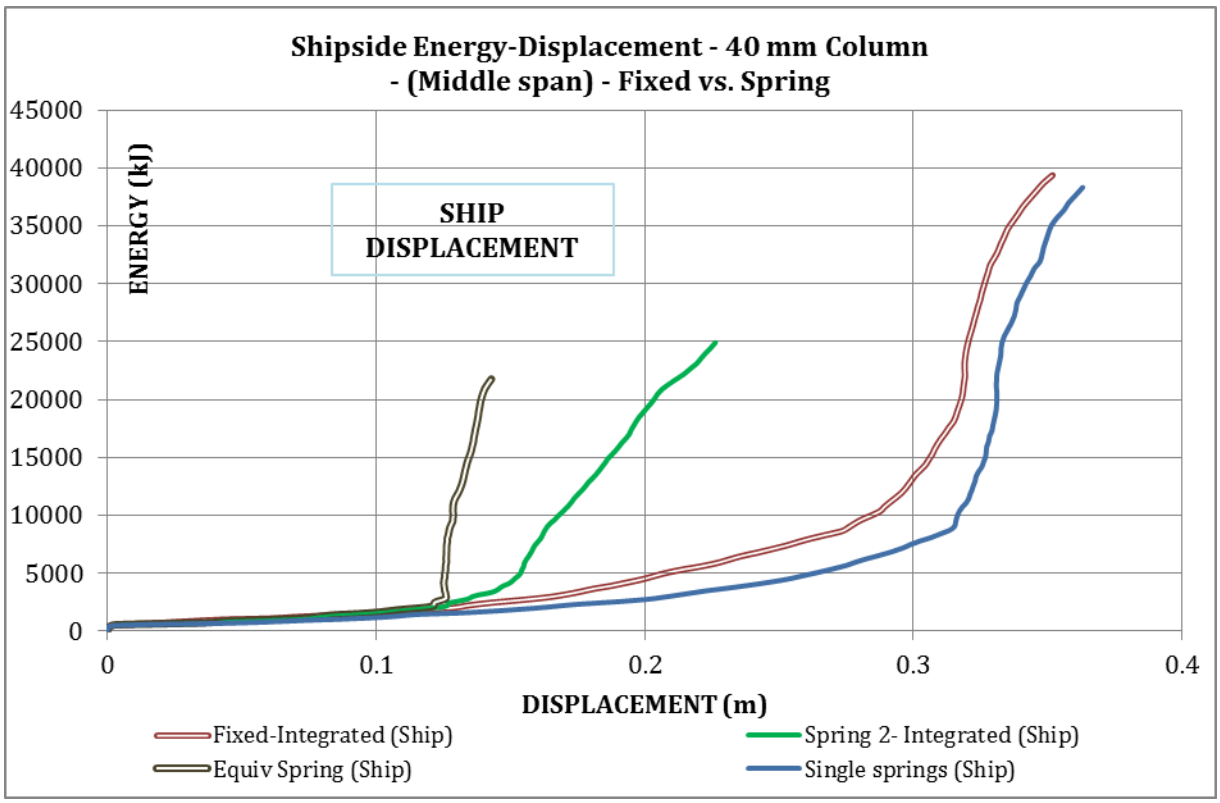

Figure 5-16 Shipside Energy-displacement Plots (Fixed vs. Spring Models)

To assure that the axial springs have been assigned in a good manner, the model was also checked with the softer spring and the firmer springs. As per discussion with Prof. Amdahl (Amdahl, Discussion, 2011), the softer springs were assigned with 1000 times less, whilst the firmer springs with 1000 times more, than the original stiffness coefficient. The force-energy-displacement comparing these three spring stiffness is shown in Figure 5-17.

To confirm the force equilibrium, the reaction forces on the springs and the springs' displacement have been checked and compared to its stiffness coefficient. It is affirmed that the equilibrium is fulfilled with a negligible deviation.

It appeared in Figure 5-17 that there is no significant deviation for the force-deformation relationships, whereas for the energy-deformation the softer springs give a lower energy-displacement.

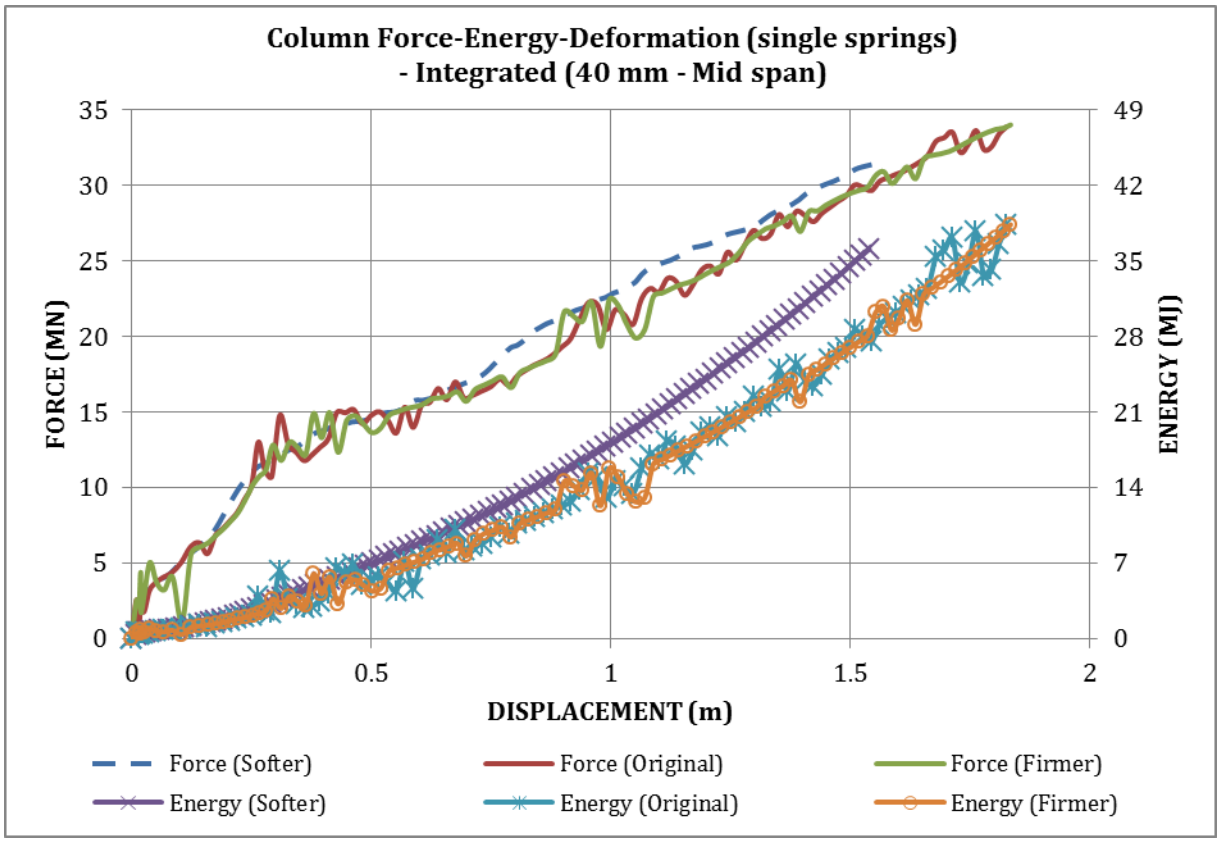

Figure 5-17 Force-Energy-displacement (Softer – Original – Firmer Single Springs)

As indicated in Figure 5-13 and Figure 5-15, the deformation on the column with axial flexibility appear to have the same tendency with the clamped-ends column. In prior, it was expected that this axial flexibility will produce a lower force-deformation curve. The prior hypothesis was that the membrane forces will be developing along with the occurrence of larger deformation on the column, such that the membrane force will generate the axial force towards its axial fixity points. It was then presumed that if the column are clamped at it ends, the constraining effect will contribute to resistance increase on the column, as discussed in section 4.2.

However, the results show a disagreement with the hypothesis. It is then guessed that the plastic strain at the interface zone is developed in the way that it allows the elongation to occur on this zone. As the results, the membrane actions is not developing as predicted, thus giving a small axial displacement and reaction force towards its fixity points.

Comparison has also been conducted for two scenarios of impact location; quarter span impact and middle span impact. Plotting the Force-Energy-deformation under one diagram, as shown in Figure 5-18, one may conclude that the impact location does not have any significant influence to the force-deformation and energy-deformation relationships.

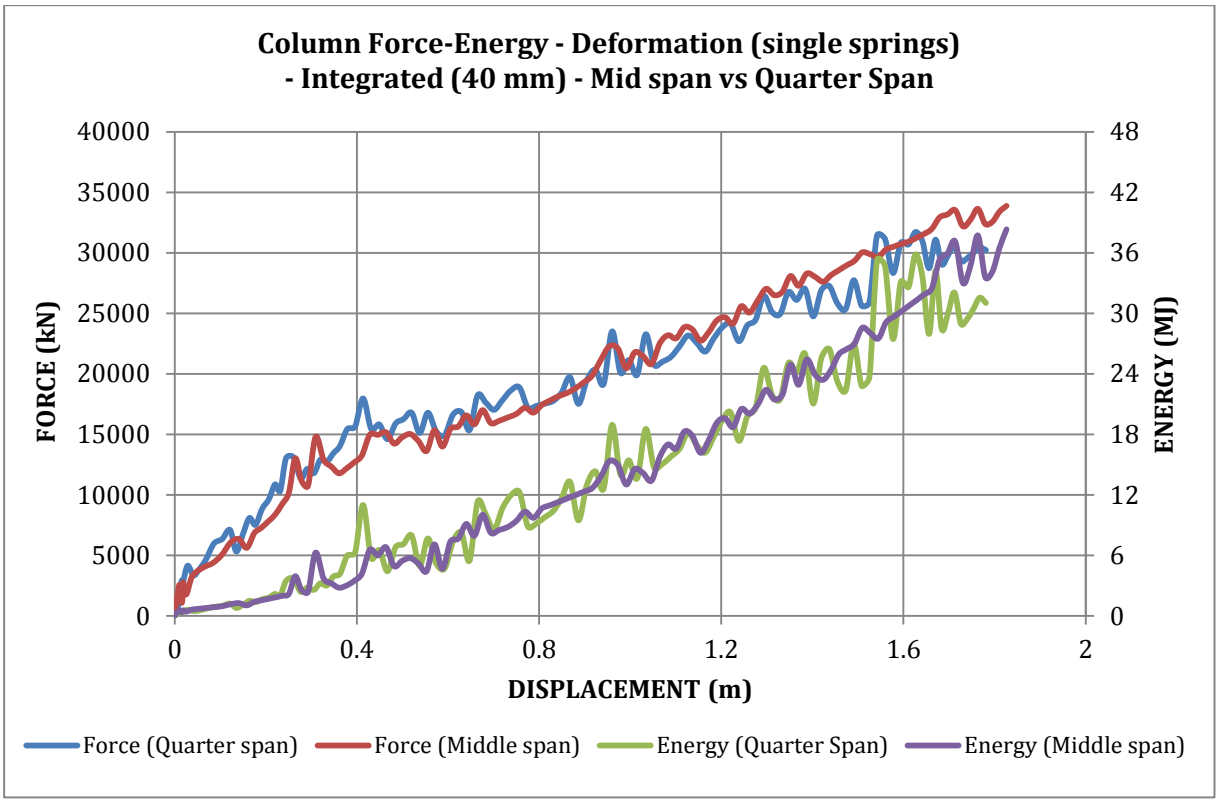

Figure 5-18 Force-Energy-deformation Plot – single springs (mid span vs. quarter span)

Appendix E provides the resistance-indentation relationships showing the influence of the single-spring model for three different column-thicknesses; 30 mm, 40mm, and 50mm.

To investigate the influence of the spring coefficients (softer, original and firmer) over three different thicknesses, the force-displacement plots are provided in appendix F .

6 Conclusions

a. The column wall thickness should be chosen according to which the design criteria aimed for. For instance, if the shared-energy design is preferred, a moderate thickness should be a viable preference. In present work, the 40 mm column had been a good example to show the shared-energy behaviour.

b. For the inclined column, the impact location is determined by the point where the striking body touches the struck body at the first strike.

c. The force demanded to generate the same displacement both on the column and shipside is slightly higher for middle span impact than for quarter span impact, for all column wall thickness assessed here.

d. The contact area of the impact increases gradually up to the height of the shipside along with the continuous motion of the shipside. The increase of contact area takes the primary role to the increase of the resistance on the column. The resistance increases significantly when the contact area cover the over the height of the shipside.

e. Comparing the plot between the middle span and the quarter span impact, the resistance after the contact area cover the height of the shipside is significantly higher for the middle span impact than for the quarter span impact. At the middle span impact, the shipside is located closer to the fixity point of the column than for the quarter span. The boundary conditions influence attempt to provide additional resistance to the column.

f. Assumption of fixed column is prudent for practical design, provided that the stiffness of the column-ends is still under elastic (linear) range. One of the ways to achieve this is by providing a good bracing system for overall jacket structures.

g. The axial flexibility does not contribute significantly to the overall resistance and deformation of the column.

h. To describe the actual process which occurs on the deformable colliding objects, the integrated (shared-energy) method should be conducted whenever viable.

7 Recommendations for Further Study

a. Sensitivity analysis on the span of jacket leg (column)

b. Consider the global deformation from the whole jacket structures

c. Impact by other part of the ship, e.g. ship bow, stern end, etc.

d. Develop a routine or algorithm to read, process, and display the interface pressure-area relationship better. (it is acknowledged that it is a tedious process and subjected to the analyser judgement)

e. Consider imperfections, welding, and the fracture criteria of the steel material model, both on the ship and on the jacket-leg

f. Larger diameter or apply for a tower

g. Assessment on the hydrodynamic effect (inertia effect) and the friction effect at the impact interface

h. Nonlinear spring stiffness model for the boundary conditions of the column

i. Assessment on the yielding zone at the contact area (interface) over the height of the shipside, considering the strain effect (elongation) on this zone

Bibliography

LS-DYNA Theory Manual. (2006, March). *Volume I, Version 971/ Rev 5*. (J. O. Hallquist, Compiler) California, U.S.A: Livermore Software Technology Corporation.

LS-DYNA Keyword User's Manual Volume 1: Version 971/Rev. 5. (2010, May). California, U.S.A : Livermore Software Technology Corporation.

Alsos, H. S. (2008). *Ship Grounding. Analysis of Ductile Fracture, Bottom Damage and Hull Girder Response. Doctoral Thesis.* Trondheim: Institutt for Marin Teknikk NTNU.

Amdahl, J. (1991). Consequences of Ship Collisions. *Seminar on Collide II Project - Risk Assessment (Collision of Ships with Offshore Platforms, RINA).* London, UK: Royal Institution of Naval Architects.

Amdahl, J. (2011, January - June). Discussion. Trondheim.

Haris, S. (2011, February to March). Discussion. Trondheim, Norway.

Hong, L., & Amdahl, J. (2007). Strength Design of FPSOs against Supply Vessel Bow Collision. *4th International Conference on Collision and Grounding of Ships* (pp. 1-10). Hamburg: Schiffbautechnische Gesellschaft e. V., Hamburg.

Khedmati, M. R., & Nazari, M. (2010, December). A Numerical Investigation into Strength and Deformation Characteristics of Preloaded Tubular Members under Lateral Impact Loads. Tehran, Iran: Elsevier.

Liu, Z. (2011, January to April). Discussion. Trondheim, Norway.

Moan, T. (2003). *TMR4190 - Finite Element Modelling and Analysis of Marine Structures.* Trondheim: Institutt for Marin Teknikk.

N-004, N. (2004). *NORSOK Standard N-004: Design of Steel Structures.* Norwegian Technology Standards Institution.

Raaholt, H. (2009). *Analysis and Design of Columns in Offshore Structures subjected to Supply Vessel Beam Collision. Master Thesis.* Trondheim: NTNU Marin Teknikk.

Skallerud, B., & Amdahl, J. (2002). *Nonlinear Analysis of Offshore Structures.* Baldock, Hertfordshire, England: Research Studies Press Ltd.

Storheim, M. (2008). *Analysis of Sructural Damage of Tankers subjected to Collision. MasterThesis.* Trondheim: NTNU Marin Teknikk.

Tavakoli, M. T. (2011, February). Discussion. Trondheim, Norway.

Tavakoli, M. T., Amdahl, J., Alsos, H. S., & Klæbo, F. (2007). Analysis of Supply Vessel Stern Impacts with a FPSO. *Proceedings 4th International Conference on Collision and Grouding of Ships (ICCGS)* (pp. 19-28). Hamburg: Schiffbautechnische Gesellschaft e. V., Hamburg.

USFOS A/S. (n.d.). USFOS: computer program for non-linear static and dynamic analysis of space frame structures. Trondheim, Norway.

Wong, M. B. (2009). *Plastic Analysis and Design of Steel Structures.* Oxford, UK: Butterworth-Heinemann.

Zhang, S. (1999). *The Mechanics of Ship Collision.* Lyngby: Department of Naval Architecture and Offshore Engineering, Technical University of Denmark.

APPENDICES

A Force-Deformation Plots

A.1 Middle Span

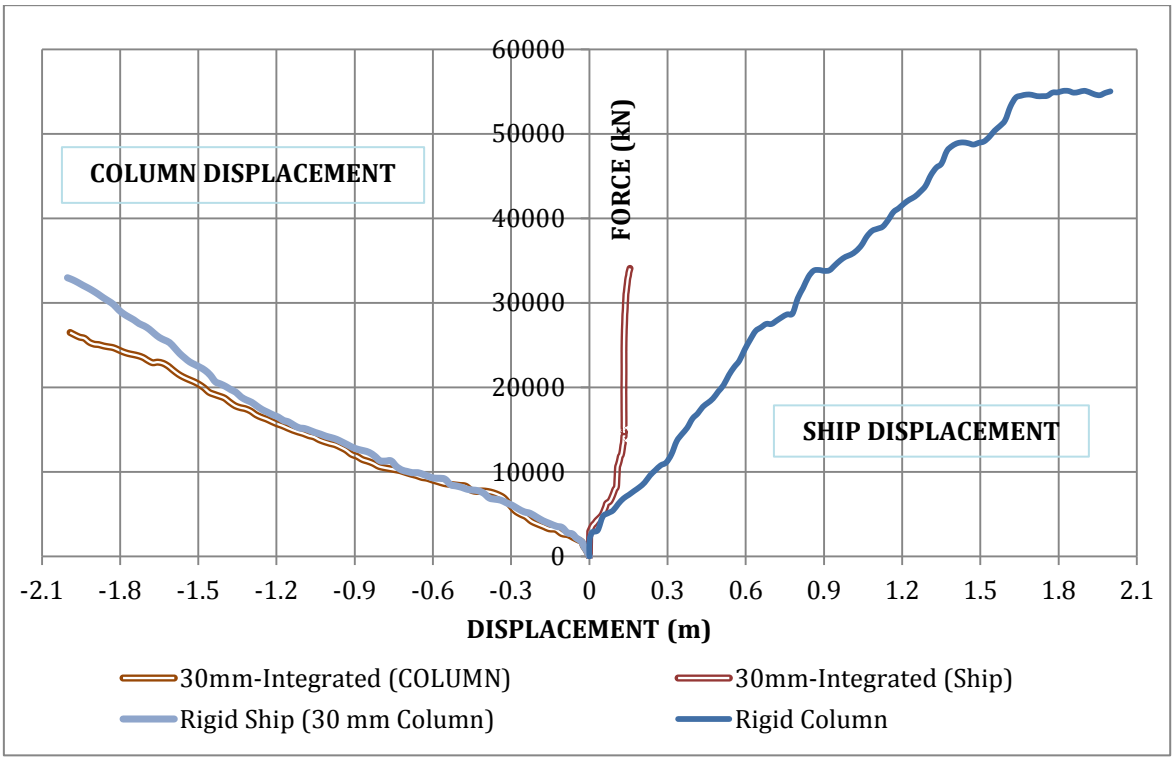

Fig. A-1 Force-Deformation – Middle Span (30 mm Column)

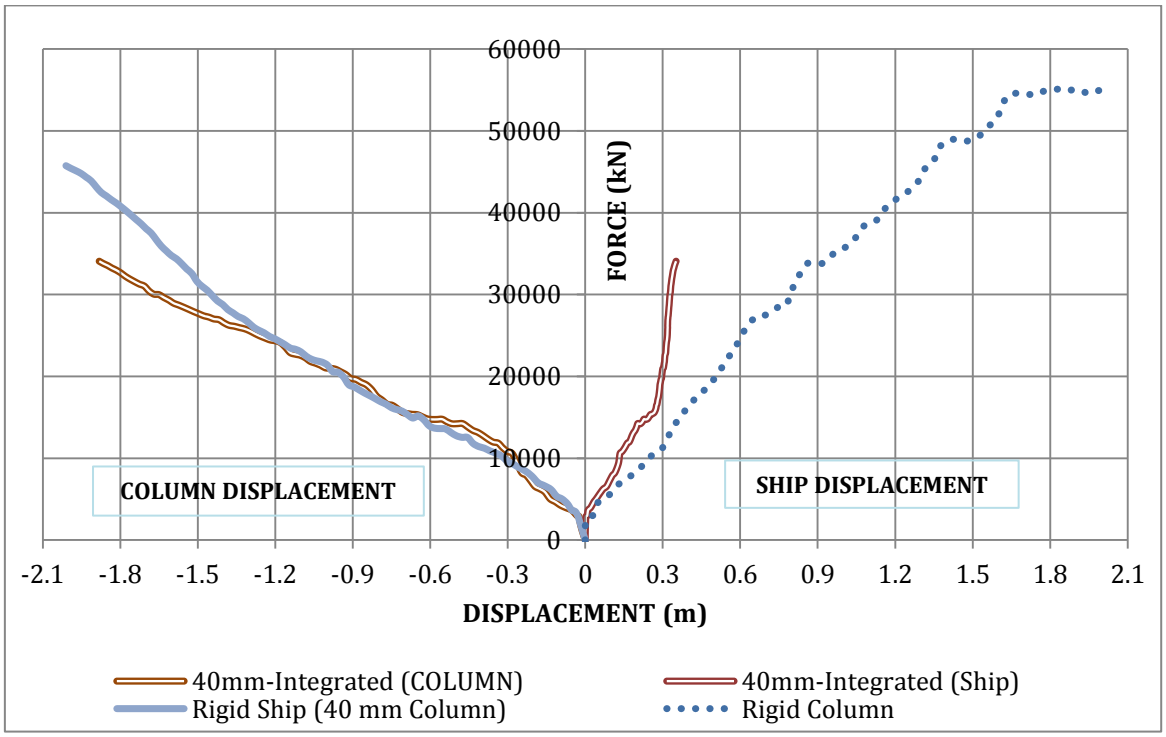

Fig. A-2 Force-Deformation – Middle Span (40 mm Column)

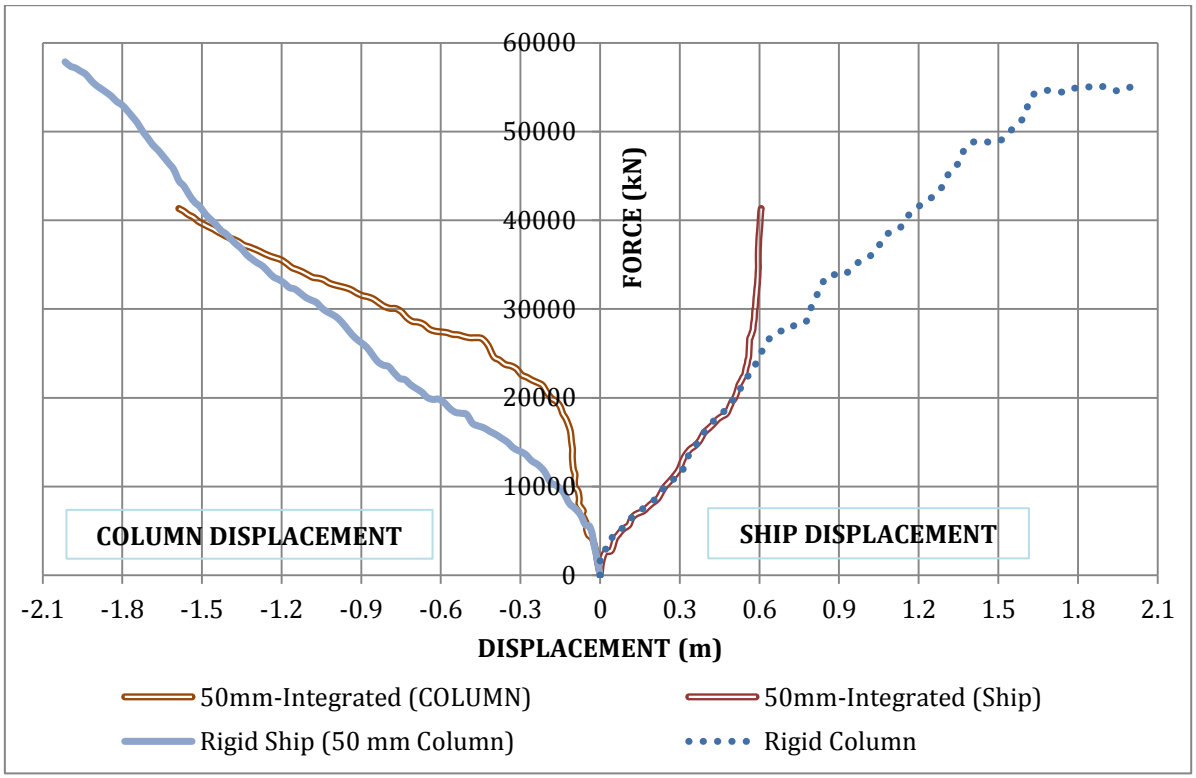

Fig. A-3 Force-Deformation – Middle Span (50 mm Column)

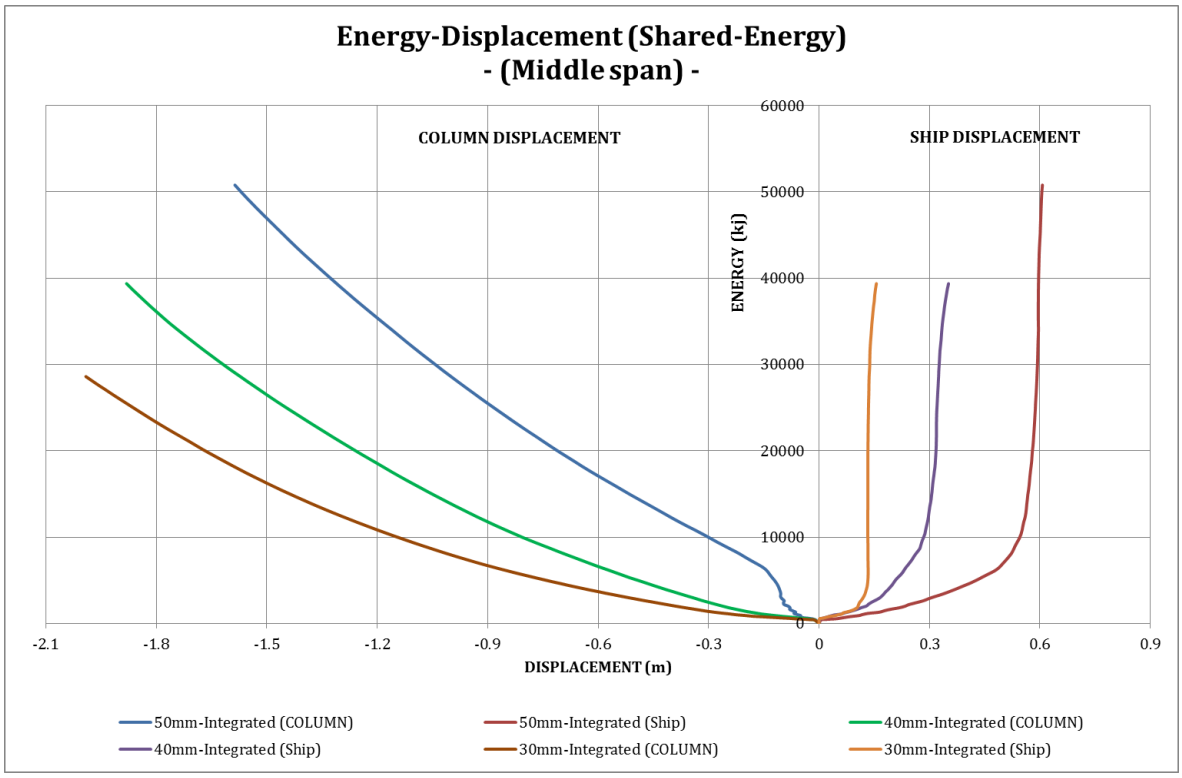

Fig. A-4 Energy-Displacement – Middle Span (Shared-Energy cases)

A.2 Quarter Span

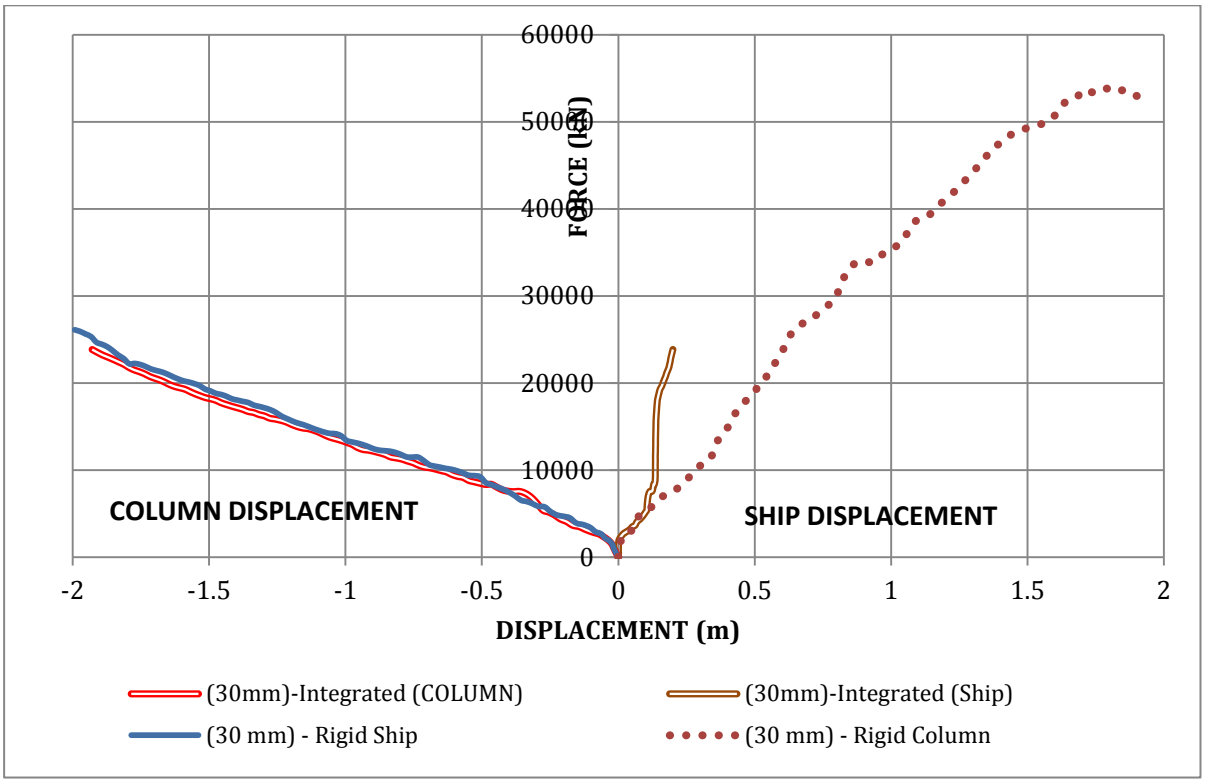

Fig. A-5 Force-Deformation – Quarter Span (30 mm Column)

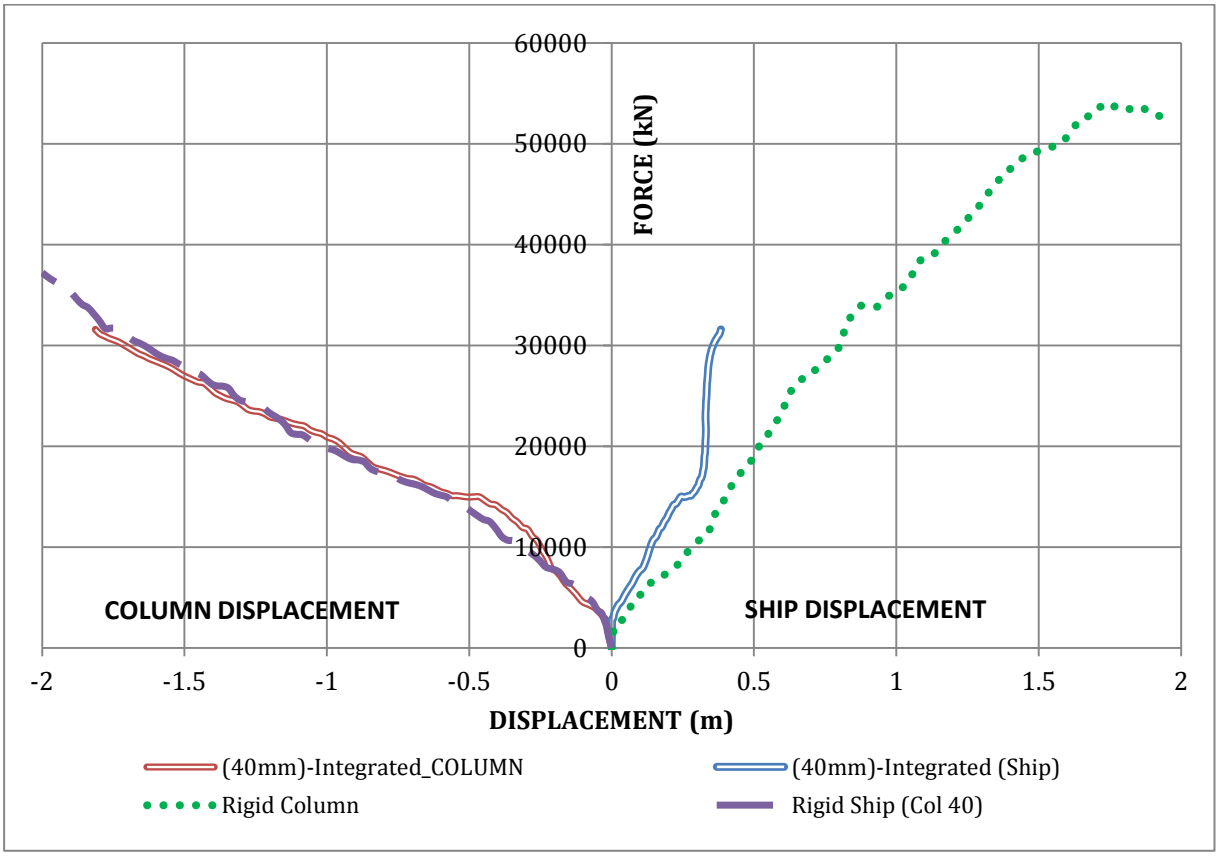

Fig. A-6 Force-Deformation – Quarter Span (40 mm Column)

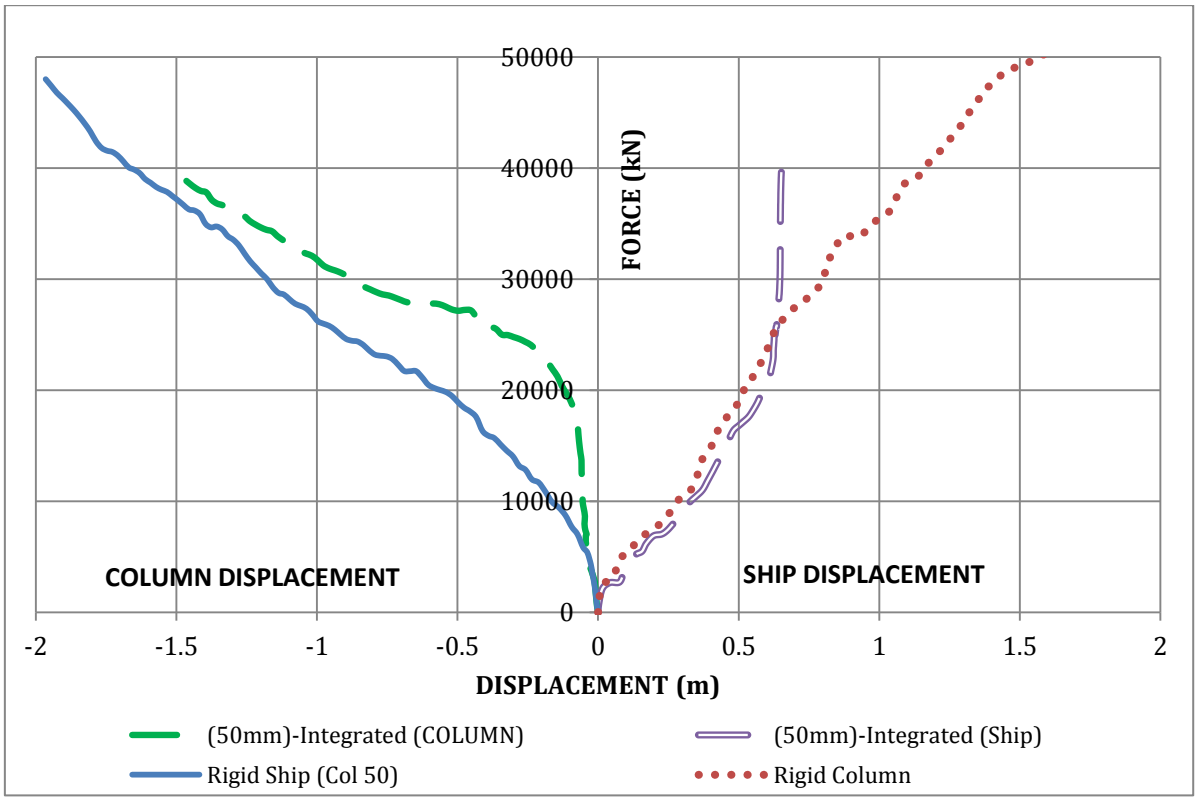

Fig. A-7 Force-Deformation – Quarter Span (50 mm Column)

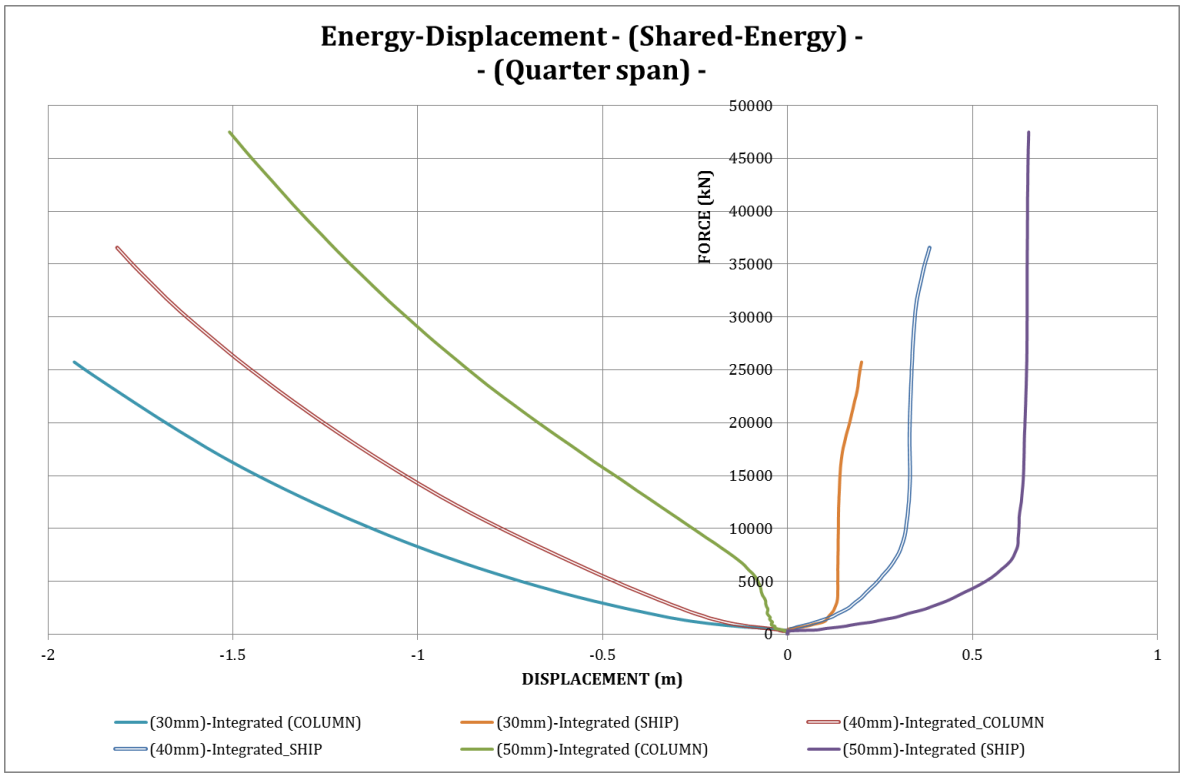

Fig. A-8 Energy-displacement – Quarter Span (Shared-Energy cases)

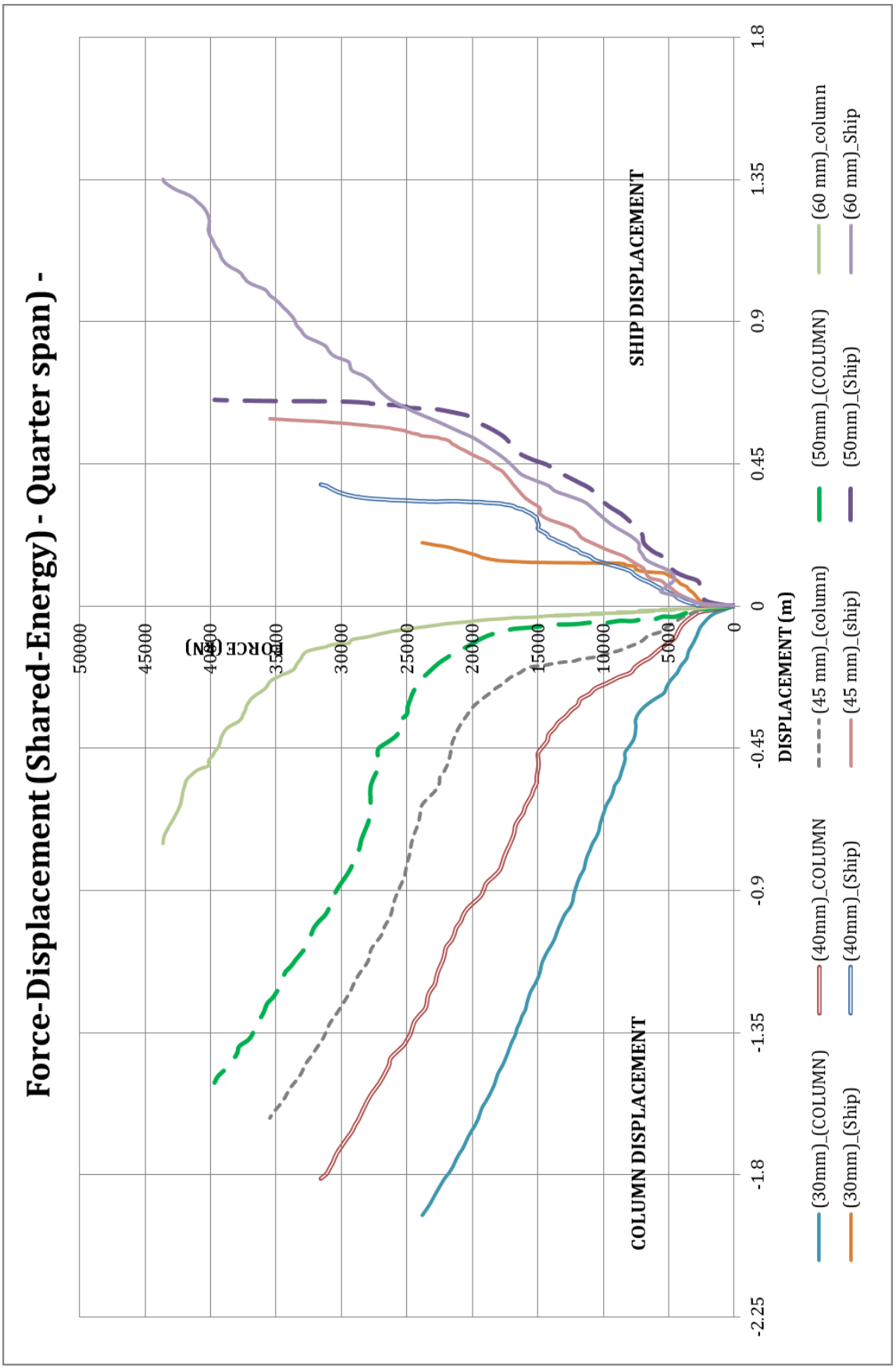

Fig. A-9 Force-Deformation – Quarter Span (Shared-Energy)

B Resistance-Indentation Plots (Middle Span versus Quarter Span)

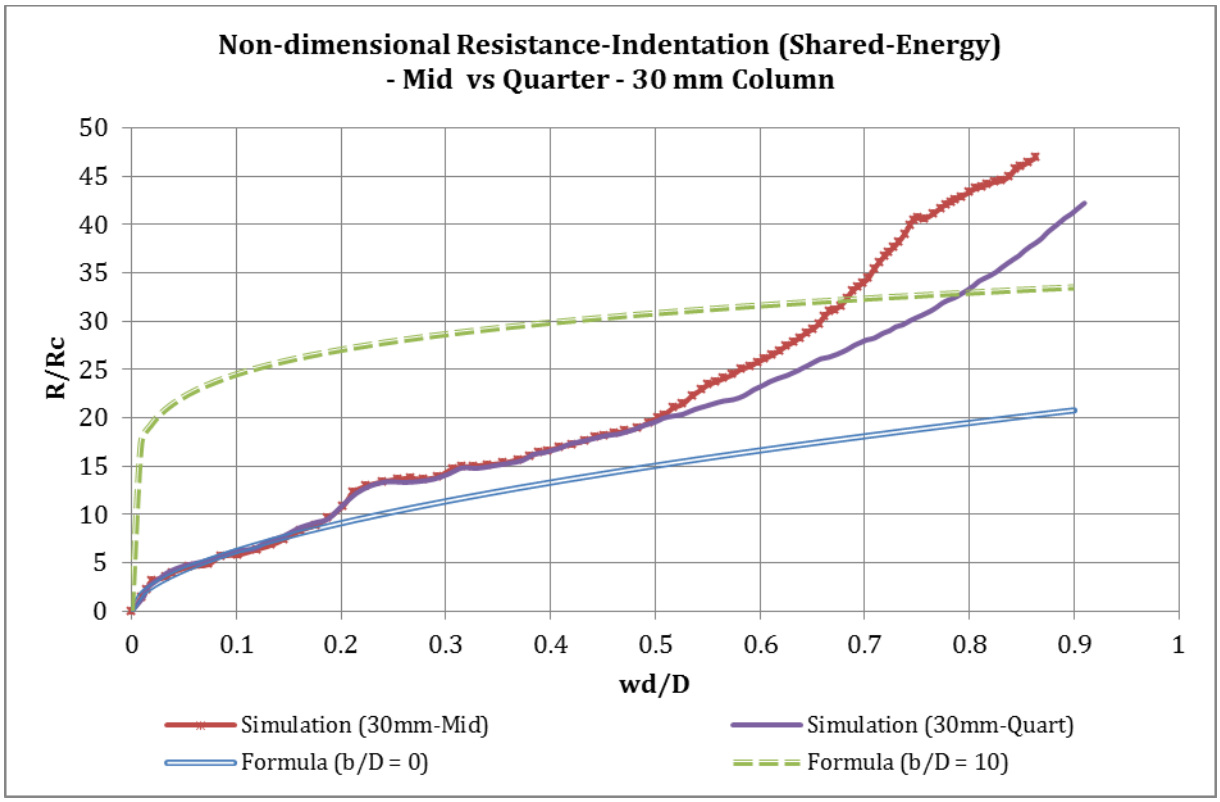

Fig. B-1 Resistance-Indentation Plot for 30 mm-thick Column

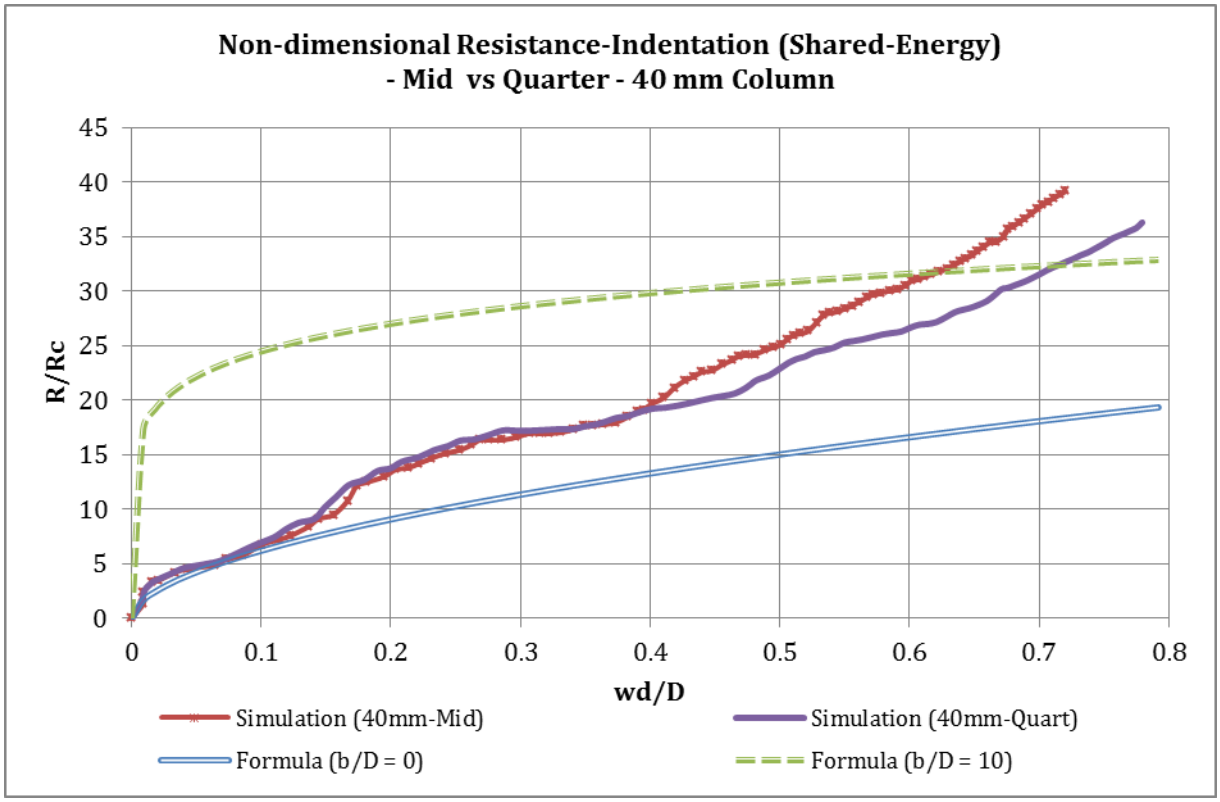

Fig. B-2 Resistance-Indentation Plot for 40 mm thick Column

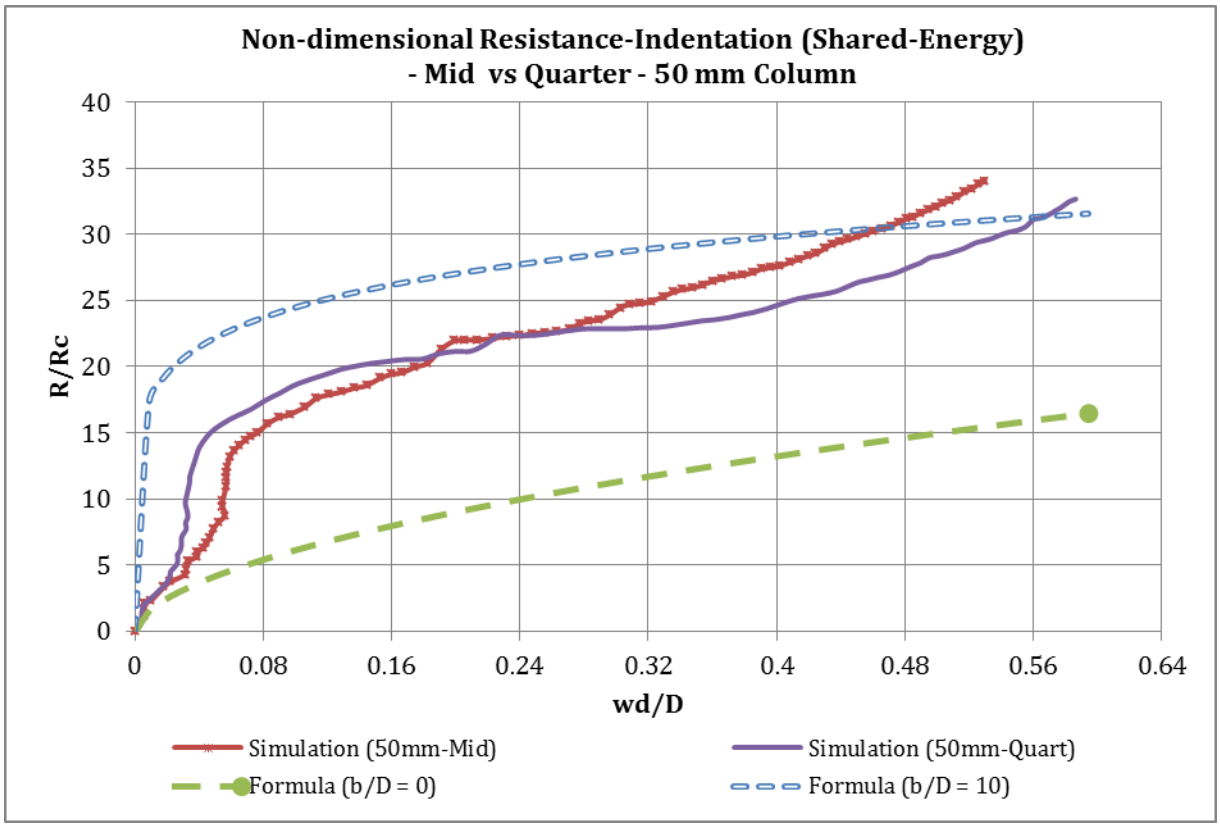

Fig. B-3 Resistance-Indentation Plot for 50 mm thick Column

C Interface Pressure-Area Plots (Inclined VS. Vertical Column)

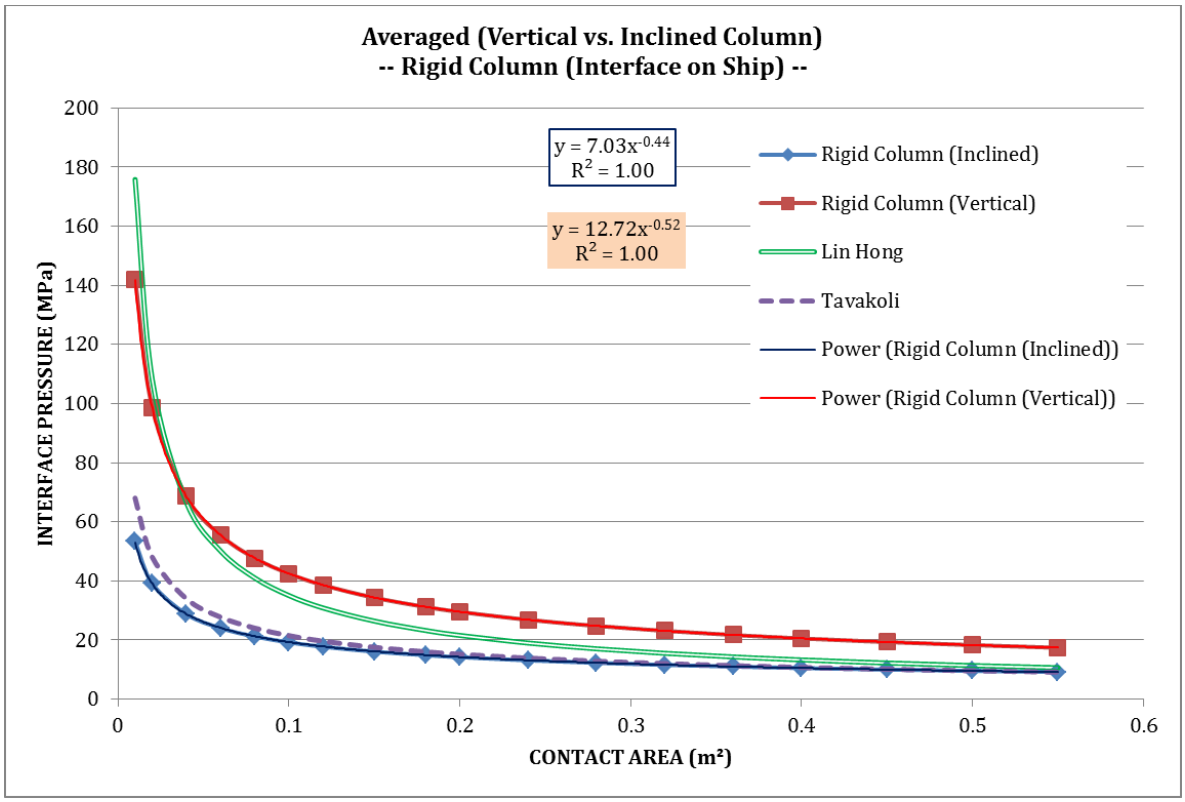

Fig. C-1 Pressure-Area – Vertical vs. Inclined Column (Rigid Column case)

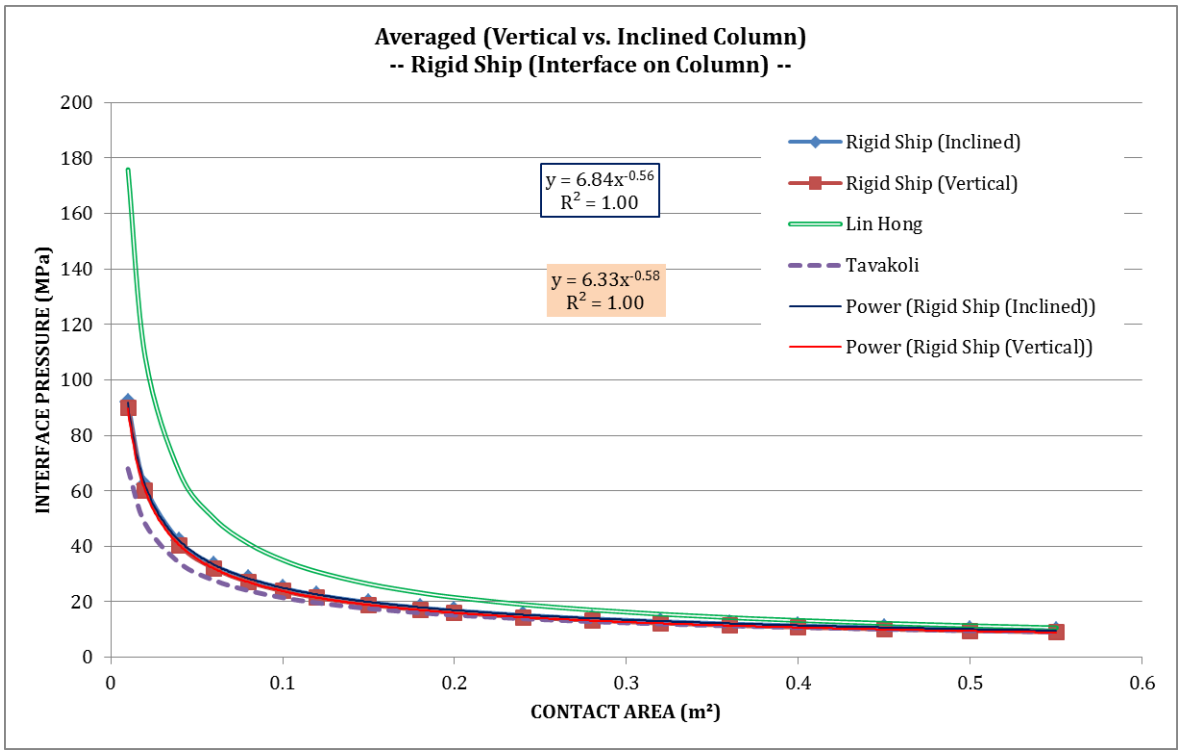

Fig. C-2 Pressure-Area – Vertical vs. Inclined Column (Rigid Ship case)

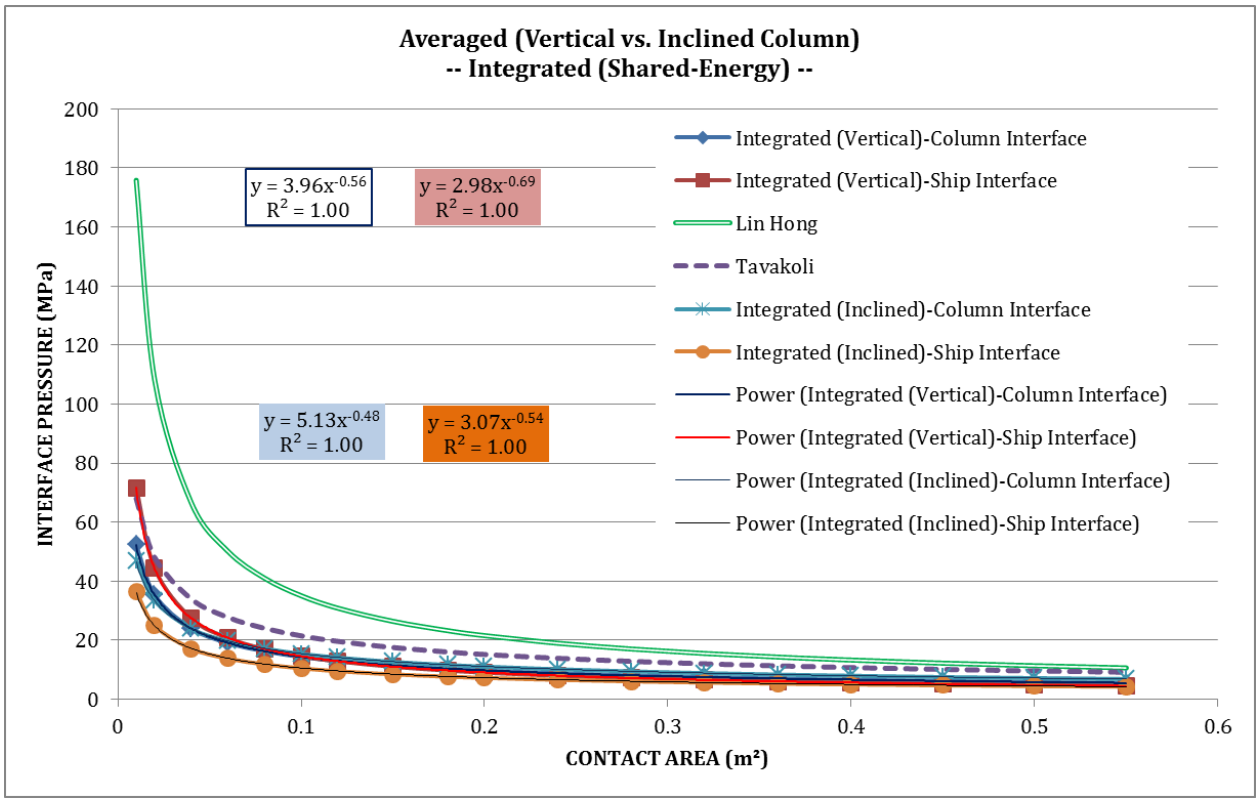

Fig. C-3 Pressure-Area – Vertical vs. Inclined Column (Shared-energy case)

D Bending Force-Deformation Plots

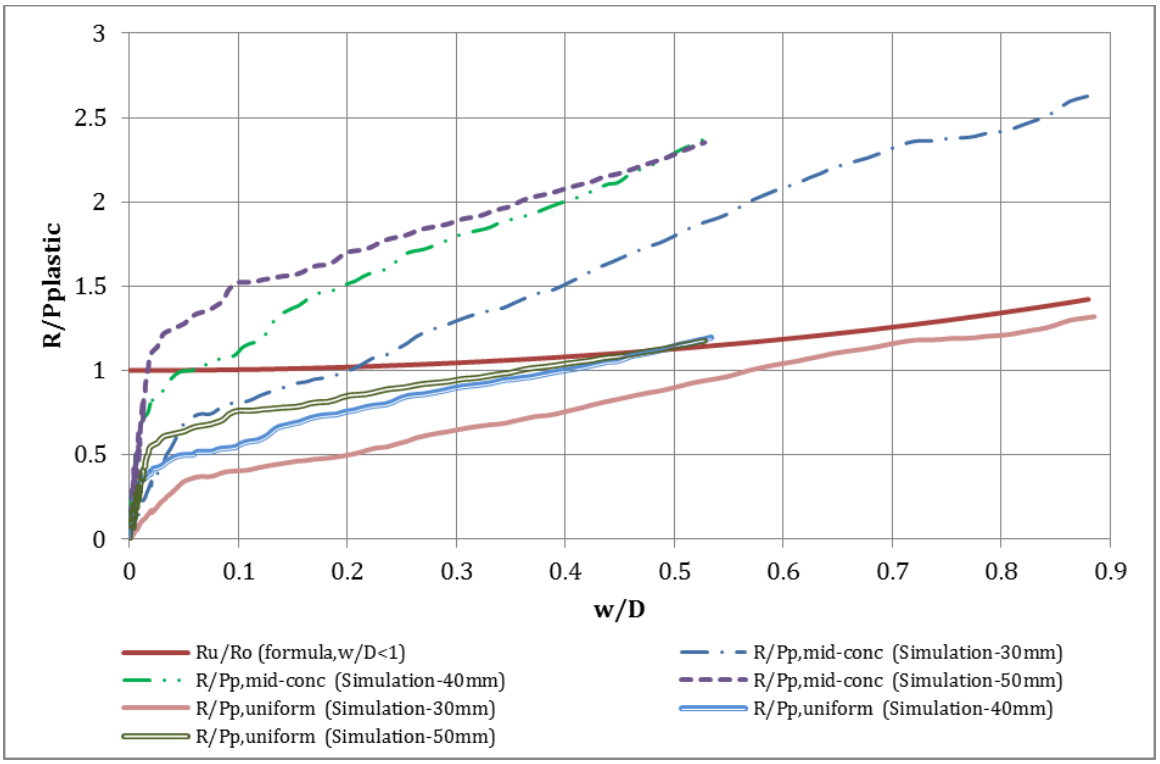

Fig. D-1 Bending Force-Deformation – Middle Span Impact

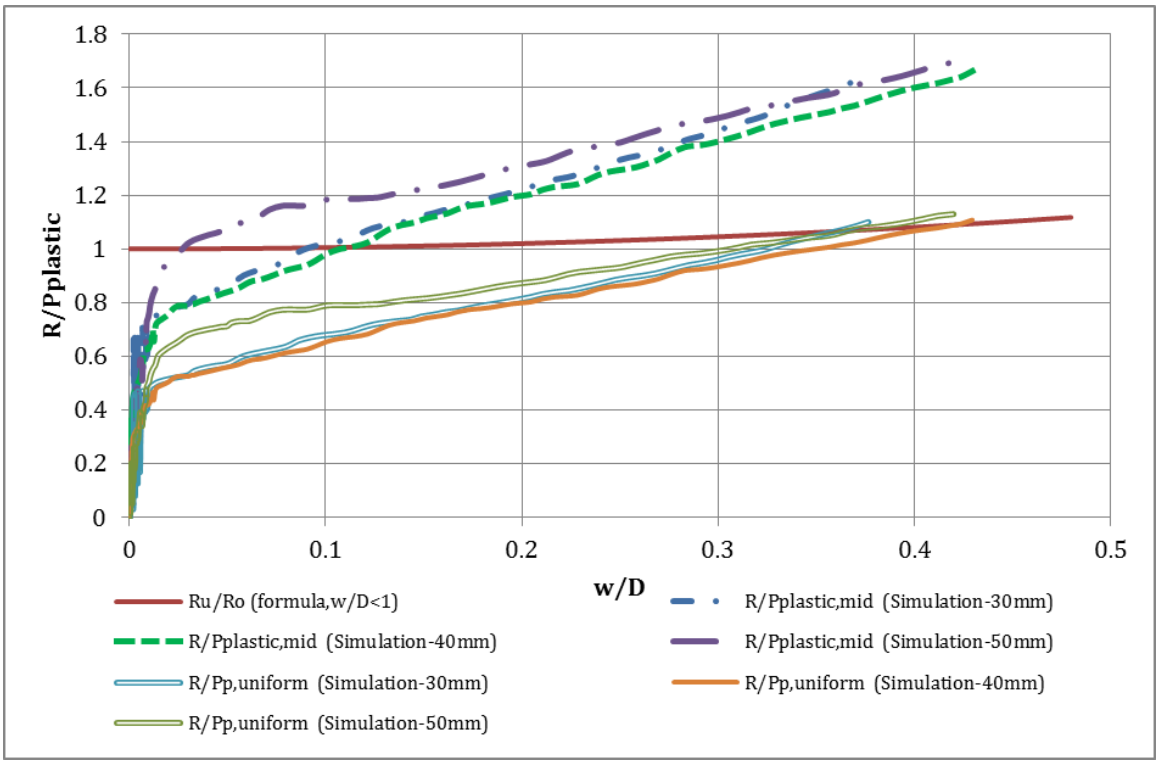

Fig. D-2 Bending Force-Deformation – Quarter Span Impact

E Resistance-Indentation Plots (Fixed- versus (single) Axial Spring-ends)

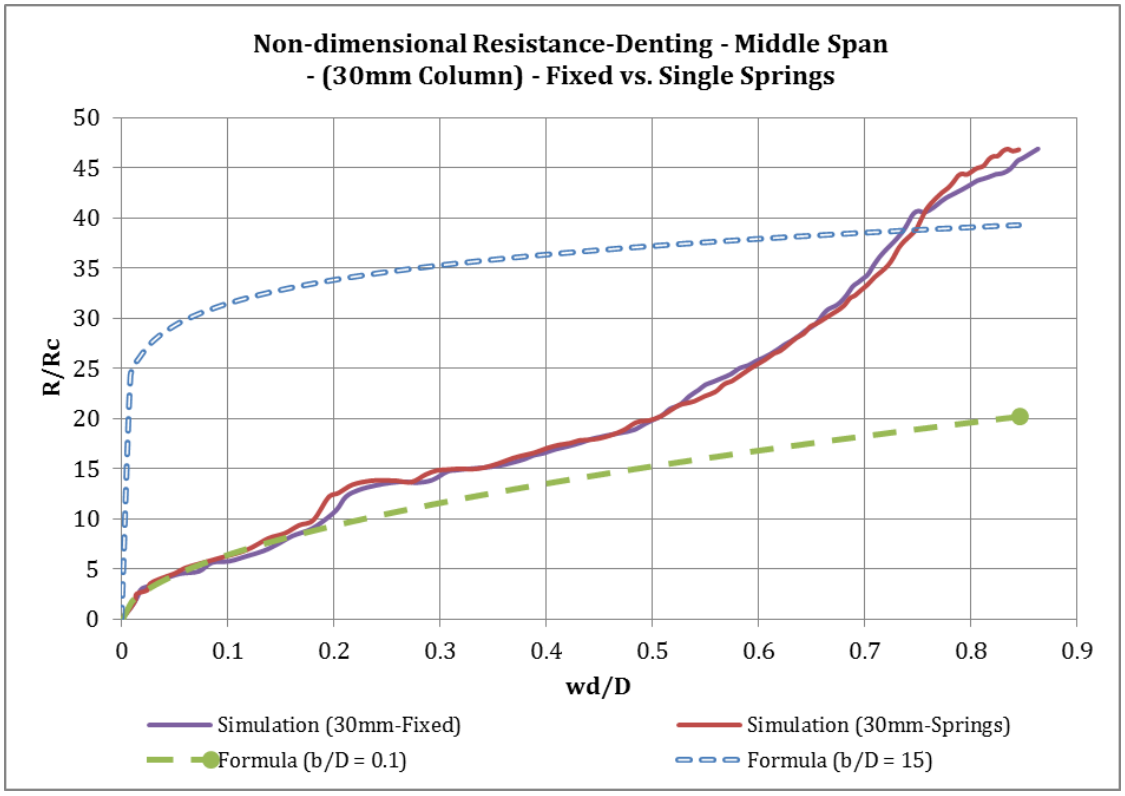

Fig. E-1 Resistance-Indentation Plot for 30 mm-thick Column (Fixed vs. Axial Spring)

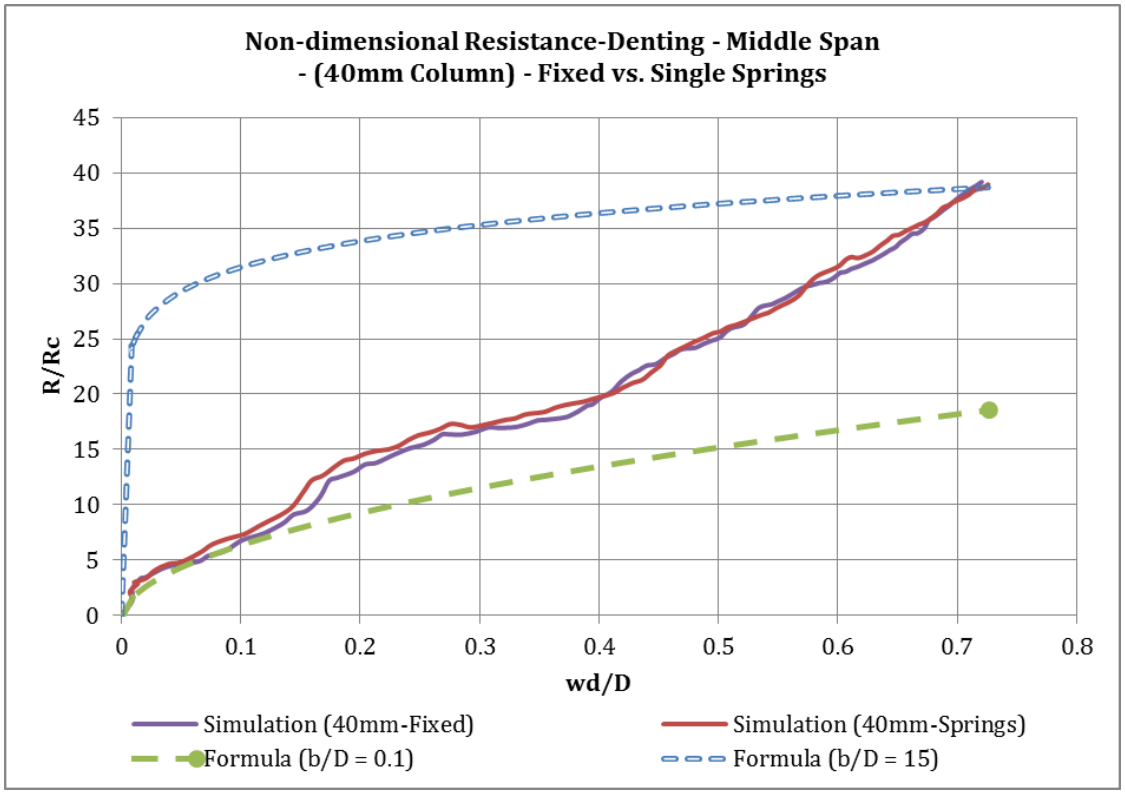

Fig. E-2 Resistance-Indentation Plot for 40 mm-thick Column (Fixed vs. Axial Spring)

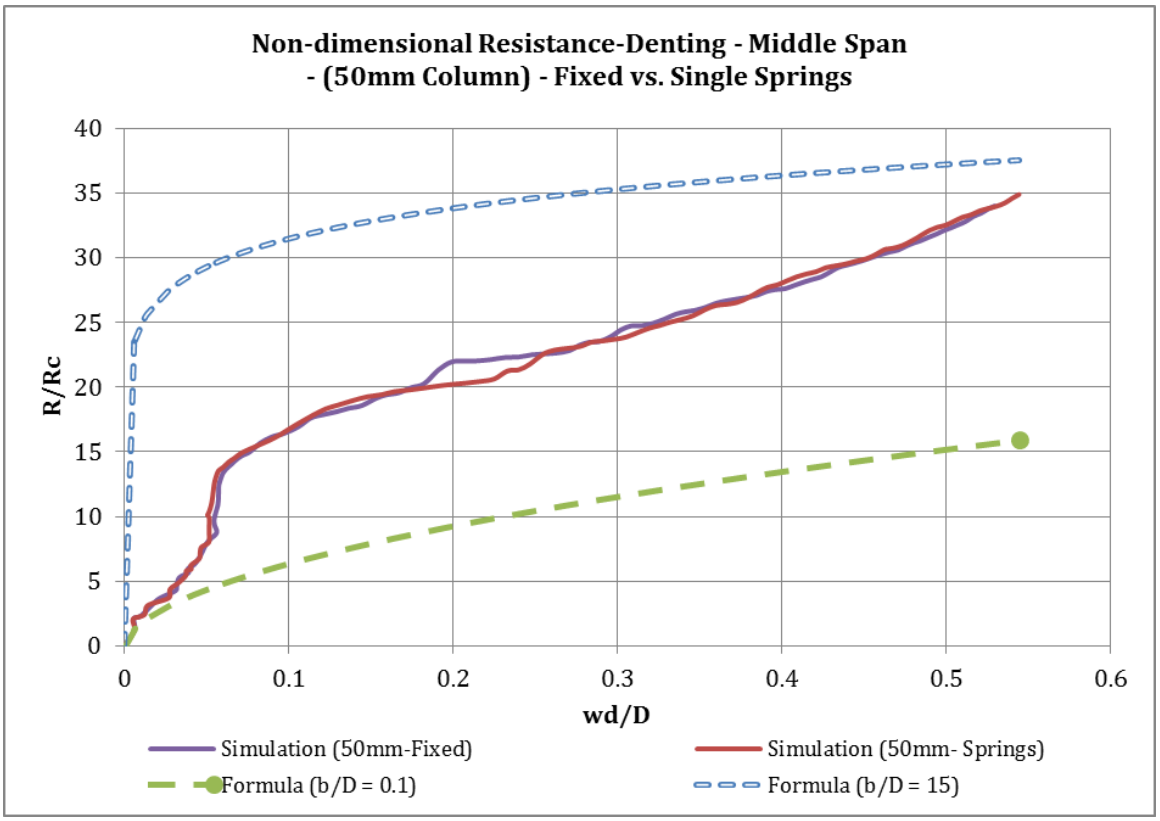

Fig. E-3 Resistance-Indentation Plot for 50 mm-thick Column (Fixed vs. Axial Spring)

F Force-Deformation Plots (Various Axial Flexibilities)

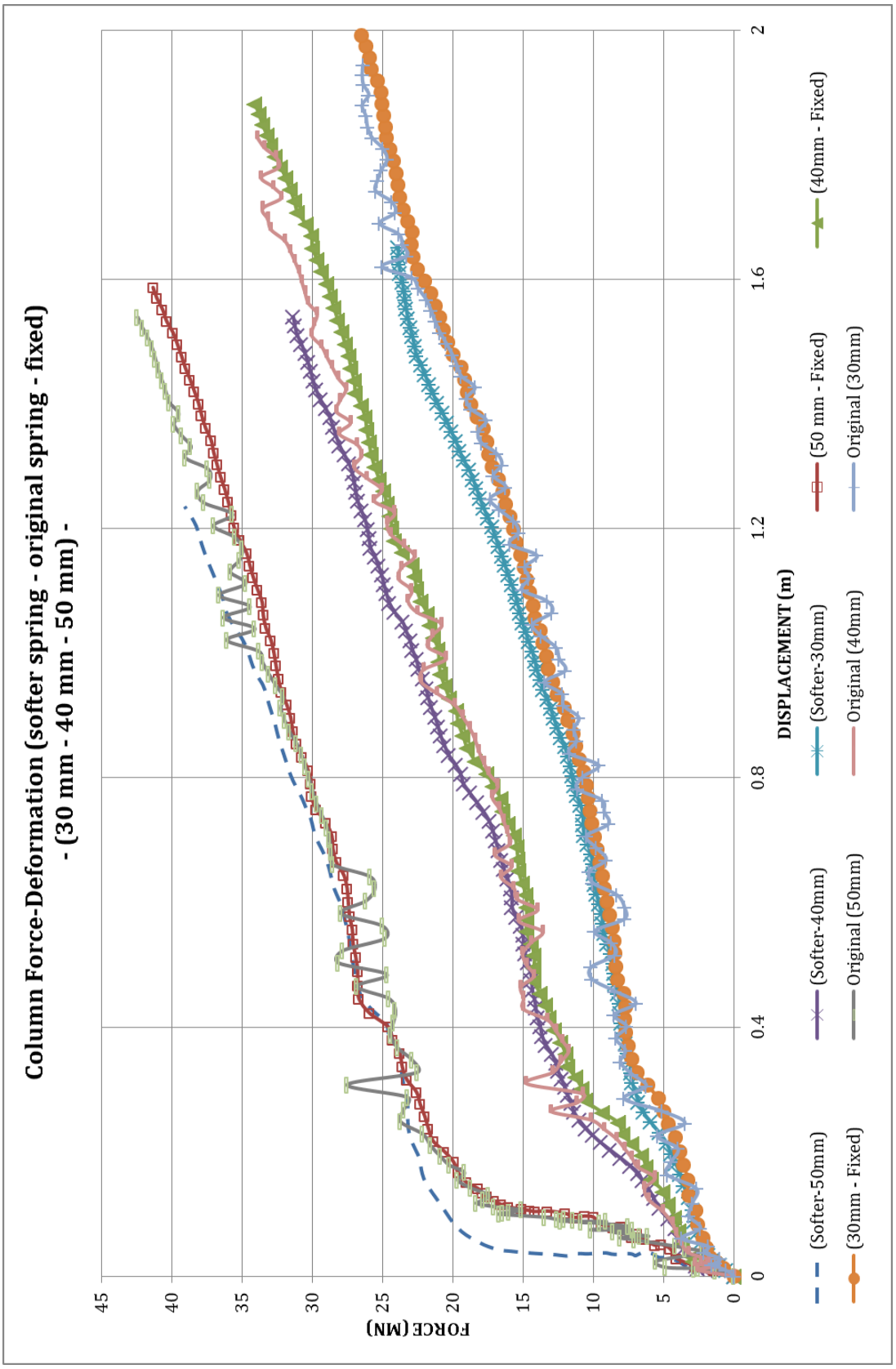

Fig. F-1 Column Force-Deformation (various axial flexibilities and thicknesses)

Content of Attached DVD or USB flash drive

- LS-DYNA output animations and input files
  - Fixed-Ends Column
    - Middle Span Impact
      - Rigid Ship
        - 30 mm Column
        - 40 mm Column
        - 50 mm Column
      - Rigid Column
      - Integrated
        - 30 mm Column
        - 40 mm Column
        - 50 mm Column
    - Quarter Span Impact
      - Rigid Ship
        - 30 mm Column
        - 40 mm Column
        - 50 mm Column
      - Rigid Column
      - Integrated
        - 30 mm Column
        - 40 mm Column
        - 50 mm Column
  - Column with Axial Springs
    - Multiple Spring Model
      - Equal Spring
      - Unequal Spring
    - Single Spring Model
      - Original Spring
      - Softer Spring
      - Firmer Spring

- Thesis Report (pdf)